

BIOPHYSICAL CHARACTERIZATION AND DIAGNOSIS OF OBESITY  
FROM ADIPOSE TISSUE BY FOURIER TRANSFORM INFRARED  
SPECTROSCOPY AND IMAGING

A THESIS SUBMITTED TO  
THE GRADUATE SCHOOL OF NATURAL AND APPLIED SCIENCES  
OF  
MIDDLE EAST TECHNICAL UNIVERSITY

BY

FATMA KÜÇÜK BALOĞLU

IN PARTIAL FULFILLMENT OF THE REQUIREMENTS  
FOR  
THE DEGREE OF DOCTOR OF PHILOSOPHY  
IN  
BIOLOGY

JANUARY 2017



Approval of the thesis:

**BIOPHYSICAL CHARACTERIZATION AND DIAGNOSIS OF OBESITY  
FROM ADIPOSE TISSUE BY FOURIER TRANSFORM INFRARED  
SPECTROSCOPY AND IMAGING**

submitted by **FATMA KÜÇÜK BALOĞLU** in partial fulfillment of the  
requirements for the degree of **Doctor of Philosophy of in Biological Sciences**  
**Department, Middle East Technical University** by,

Prof. Dr. Gülbin Dural Ünver

Dean, **Graduate School of Natural and Applied Sciences**

Prof. Dr. Orhan Adalı

Head of Department, **Biological Sciences**

Prof. Dr. Feride Severcan

Supervisor, **Biological Sciences Dept., METU**

**Examining Committee Members:**

Assoc. Prof. Dr. Çağdaş D. Son

Biological Sciences Dept., METU

Prof. Dr. Feride Severcan

Biological Sciences Dept., METU

Assoc. Prof. Dr. Tülin Yanık

Biological Sciences Dept., METU

Assist. Prof. Dr. Özlem Bozkurt Girit

Biophysics Dept., Adnan Menderes University

Assist. Prof. Dr. Ayça Doğan Mollaoğlu

Physiology Dept., Istanbul Kemerburgaz University

**Date: 27.01.2017**

**I hereby declare that all information in this document has been obtained and presented in accordance with academic rules and ethical conduct. I also declare that, as required by these rules and conduct, I have fully cited and referenced all material and results that are not original to this work.**

Name, Last name: Fatma KÜÇÜK BALOĞLU

Signature:

## **ABSTRACT**

# **BIOPHYSICAL CHARACTERIZATION AND DIAGNOSIS OF OBESITY FROM ADIPOSE TISSUE BY FOURIER TRANSFORM INFRARED SPECTROSCOPY AND IMAGING**

Küçük Baloğlu Fatma

Ph.D., Department of Biological Sciences

Supervisor: Prof. Dr. Feride Severcan

January 2017, 157 pages

Obesity is a heterogeneous disorder originating from the enlargement of visceral (VAT) and subcutaneous (SCAT) adipose tissue mass in the body and this process usually results in disturbed glucose and lipid metabolism. The first part of this study aimed to characterize and compare VAT and SCAT with regard to biomolecular content and also investigate transdifferentiation between white and brown adipocytes. Regarding this aim, Fourier transform infrared (FTIR) microspectroscopy and uncoupling protein 1 (UCP1) immunohistological staining was used in VAT and SCAT of male Berlin fat mice inbred (BFMI) lines, which are spontaneously obese. The results indicated a remarkable increase in the lipid/protein ratio, accompanied with a decrease of UCP1 protein content which

might be due to the transdifferentiation of brown to white adipocytes in obese groups. Additionally, the lower unsaturation/saturation lipid ratio, the longer hydrocarbon acyl chain length of lipids and the higher amount of triglycerides were obtained in both adipose tissues of mice lines compared to control line. The results also revealed that SCAT was more prone to obesity-induced structural changes than VAT.

The excess deposition of triglycerides in adipose tissue is the main reason of obesity and this process causes the excess release of fatty acids to the circulatory system leading to insulin resistance. The second part of this study mainly aimed to propose triglyceride band located at  $1770\text{-}1720\text{ cm}^{-1}$  spectral region as a sensitive obesity related biomarker. For this reason, the diagnostic potential of FTIR spectroscopy coupled with hierarchical cluster analysis (HCA) and principal component analysis (PCA) was used in SCAT and VAT samples obtained from control and four different obese male BFMI mice lines. Successful discrimination of the obese, obesity related insulin resistant and control groups were achieved with high sensitivity and specificity. The results revealed the power of FTIR spectroscopy coupled with chemometric approaches in internal diagnosis of abdominal obesity based on the spectral differences in the triglyceride region.

Gender is an important factor in the evaluation of obesity, hence the purpose of the third part of the study is to investigate gender-based differences in obesity by comparing biomolecular content of SCAT and VAT in male and female mice lines. In accordance with this comparative approach, ATR-FTIR spectroscopy coupled with multivariate data analysis was applied to the spectra of some special regions to differentiate male and female samples. To determine gender-based differences in the effect of obesity on VAT and SCAT in obese mice lines, the biomolecular characteristics of these tissues were compared in male and female BFMI mice by FTIR microspectroscopy. UCP1 immunohistological staining was also performed to compare the appearance of brown and white adipocytes in different genders. The results indicated that obesity indicators were more significant in SCAT of female mice while they were more significant in VAT of male mice. Consequently, the effects of obesity on male's health can be more harmful than females.

**Keywords:** Obesity, Visceral Adipose Tissue, Subcutaneous Adipose Tissue, White Adipose Tissue, Brown Adipose Tissue, gender-based effect, UCP1 Protein, FTIR, ATR, Spectroscopy, Transdifferentiation, Diagnosis, Principal Component Analysis; Hierarchical Cluster Analysis.





## ÖZ

# **OBEZİTENİN ADİPOZ DOKUDA FOURIER DÖNÜŞÜMLÜ KIZİLÖTESİ SPEKTROSKOPİSİ VE GÖRÜNTÜLEMESİ İLE BİYOFİZİKSEL KARAKTERİZASYONU VE TEŞHİSİ**

Küçük Baloğlu Fatma

Ph.D., Biyolojik Bilimler Bölümü

Tez Yöneticisi: Prof. Dr. Feride Severcan

Ocak 2017, 157 Sayfa

Obezite, viseral (VAT) ve subkütan (SCAT) adipoz dokunun büyümesinden kaynaklanan heterojen yapılı bir hastalıktır ve sözkonusu süreç çoğunlukla zarar görmüş glukoz ve lipit metabolizması ile sonuçlanmaktadır. Çalışmanın birinci kısmında VAT ve SCAT'ı moleküler içerik bakımından karakterize etmek ve karşılaştırmak, ayrıca beyaz ve kahverengi adipoz dokular arasındaki transdiferansiyonu araştırmak amaçlanmıştır. Bu sebeple kendiliğinden obez olan erkek Berlin lipit inbred fare (BFMI) hatlarına ait VAT ve SCAT dokularına Fourier Dönüşümlü Kızılötesi (FTIR) Mikrospektroskopisi ve uncoupling protein 1 (UCP1) immünohistolojik boyaması uygulanmıştır. Sonuçlar lipit/protein oranında anlamı bir artış ile birlikte kahverengi ve beyaz adipozitlerin transdiferasyonundan kaynaklanmış olabilecek bir UCP1 protein miktarı düşüşü

göstermiştir. Buna ek olarak, fare hatlarına ait iki tip adipoz dokusunda da kontrol hattına göre daha düşük doymamış/doymuş yağ oranı, daha uzun hidrokarbon açıl zincir uzunluğu ve daha yüksek miktarda trigliserit tespit edilmiştir. Sonuçlar ayrıca SCAT'ın VAT'a göre obezite kaynaklı yapısal değişimlere daha yatkın olduğunu ortaya koymuştur.

Trigliseritlerin adipoz dokuda aşırı birikimi obezitenin ana sebebidir ve bu süreç serbest yağ asitlerinin yoğun bir şekilde dolaşıma katılmasına neden olarak insulin direncine yol açar. Çalışmamızın ikinci kısmı temelde 1770-1720  $\text{cm}^{-1}$  spektral bölgesinde bulunan trigliserit bantını bir duyarlı obezite biyobelirteci olarak sunmaktır. Bu nedenle. Hiyerarşik Kümeleme Analizini (HCA) ve Temel Bileşen Analizi (PCA) ile birlikte kullanılan FTIR spektroskopisinin teşhissel potansiyeli, kontrol ve 4 farklı obez BFMI erkek fare hatlarına ait SCAT ve VAT dokuları üzerinde uygulanmıştır. Kontrol, obez, obezite kaynaklı insulin dirençli gruplar yüksek duyarlılık ve özgüllük ile birbirinden başarıyla ayrılmıştır. Sonuçlar, trigliserit bölgesindeki spektral değişimlere dayanan abdominal obezitenin dahili teşhisinde, kemometrik yaklaşımlarla beraber FTIR spektroskopisinin gücünü ortaya koymuştur.

Cinsiyet, obezitenin değerlendirilmesi için önemli bir faktördür, bu sebeple çalışmanın üçüncü kısmının amacı dişi ve erkek fare hatlarına ait VAT ve SCAT dokularının moleküler içeriğinin karşılaştırması yolu ile obezitede cinsiyete bağlı farklılıklarının araştırılmasıdır. Bu karşılaştırmacı yaklaşımla uyumlu olarak, çok değişkenli veri analiz ile birlikte ATR-FTIR spektroskopisi dişi ve erkek örneklerin ayrımı amacıyla bazı özel spektral bölgelerde uygulanmıştır. Obezitenin VAT ve SCAT üzerindeki etkilerinin cinsiyete bağlı değişimlerini saptamak için bu dokuların makromoleküler karakteristikleri erkek ve dişi BFMI farelerde FTIR spektroskopisi ile karşılaştırılmıştır. UCP1 immunohistolojik boyama ise farklı cinsiyetlerde kahverengi ve beyaz adipositlerin görünümünü karşılaştırmak amacıyla uygulanmıştır. Sonuçlar obezite belirteçlerinin dişi farelere ait SCAT dokusunda ve erkek farelere ait VAT dokusunda daha anlamlı olduğunu göstermiştir. Sonuç olarak, obezitenin erkek sağlığı üstüne etkileri dişilere nazaran daha zararlı olabilir.

**Anahtar Kelimeler:** Obezite, Visceral Adipoz Doku, Subkütan Adipoz Doku, Beyaz Adipoz Doku, Kahverengi Adipoz Doku, Cinsiyete Bağlı Değişim, UCP1 Protein, FTIR, ATR, Spektroskopi, Transdiferansiyon, Teşhis, Hiyerarşik Kümeleme Analizi, Temel Bileşen Analizi.



**Dedicated to my devoted family,**

## ACKNOWLEDGEMENTS

First and foremost, I would like to express my deepest appreciation to my supervisor Prof. Dr. Feride SEVERCAN for her endless support, patience motivation and immense knowledge. Without her inspiring guidance and encouragement, I couldn't have accomplished this thesis successfully.

I would also like to thank to my PhD Thesis Committee Members Assoc. Prof. Dr. Çağdaş D. SON, Assoc. Prof. Dr. Tülin YANIK, Assist. Prof. Dr. Özlem BOZKURT GİRİT and Assist. Prof. Dr. Ayça DOĞAN MOLLAOĞLU.

I would like to express my special thanks to Assist. Prof. Dr. Özlem BOZKURT GİRİT, Assist. Prof. Dr. Şebnem GARİP USTAOĞLU, Assist. Prof. Dr. Ayça DOĞAN MOLLAOĞLU, Dr. Dilek YONAR for their precious and endless help, concern support and lovely attitude throughout the progress of my thesis.

I would like to extend my thanks to my friends in Lab-146, Dr. Nihal ŞİMŞEK ÖZEK, Seher GÖK, Dr.Nuri ERGEN, Dr.Sherif ABBAS and Dr.Rafig GURBANOV for their great help, support and considerable advices.

I would like to give my deepest thanks to my husband Onur BALOĞLU for his endless patience, support and love during my all academic life.

Words failed me to express my appreciation to my mother Ayten KÜÇÜK, my father Mevlüt KÜÇÜK, my sister Funda N. KÜÇÜK and my brother M. Eren KÜÇÜK for their love, constant support, care and understanding throughout my life. I wouldn't be here without their encouragement. I dedicate this work to my family.

I was supported by TUBITAK 2211-A National Scholarship Programme for PhD Students during my doctorate and this study was also supported by the Scientific and Technical Research Council of Turkey (TUBITAK) through SBAG-110S235 research fund.

## TABLE OF CONTENTS

|   |       |
|---|-------|
| ABSTRACT .....  | v     |
| ÖZ .....  | ix    |
| ACKNOWLEDGEMENTS .....  | xiv   |
| TABLE OF CONTENTS .....   | xv    |
| LIST OF TABLES .....  | xvii  |
| LIST OF FIGURES .....   | xviii |
| LIST OF ABBREVIATIONS .....   | xxiii |
| CHAPTERS  |       |
| 1. INTRODUCTION .....   | 1     |
| 1.1. Obesity.....   | 1     |
| 1.1.1. Diagnosis of Obesity .....   | 2     |
| 1.1.2. Causes of Obesity.....   | 4     |
| 1.1.3. Adipose Tissue and Obesity.....  | 5     |
| 1.1.4. Obesity and Insulin Resistance .....                                   | 14    |
| 1.1.5. The Berlin Fat Mouse Inbred (BFMI) Lines as Mouse Models for Obesity.. | 17    |
| 1.2. Electromagnetic Radiation and Basics of Spectroscopy .....               | 18    |
| 1.2.1. Basis of Infrared Spectroscopy .....                                   | 21    |
| 1.2.2. Fourier Transform Infrared Spectroscopy (FTIR) .....                   | 23    |
| 1.3. Chemometrics in FTIR Spectroscopy.....                                   | 30    |
| 1.3.1. Hierarchical Cluster analysis (HCA) .....                              | 30    |

|   |     |
|---|-----|
| 1.3.2. Principal Component Analysis (PCA) .....   | 31  |
| 1.4. Aim of the Study .....   | 32  |
| 2. MATERIALS AND METHODS .....  | 33  |
| 2.1. Animal Studies, Feeding and Husbandry Conditions .....   | 33  |
| 2.2. FTIR Microspectroscopic Studies .....  | 34  |
| 2.2.1. Sample Preparation .....   | 34  |
| 2.2.2. FTIR Microspectroscopic Data Collection and Analysis.....  | 35  |
| 2.3. Immunohistological Staining .....  | 37  |
| 2.4. ATR-FTIR Spectroscopic Studies.....  | 38  |
| 2.5. Hierarchical Cluster Analysis (HCA) .....  | 39  |
| 2.6. Principle Component Analysis (PCA) .....   | 41  |
| 2.7. Statistics .....   | 41  |
| 3. RESULTS AND DISCUSSION .....   | 43  |
| Part 1: FTIR imaging of structural changes in visceral and subcutaneous adiposity and transdifferentiation from brown to white adipocyte..... | 43  |
| Part 2: Triglyceride Dependent Differentiation of Obesity in Adipose Tissues by FTIR Spectroscopy Coupled with Chemometrics .....             | 62  |
| Part 3: Investigation of gender-based differences in the effect of obesity on adipose tissue.....   | 78  |
| 4. CONCLUSION .....   | 113 |
| REFERENCES .....  | 117 |
| APPENDIX .....  | 149 |
| CURRICULUM VITAE .....  | 151 |



## LIST OF TABLES

### TABLES

|   |    |
|---|----|
| <b>Table 1.</b> The spectral regions and baseline points for particular infrared bands used in calculation of band area ratios.....                                       | 36 |
| <b>Table 2.</b> Definitions for sensitivity and specificity during hierarchical cluster analysis based on FTIR data. ....   | 40 |
| <b>Table 3.</b> General band assignment of FTIR spectrum of an adipose tissue(Dogan et al., 2013; Kneipp et al., 2000; Naumann Dieter, Fabian Heinz, 2009).....           | 45 |
| <b>Table 4.</b> The band area and band position values of the amide I band in male control (DBA/2J) and obese (BFMI lines) mice gonadal and inguinal adipose tissues..... | 55 |
| <b>Table 5.</b> The alterations in band area values of the triglyceride band for the control and obese lines in SCAT and VAT.....   | 66 |
| <b>Table 6.</b> General band assignment of FTIR spectrum of adipose tissues based on literature. ....   | 82 |
| <b>Table 7.</b> Definitions and obtained values for sensitivity and specificity during HCA based on male and female spectral data in VAT and SCAT.....                    | 90 |

## LIST OF FIGURES

### FIGURES

|  |    |
|--|----|
| <b>Figure 1.</b> Prevalence of obesity in the world (2014). .....  | 2  |
| <b>Figure 2.</b> The International Classification of adult underweight, overweight and obesity according to BMI. ....  | 3  |
| <b>Figure 3.</b> Fundamental principles of energy balance. ....  | 5  |
| <b>Figure 4.</b> Adipocytes of adipose tissue, Brown and White adipocyte phenotypes. ....  | 8  |
| <b>Figure 5.</b> Characteristics of white and brown fat. ....  | 9  |
| <b>Figure 6.</b> Localization of VAT and SAT in the body (Cinti 2005). ....  | 10 |
| <b>Figure 7.</b> Dysfunctional adipose tissue in obesity (van Kruijsdijk, van der Wall, and Visseren 2009).....  | 14 |
| <b>Figure 8.</b> Secretion of inflammatory adipokines from adipose tissue in obese state. ....   | 17 |
| <b>Figure 9.</b> An electromagnetic wave.....  | 18 |
| <b>Figure 10.</b> Typical energy-level diagram .....   | 19 |
| <b>Figure 11.</b> The electromagnetic spectrum .....   | 21 |
| <b>Figure 12.</b> Simple layouts of the vibrational modes associated to a molecular dipole moment change detectable in an IR absorption spectrum. ....           | 22 |
| <b>Figure 13.</b> A typical mid-IR transmission spectrum showing in a schematic way typical absorptions lines associated to vibrational modes of molecules. .... | 23 |
| <b>Figure 14.</b> A) Schematic diagram of a Michelson interferometer configured for FTIR B) The general system flowchart of FTIR. ....                           | 24 |
| <b>Figure 15.</b> A multiple reflection ATR-FTIR system (T. D. Wang et al. 2007).....  | 28 |
| <b>Figure 16.</b> Schematic diagram representing the working principle of FTIR microspectroscopy.....  | 29 |

|  |    |
|--|----|
| <b>Figure 17.</b> Representative FTIR spectra of IF adipose tissue of male control DBA/J2 and obese BFMI861 lines in the 4000-750 $\text{cm}^{-1}$ region.....   | 44 |
| <b>Figure 18.</b> Representative images of the lipid/protein ratio in SCAT and VAT of the control and BFMI lines. ....   | 47 |
| <b>Figure 19.</b> Representative images of the $\text{CH}_2/\text{CH}_3$ antisymmetric ratio in SCAT and VAT of the control and BFMI lines. ....   | 48 |
| <b>Figure 20.</b> Representative images of the olefinic/protein ratio in SCAT and VAT of control and BFMI lines. ....  | 49 |
| <b>Figure 21.</b> Representative images of the carbonyl/lipid in SCAT and VAT of the control and BFMI lines.....   | 50 |
| <b>Figure 22.</b> Representative images of the amide I/amide II in SCAT and VAT of the control and BFMI lines.....   | 51 |
| <b>Figure 23.</b> The bar graphs of the lipid/protein, $\text{CH}_2$ symmetric/ $\text{CH}_2$ antisymmetric, $\text{CH}_2/\text{CH}_3$ antisymmetric, olefinic/lipid, carbonyl/lipid, $\text{CH}_2$ antisymmetric/lipid, amide I/ amide II, amide I/ amide I + amide II ratios of control (DBA/J2) and 4 different obese (BFMI) male mice lines. (GF: VAT; IF: SCAT). .... | 53 |
| <b>Figure 24.</b> Microscopic images of immunohistological UCP1 staining results of SCAT and VAT belong to the control and obese lines under 40X magnification. ....   | 60 |
| <b>Figure 25.</b> PCA loading plots for VAT (A) and SCAT (B) of control and obese groups in the 1800–1000 $\text{cm}^{-1}$ spectral region. The triglyceride region is shown by arrow. ....  | 64 |
| <b>Figure 26.</b> Representative ATR-FTIR spectra of the control and obese lines in the 1800–1000 $\text{cm}^{-1}$ spectral region and enlarged panel of baseline corrected version of the triglyceride region (1770-1720 $\text{cm}^{-1}$ ). The spectra were normalized to the band located at 3300 $\text{cm}^{-1}$ .....   | 65 |
| <b>Figure 27.</b> Correlation between VAT and SCAT. Spearman correlation coefficient (r) and p value are provided on each panel. Calculations were performed using GraphPad (Prism version 6). ....  | 67 |
| <b>Figure 28.</b> Hierarchical clustering of BFMI lines (852, 856, 860, 861) in SCAT (A) and VAT (B) in the 1770-1720 $\text{cm}^{-1}$ spectral region. PC1 versus PC2 scores plot of the second derivative vector normalized spectra in the same range of BFMI lines in SCAT (C) and  |    |

VAT (D). Obese group (BFMI852-856) (red), obesity related insulin resistant group (BFMI860-861) (blue).....69

**Figure 29.** Hierarchical clustering of control, obese and obesity related insulin resistant groups in SCAT (A) and VAT (B) in the 1770-1720  $\text{cm}^{-1}$  spectral region. Control group (black), obese group (BFMI852-856) (red), obesity related insulin resistant group (BFMI860-861) (blue).....72

**Figure 30.** PCA loading plots of control, obese and obesity related insulin resistant groups for SCAT (A) and VAT (B) samples in the 1770–1720  $\text{cm}^{-1}$  spectral region. PC1 versus PC2 scores plot of the second derivative vector normalized spectra in the same range of SCAT (C) and VAT (D). Control group (black), obese group (BFMI852-856) (red), obesity related insulin resistant group (BFMI860-861) (blue).....74

**Figure 31.** PC1 versus PC2 score plots of control, obese and obesity related insulin resistant groups for SCAT (A) samples in the 1770–1720  $\text{cm}^{-1}$  spectral region. Leave-one-out cross validation for SCAT (B) in the same region. Control group (black), obese group (BFMI852-856) (red), obesity related insulin resistant group (BFMI860-861) (blue). ...76

**Figure 32.** PC1 versus PC2 score plots of control, obese and obesity related insulin resistant groups for VAT (A) samples in the 1770–1720  $\text{cm}^{-1}$  spectral region. Leave-one-out cross validation for VAT (B) in the same region. Control group (black), obese group (BFMI852-856) (red), obesity related insulin resistant group (BFMI860-861) (blue). ...77

**Figure 33.** The representative FTIR spectra of male and female VAT samples (BFMI860) in the 4000-650  $\text{cm}^{-1}$  region. ....79

**Figure 34.** The representative FTIR spectra of male and female SCAT samples (BFMI860) in 4000-650  $\text{cm}^{-1}$  region.....79

**Figure 35.** Representative infrared spectra of VAT samples of male and female mice in the 3050-2800  $\text{cm}^{-1}$  and 1800-1000  $\text{cm}^{-1}$  regions. (The spectra were baseline corrected and normalized with respect to the Amide A band for visual demonstration). ....80

**Figure 36.** Representative infrared spectra of SCAT samples of male and female mice in the 3050-2800  $\text{cm}^{-1}$  and 1800-1000  $\text{cm}^{-1}$  regions. (The spectra were baseline corrected and normalized with respect to the Amide A band for visual demonstration). ....81

|   |    |
|---|----|
| <b>Figure 37.</b> PC1 versus PC2 scores plot of the second derivative vector normalized spectra in the whole range of VAT.....  | 83 |
| <b>Figure 38.</b> PC1 versus PC2 scores plot of the second derivative vector normalized spectra in the whole range of SCAT.....   | 83 |
| <b>Figure 39.</b> PCA loading plots of male and female groups for VAT samples in the C-H region (3025–2800 cm <sup>-1</sup> ) (above). PC2 versus PC6 scores plot of the second derivative vector normalized spectra in the same range of VAT (below). ....           | 85 |
| <b>Figure 40.</b> PCA loading plots of male and female groups for VAT samples in the fingerprint region (1800–1000 cm <sup>-1</sup> ) (above). PC1 versus PC3 scores plot of the second derivative vector normalized spectra in the same range of VAT (below). ....   | 86 |
| <b>Figure 41.</b> PCA loading plots of male and female groups for SCAT samples in the C-H region (3025–2800 cm <sup>-1</sup> ) (above). PC5 versus PC6 scores plot of the second derivative vector normalized spectra in the same range of SCAT (below). ....         | 87 |
| <b>Figure 42.</b> PCA loading plots of male and female groups for SCAT samples in the fingerprint region (1800–1000 cm <sup>-1</sup> ) (above). PC5 versus PC6 scores plot of the second derivative vector normalized spectra in the same range of SCAT (below). .... | 88 |
| <b>Figure 43.</b> Hierarchical clustering of the male and female groups in the C-H region (A) and the fingerprint region (B) belonging to the VAT samples. Male group (blue), female group (red).....   | 91 |
| <b>Figure 44.</b> Hierarchical clustering of the male and female groups in the C-H region (A) and the fingerprint region (B) belonging to the SCAT samples. Male group (blue), female group (red).....  | 92 |
| <b>Figure 45.</b> Representative images of the lipid/protein ratio in VAT of male and female groups.....  | 94 |
| <b>Figure 46.</b> Representative images of the lipid/protein ratio in SCAT of male and female groups.....   | 95 |
| <b>Figure 47.</b> Representative images of the olefinic/lipid ratio in VAT of male and female groups.....   | 96 |
| <b>Figure 48.</b> Representative images of the olefinic/lipid ratio in SCAT of male and female groups.....  | 97 |

|  |     |
|--|-----|
| <b>Figure 49.</b> Representative images of the carbonyl/lipid ratio in VAT of male and female groups. ....   | 98  |
| <b>Figure 50.</b> Representative images of the carbonyl/lipid ratio in SCAT of male and female groups. ....  | 99  |
| <b>Figure 51.</b> Representative images of the amide II/amide I ratio in VAT of male and female groups. ....   | 100 |
| <b>Figure 52.</b> Representative images of the amide II/amide I ratio in SCAT of male and female groups. ....  | 101 |
| <b>Figure 53.</b> The bar graphs of the lipid/protein, olefinic/lipid, carbonyl/lipid, amide I/amide II ratios of male and female groups in VAT. ....        | 103 |
| <b>Figure 54.</b> The bar graphs of the lipid/protein, olefinic/lipid, carbonyl/lipid, amide I/amide II ratios of male and female groups in SCAT. ....       | 104 |
| <b>Figure 55.</b> . Microscopic images of immunohistological UCP1 staining results of male and female groups belong to the VAT under 40X magnification. .... | 109 |
| <b>Figure 56.</b> Microscopic images of immunohistological UCP1 staining results of male and female groups belong to the SCAT under 40X magnification. ....  | 110 |

## LIST OF ABBREVIATIONS

|       |  |
|-------|--|
| ATR   | Attenuated Total Reflectance           |
| BaF2  | Barium Fluoride                        |
| BAT   | Brown Adipose Tissue                   |
| BFMI  | Berlin Fat Mouse Inbred                |
| FFA   | Free Fatty Acid                        |
| FTIR  | Fourier Transform Infrared             |
| GF    | Gonadal Fat                            |
| HCA   | Hierarchical Cluster Analysis          |
| HFD   | High Fat Diet                          |
| IF    | Inguinal Fat                           |
| ipGTT | Intraperitoneal Glucose Tolerance Test |
| ipITT | Intraperitoneal Insulin Tolerance Test |
| PCA   | Principal Component Analysis           |
| PUFA  | Polyunsaturated Fatty Acid             |
| SCAT  | Subcutaneous Adipose Tissue            |
| SBD   | Standard Breeding Diet                 |
| VAT   | Visceral Adipose Tissue                |
| WAT   | White Adipose Tissue                   |





## **CHAPTER I**

### **1. INTRODUCTION**

#### **1.1. Obesity**

Obesity is an epidemic disease resulting from the modern life leading to a growing number of people of many social circumstances as a worldwide problem. As a result of modern life, there is an increment in sedentary lifestyle and an augmentation in food consumption with high fat content, obesity is turning into one of the considerable risk factor for human health (Reaven, 1997). The WHO reported that overweight adults were more than 1.4 billion and over 200 million men and approximately 300 million women of them were obese (Figure 1) (WHO, 2014). Epidemiological investigations estimated that 2.16 billion people worldwide will be overweight and 1.12 billion will be obese by the year 2030 (Kastorini et al., 2011). When Turkey is in concern, Turkish population has higher obesity prevalence than most of the European countries, so it was found that 19.9% of Turkish Population is obese and 33.7% of them is overweight while 42.2% is in the normal range (Turkish Statistical Institute, 2014).

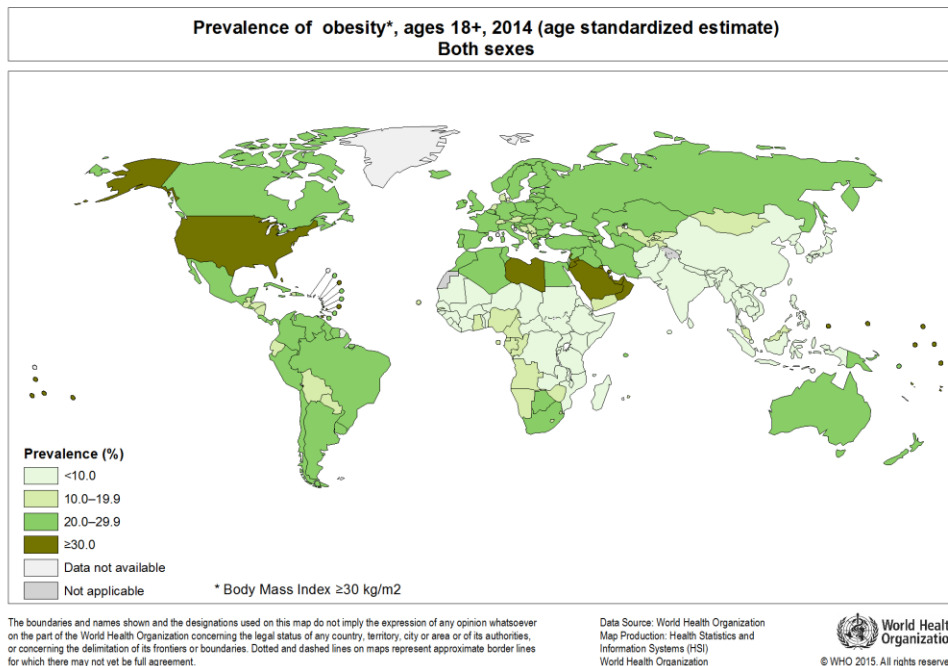


**Figure 1.** Prevalence of obesity in the world (2014).

### 1.1.1. Diagnosis of Obesity

Body weight, body mass index (BMI), waist circumference (WC) and waist–hip ratio are widespread methods for the diagnosis of obesity (Sonmez et al., 2003). The body mass index and waist circumference are two methods that are widely used to estimate whether a person has a healthy weight or not. BMI is calculated as weight in kilograms divided by height in meters squared ( $\text{kg/m}^2$ ). The BMI cutoffs have been established to identify normal healthy range (18.50 - 24.99), overweight ( $\text{BMI} \geq 25 \text{ kg/m}^2$ ) or obese ( $\text{BMI} \geq 30 \text{ kg/m}^2$ ) individuals (WHO, 1995; World Health Organization & Organization, 2004). The WC is measured at a level halfway between the lowest rib and the iliac crest. The probability of obesity related diseases are categorized as high if women have a WC longer than 88 cm and men have a WC longer than 102 cm (WHO, 2008). On the other hand, waist–hip ratio is calculated to estimate the localization of abdominal fat and to have information of central obesity (Pouliot et al., 1994). Nowadays, BMI is a fundamental

index for diagnosis of obesity for the measurement of total body fat in clinical trials (Gray & Fujioka, 1991) (Figure 2) (WHO, 2016).

| Classification      | BMI(kg/m <sup>2</sup> )  |                           |
|---------------------|--------------------------|---------------------------|
|                     | Principal cut-off points | Additional cut-off points |
| <b>Underweight</b>  | <b>&lt;18.50</b>         | <b>&lt;18.50</b>          |
| Severe thinness     | <16.00                   | <16.00                    |
| Moderate thinness   | 16.00 - 16.99            | 16.00 - 16.99             |
| Mild thinness       | 17.00 - 18.49            | 17.00 - 18.49             |
| <b>Normal range</b> | <b>18.50 - 24.99</b>     | <b>18.50 - 22.99</b>      |
|                     |                          | <b>23.00 - 24.99</b>      |
| <b>Overweight</b>   | <b>≥25.00</b>            | <b>≥25.00</b>             |
| Pre-obese           | 25.00 - 29.99            | 25.00 - 27.49             |
|                     |                          | 27.50 - 29.99             |
| <b>Obese</b>        | <b>≥30.00</b>            | <b>≥30.00</b>             |
| Obese class I       | 30.00 - 34.99            | 30.00 - 32.49             |
|                     |                          | 32.50 - 34.99             |
| Obese class II      | 35.00 - 39.99            | 35.00 - 37.49             |
|                     |                          | 37.50 - 39.99             |
| Obese class III     | ≥40.00                   | ≥40.00                    |

Source: Adapted from WHO, 1995, WHO, 2000 and WHO 2004.

**Figure 2.** The International Classification of adult underweight, overweight and obesity according to BMI.

While prevalence of obesity in the world continues to increase dramatically, these conventional measurement techniques identify obesity poorly. To give an example, increased adiposity and decreased muscle mass within body composition occur with aging, and hence the result of diagnosis process of obesity can be complicated and misleading with these methods (Batsis et al., 2015). On the other hand, there is no well-accepted definition of abdominal obesity, especially in the existence of different ethnic groups culminating in heterogeneity in composition of abdominal tissue and alterations in metabolic effects of obesity in the body (Misra et al., 2005). Therefore, there is a requirement for a practical and accurate method to detect biomarkers of obesity and obesity related metabolic diseases. Recently, it has been reported that triglyceride is

promising predictor of the amount of VAT therefore it can be used as a marker to estimate visceral adiposity (Huang et al., 2015).

### **1.1.2. Causes of Obesity**

Obesity is a complicated multifactorial chronic disease originating from interrelated influences of many factors e.g. genetic, physiological, social, behavioral effects. Many researches have shown that there is a strong link between obesity and genetics (Cinti, 2009). If someone's parent is obese, the risk of the obesity increases significantly. In addition, if obesity is present throughout early childhood, possibilities are high that an individual will be obese during her or his life. Investigations have showed that someone's BMI can be attributed to genetic influences, with a 25-50% possibility that a child with one obese parent will be overweight, and a 75% possibility with two obese parents (Cannon & Nedergaard, 2004).

The environment is one of the major determinants of overweight and obesity. Environmental effects on overweight and obesity are closely related to physical activity and food intake behaviors (Sallis & Glanz, 2009). If calorie intake is more than requirement, it will be stored essentially as body fat. If the stored body fat does not consume with physical activity, it will cause overweight or obesity (Figure 3)(Prieto-Hontoria et al., 2011). A number of studies indicated that individuals on a high-fat diet are more prone to become overweight (Popkin et al.,1995).

Modern life is becoming sedentary and consequently the decline in energy expenditure can be seen with modernization and other societal changes. With the growing popularity of sedentary activities has been associated with an increased risk of obesity (Wadden & Stunkard, n.d.).

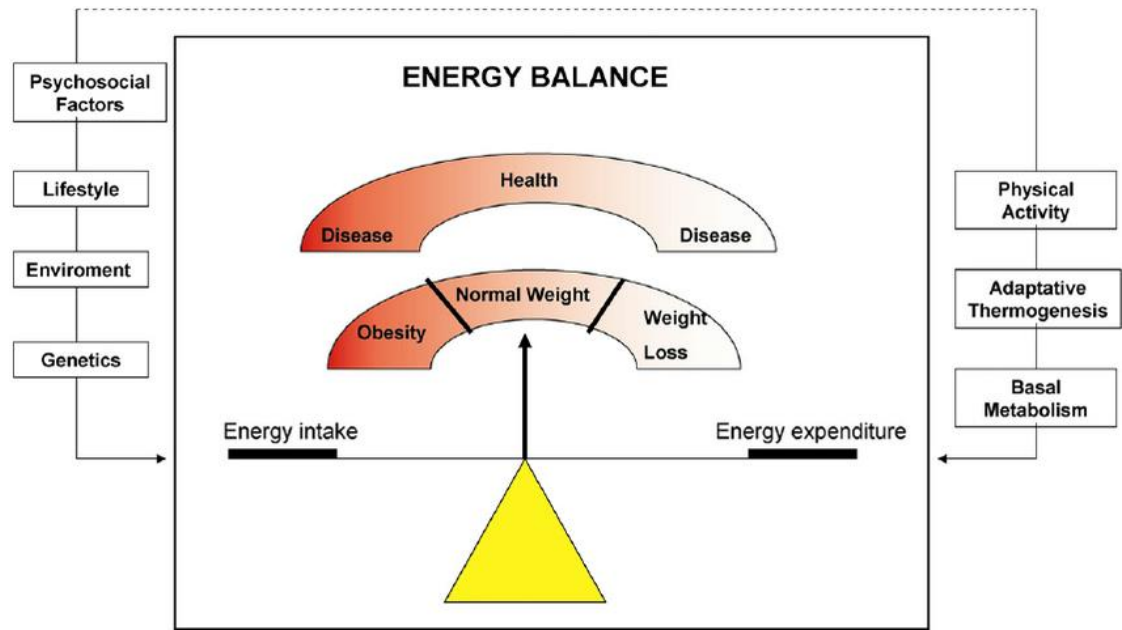


**Figure 3.** Fundamental principles of energy balance.

### 1.1.3. Adipose Tissue and Obesity

Adipose tissue is a complicated, crucial, and highly active metabolic and endocrine organ. Adipocytes are the cells that primarily constitute adipose tissue. Besides adipocytes, adipose tissue also includes the stromal vascular fraction (SVF) of cells including fibroblasts, vascular endothelial cells and a variety of immune cells such as macrophages. Adipose tissue is the primary storage location for excess energy but it can be also defined as an endocrine organ. Adipose tissue is not only replies to afferent signals from endocrine system and the central nervous system but also releases many components having crucial endocrine functions. These components involve leptin, adiponectin, tumor necrosis factor alpha (TNF $\alpha$ ), interleukin 6 (IL-6), plasminogen activator inhibitor-1, proteins of the renin-angiotensin system, and resistin (Kershaw & Flier, 2004). They are responsible for the controlling of immune system, thermogenesis, and also neuroendocrine function (Ahima, 2006).

#### **1.1.3.1. Adipocytes**

Adipocytes work as buffers along satiety as they can absorb free fatty acids (FFAs) and triglycerides as energy rich molecules. FFAs are main membrane constituents in the cells therefore they are enable to affect the fluidity of membrane and functions of channels and receptor. The excess deposition of FFAs and the accumulation as triglycerides are basics in obesity. Since hormone like effects of FFA are associated with the control of gene expression in pre-adipocytes, they have a direct impact on adipocyte proliferation and differentiation (Duplus et al., 2000; Garaulet et al., 2006). Since insulin is a strong inhibitor of hormone sensitive lipase (HSL), it has a crucial status in the regulation of adipocyte fat content. HSL is responsible for the hydrolysis of triglycerides to FFAs and a fundamental activator of lipoprotein lipase (LPL) for increasing FFA uptake by ensuring hydrolysis of triglycerides (Hajer et al., 2008). The smaller adipocytes are more sensitive to insulin and they become dysfunctional when they enlarge extremely (hypertrophy). Large adipocytes turn into insulin resistant preventing a react to the anti-lipolytic effect of insulin. These complications result in obesity and insulin resistance (Freedland, 2004; Garaulet et al., 2006; Ibrahim, 2010; Rajala & Scherer, 2003).

Adipocytes are complex cells composing a number of signals including cytokines, hormones and growth factors. These components can affect the neighboring cells and target tissues associated with energy metabolism, physiologic and pathologic processes (Coelho et al., 2013).

#### **1.1.3.2. White and Brown Adipose Tissue (WAT and SCAT)**

Adipose cell, also called adipocyte or fat cell, is basically a connective tissue cell specialized to synthesize and store large amounts of fat. There are two types of adipocytes: white adipocytes contain large lipid droplets, a small amount of cytoplasm, and decentralized nucleus; while brown adipocytes contain lipid droplets of varied size, a large amount of cytoplasm, a lot of mitochondria, and round, centralized nucleus (Figure 4)

(Cinti, 2006). White adipocytes are globular cells whose changeable size principally depends on the size of the single lipid droplet accumulated in them. These lipid droplets are composed of triglycerides and they take up more than 90% of the cell volume. White adipocytes account for storing of energetic molecules to provide energy to the cells between the durations of food intakes. Brown adipocytes also include triglycerides as multiple small vacuoles; they have generally polygonal shape with a variable diameter. Mitochondria are the most characteristic organelles of brown adipocytes. The color of brown adipocytes proceeds from its high mitochondrial density and high vascularization (Cinti, 2009; Saelens et al., 2012). Since brown adipocytes are responsible for thermogenesis, they have an entirely different role than white adipocytes. As a critical role, brown adipocytes pass the energy obtained from nourishment to thermal energy (Cannon & Nedergaard, 2004; Klaus et al., 1991). These two types of adipocytes constitute two different types of adipose tissue namely white adipose tissue (WAT) and brown adipose tissue (BAT). Amounts of these tissues in the body show variation with respect to age, gender, strain and environmental elements. The adipose tissues are classified based on their colors because there are alterations in histological composition between WAT and BAT (Cinti, 2006).

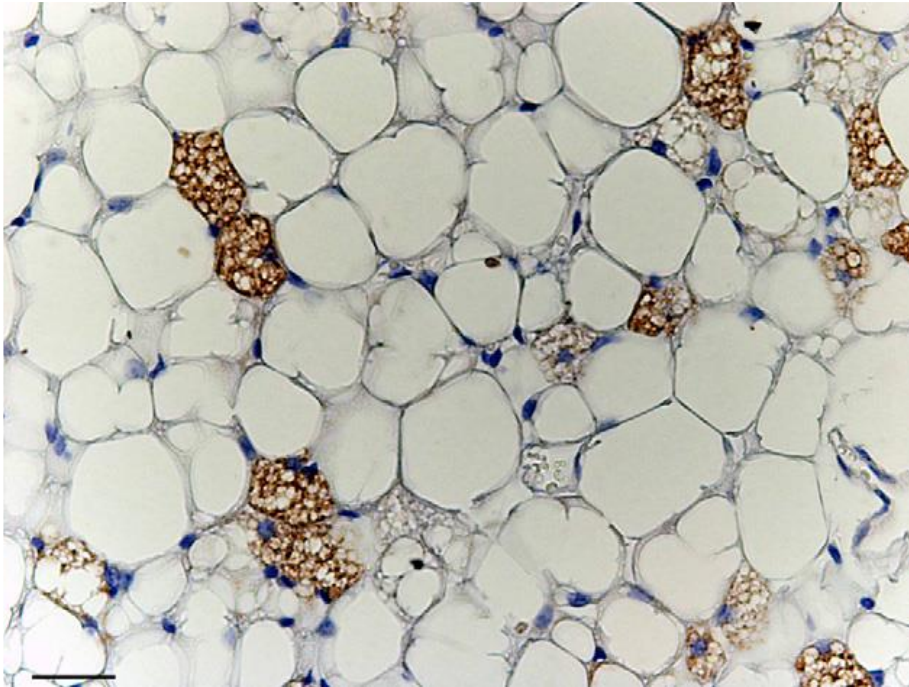


**Figure 4.** Adipocytes of adipose tissue, Brown and White adipocyte phenotypes.

The conventional function of WAT is that it supplies a long term energy fuel stock which can be mobilized during lack of food by releasing of fatty acids for oxidation in related organs (Trayhurn et al., 2011). Moreover, WAT secretes a range of fundamental components affecting the metabolism of the whole system like leptin which can affect especially the eating behavior (Zhang et al., 1994). Leptin is a hormone of long-term regulation of energy balance, suppressing food intake and then inducing weight loss.

BAT and WAT differ from each other in many respects (Figure 5). BAT have a completely different role than WAT since it is responsible for thermogenesis. Since BAT requires more oxygen, it has more capillaries than WAT. Nerve supply is also more intense in BAT than in WAT. On the other hand, BAT can pass the energy gained from nourishment to energy (Cannon & Nedergaard, 2004; Klaus et al., 1991). Uncoupling protein 1 (UCP1) that is specifically expressed in BAT is responsible for this conversion of the energy that is not utilized in oxidative metabolism (Cannon et al., 1982). Noradrenaline is capable to activate the beta-3-adrenoceptors which promotes brown adipocytes to form heat. The



brown adipocytes can lose most of their brown characteristics, when they are not stimulated adrenergically, this process cause transdifferentiation of brown adipocytes into white adipocytes (Cinti, 2006, 2008). This morphological transformation is reversible and it occurs with UCP-1 gene inhibition and leptin gene activation (Cancello et al., 1998). BAT phenotype in adipose tissues is so crucial in rodents for the inhibition of various metabolic diseases such as obesity and diabetes (Cinti, 2006).

|                         | White fat   | Brown fat  |
|-------------------------|---|--|
| Function                | Energy storage  | Heat production  |
| Morphology              | Single lipid droplet<br>Variable amount of mitochondria                       | Multiple small vacuolae<br>Abundant mitochondria   |
| Characteristic proteins | Leptin  | UCP1   |
| Development             | From Myf5-negative progenitor cells   | From Myf5-positive progenitor cells (but there are also Myf5-negative brown fat cells which are derived from other lineages) |
| Human data              | Large amounts are associated with increased risk of obesity-related disorders | Large amounts are associated with decreased risk of obesity-related disorders  |
| Impact of aging         | Increases with age relative to total body weight                              | Decreases with age   |

**Figure 5.** Characteristics of white and brown fat.

### 1.1.3.3. Visceral and Subcutaneous Adipose Tissue (VAT and SCAT)

Adipose tissue can be approved as a crucial, complicated and metabolically active endocrine organ having a distribution in a variety of locations in whole body differently from the other organs (Cinti, 2005; Kershaw & Flier, 2004). The murine adipose organ composed of two main subcutaneous storages (anterior and posterior) and several visceral storages (mediastinal, omental, mesenteric, perirenal, retroperitoneal, perigonadal, and perivesical) (Figure 6) (Saely et al., 2012). Other lipid storages are present in close connection with skeletal muscles and in organs such as parathyroid gland, bone marrow, parotid gland, pancreas, and lymph nodes (Cinti, 2009).

The locational fat distribution is more critical than whole fat content in the body in the matter of obesity-linked metabolic diseases (Oka et al., 2010). It has been reported that the more than 80% of total body fat constituted from SCAT in the body and approximately 10–20% from VAT in adults (Abate et al., 1995). SCAT consist of two different anatomical layers where superficial and deep layers are separated by the fascia superficialis (Scarpa's fascia). Subcutaneous fat depots represent 80 % of the whole fat mass in normal weight subjects. VAT is an intraperitoneal adipose tissue and it primarily consist of the omental and mesenteric fat depots (Lafontan & Berlan, 2003).

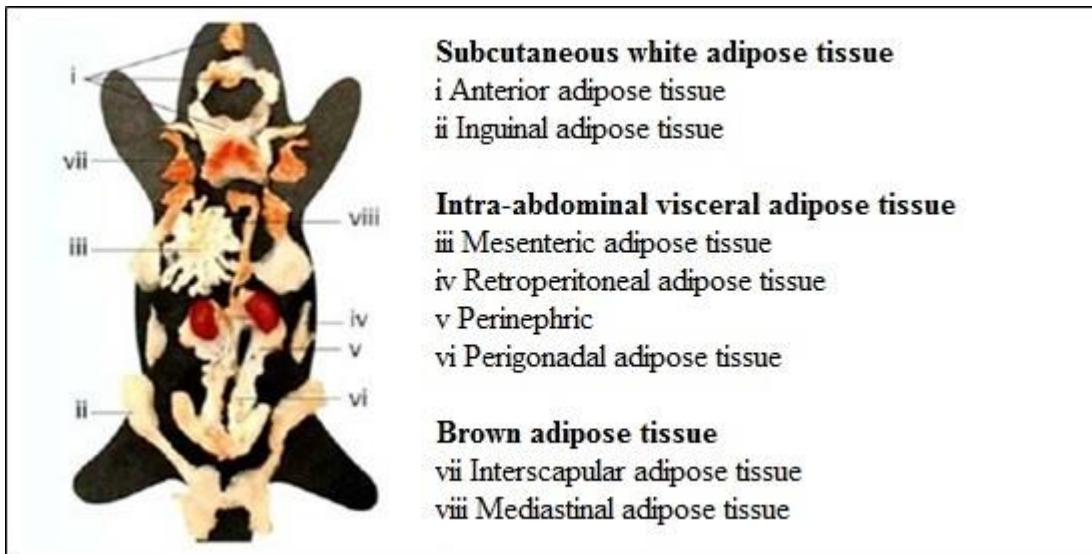


**Figure 6.** Localization of VAT and SAT in the body (Cinti, 2005).

SCAT and VAT differ from each other in respect to the type of adipocytes, lipolysis process, endocrine functions and their reaction to insulin and other hormones (Ibrahim, 2010). VAT has a crucial role in the expression of inflammatory cytokines and secretion of various of hormones causing the metabolic effects of obesity since it possesses a special position near portal vein (Björntorp, 1990; Freedland, 2004; Ibrahim, 2010; Oka et al., 2010; Rytka et al., 2011). VAT is also different from the SCAT due to the fact that visceral adipocytes have more lipolytic activity metabolically and they more active than

subcutaneous adipocytes (Arner, 1995; Lemieux & Després, 1994). VAT involves greater number of large adipocytes contrary to SCAT, which contains the small adipocytes. These small adipocytes are more insulin-sensitive and more prone to free fatty acid (FFA) and triglyceride (TG) uptake in order to avoid their storage in non-adipose tissue (Mårin et al., 1992; Misra & Vikram, 2003). On the other hand, VAT may have a role in lipolysis of central SCAT causing the release of peripheral FFA (Freedland, 2004). VAT is more sensitive to the catecholamine induced lipolysis and less sensitive to the antilipolysis action of insulin therefore VAT possesses a higher glucose uptake upon insulin stimulation, thus it becomes more insulin resistant than SCAT (Abate et al., 1995; Arner, 1999; Frayn, 2000).

VAT has more vascular structure which is rich in blood supply and more nerve cells than SCAT and they also differ in capacity to produce and secrete adipokines (Ibrahim, 2010). Leptin as one of the main adipokine is expressed in adipose tissue and its levels increase in keeping with the accumulation of triglycerides in adipose tissue (Tritos & Mantzoros, 1997). Since SCAT is capable to store more TG, this makes the SCAT the major source of leptin hormone (Wajchenberg, 2000). Adiponectin as another crucial adipokine is predominantly expressed in VAT compared to SCAT (Freedland, 2004; Motoshima et al., 2002). Additionally, plasma levels of adiponectin are correlated with body weight negatively (Cnop et al., 2003). There are more several inflammatory cytokines such as TNF- $\alpha$ , IL-6 and CRP are obtained in VAT compared to SCAT (Lemieux et al., 2001; Pepys & Hirschfield, 2003; Weisberg et al., 2003). Obesity could be identified as the expansion of VAT and SCAT mass in the body causing alterations in cellular biology, i.e. disturbed glucose and lipid metabolism. Though, abdominal obesity is determined by the storage of both VAT and SCAT in the body, VAT is thought to have more critical role in the metabolism of obesity (Freedland, 2004).

#### **1.1.3.4. Adipose Tissue in Obesity**

Obesity is resulted from a chronic imbalance between the level of energy intake and consumption causing extreme weight gain. Obesity constitutively results in storage of triglycerides in different adipose tissues (Shulman, 2000). The increase in fat mass results in the greater adipocyte size (hypertrophy) and increased numbers of adipocytes (hyperplasia). The hypertrophy, hyperplasia, or both of them occur in return for energy imbalance may alter the location of the adipose tissue (de Ferranti & Mozaffarian, 2008). The VAT deposition occurs only if SCAT capacity has been reached the maximum in early stage of obesity (Drolet et al., 2008). These changes related with adipocyte hypertrophy could be the first steps toward adipocyte dysfunction (Figure 7).

Extreme lipid storage causes functional disorders in endoplasmic reticulum (ER) that is central to the pathophysiologic effects of obesity. The ER arranges lipid storage, modulation of fatty acid uptake, storage of fatty acids as triglycerides, and packaging of triglycerides into lipid droplets to serve as energy stores. Due to energy imbalance and adiposity, excessive charge on the ER end up with “ER stress” causing dysfunctions in lipid metabolism (de Ferranti & Mozaffarian, 2008). On the other hand, when ER reaches a particular point, it begins to deliver of unfolded and/or misfolded proteins. For eliminating this damage, ER composes an unfolded protein response (UPR). The UPR is a cellular respond process by modifying regulatory pathways to increase clearance of the abnormally folded proteins. As a result, if ER stress cannot be stabilized, UPR can result in apoptosis (Gregor & Hotamisligil, 2007; Mittra et al., 2008).

With obesity, some inflammatory components named as adipokines are altered in adipose tissue. Adipokines, including adiponectin, leptin, and resistin, are mainly produced by adipocytes that affect energy and lipid metabolism and have a crucial role in the pathophysiology of obesity and its systemic health effects (Arita et al., 2012; Tilg & Moschen, 2006). The construction of many adipokines is upregulated in obesity and these proinflammatory proteins are associated with obesity-related metabolic diseases. As an

adipokine, leptin controls the feeding behavior and is positively correlated with adipose tissue mass, therefore obese people have elevated amounts of leptin (Friedman & Halaas, 1998). Leptin stimulates synthesis of IL-6 and TNF $\alpha$  by macrophages and also activates macrophages (Tilg & Moschen, 2006). TNF has a vital role in inflammatory and autoimmune diseases as a proinflammatory cytokine that is primarily produced by monocytes and macrophages. In experimental animal models of obesity and type 2 diabetes, increased amount of TNF expression was obtained in the adipose tissues (Hotamisligil et al., 1993). It has been reported that the increased levels of TNF were obtained in the adipose tissue and plasma of obese people, and when these people lose weight, a decrease in TNF expression was obtained (Kern et al., 1995; Ziccardi et al., 2002). IL-6 is another proinflammatory cytokine that also increased in obese adipose tissue. The IL-6 expression in adipose tissue from obese people is 10 time more than lean people (Fried et al., 1998). It has been reported that adipose tissue produces almost one-third of total circulating IL-6 and the increased secretion of IL-6 in case of obesity promotes to metabolic dysfunction (Ouchi, et al., 2011). Adiponectin is an anti-inflammatory factor that protects to body from obesity related metabolic dysfunction. Adiponectin levels in the plasma and adipose tissue decrease in obese subjects in comparison to lean subjects (Hosogai et al., 2007; Ryo et al., 2004)). The production of adiponectin by adipocytes is inhibited by pro-inflammatory components such as TNF and IL-6 in case of obesity and obesity related diseases.

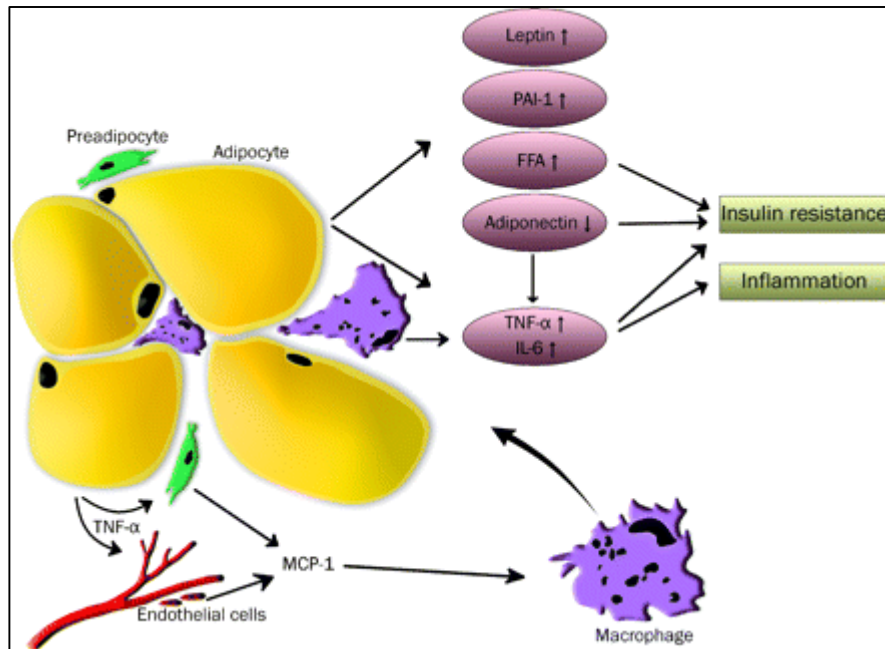


**Figure 7.** Dysfunctional adipose tissue in obesity (van Kruijsdijk et al., 2009)

#### 1.1.4. Obesity and Insulin Resistance

Obesity is related to enhanced release of fatty acids and triglycerides into the circulation (Campbell et al., 1994). Since the storage capacity of SCAT is limited because of the increase in hypertrophy, VAT stores also accumulate excess lipids (Bonora et al., 1992). This extreme accumulation and catabolism of triglycerides in VAT result in the excess release of FFAs into the hepatic portal vein (Björntorp, 1990). Elevated levels of these circulating FFAs and triglycerides from adipose tissue into the circulation augment the delivery of FFAs to the liver, skeletal muscle, which can cause insulin resistance (Boden & Shulman, 2002).

Adipose tissue is an important insulin-responsive tissue, and in adipose tissue, insulin stimulates accumulation of triglycerides by inducing the differentiation of pre-adipocytes to adipocytes and increasing the uptake of glucose and fatty acids arise from circulation (Kahn & Flier, 2000). FFAs and various adipokines released from adipose tissue cause

abnormalities in insulin signaling. FFAs and their metabolites, such as acyl-coenzyme A, ceramides and diacylglycerol, can damage insulin signaling by inducing protein kinases such as protein kinase C, MAPK, c-Jun N-terminal kinase (JNK), and the inhibitor of nuclear factor  $\kappa$ B kinase  $\beta$  (Schenk et al., 2008). In addition, obesity induces a phenotypic switch in adipose tissue from anti-inflammatory (M2) to pro-inflammatory (M1) macrophages. The excess consumption of high energy foods causes macrophage infiltration to the adipose tissue and this process reduces activated M2 macrophages and increases in classically activated M1 macrophages that express inflammatory cytokines such as IL-6 and TNF $\alpha$  which affect insulin sensitivity directly. Macrophages lead to insulin resistance indirectly by increasing adipocyte size and changed expression of adipokines and release of excess FFAs, resulting in abnormal accumulation of triglyceride in non-adipose tissues (Heilbronn & Campbell, 2008).

Obesity induced inflammation of adipose tissue is the crucial process resulting in activation of proinflammatory pathways which contribute insulin signaling and insulin resistance (Figure 8) (Jung & Choi, 2014). The adipocytes in obesity are characterized by inflammation mediators producing a large number of inflammatory cytokines and chemokines, such as TNF-alpha, IL-6, monocyte chemoattractant protein-1 (MCP-1), and adiponectin as an anti-inflammatory adipokine (Hsieh, 2011). When these inflammatory pathways are activated in adipocytes, they damage triglyceride storage and enhance release of FFAs, inducing insulin resistance in muscle and liver (Guilherme et al., 2008). One major key point in the energy balance regulation and adipose tissue metabolism is leptin (Zhang et al., 1994). SCAT is responsible of 80% of leptin production. In adipose tissue, mRNA expression of leptin is precisely related to severity of obesity. Since an increase of leptin is associated with an increase of fat mass, leptin is accepted as an indicator of total fat mass (Vidal et al., 1996). Although the main effect of leptin is the control of energy expenditure and food intake, it impairs insulin signaling in murine adipocytes (Müller et al., 1997; Pérez et al., 2004). In fact, the leptin-signaling pathway activates suppressor of cytokine signaling (SOCS)-3, which might inhibit insulin signaling (Howard & Flier, 2006). As a proinflammatory cytokine, TNF- $\alpha$  makes contribution to

the pathogenesis of obesity and insulin resistance. In case of obesity and insulin resistance, TNF- $\alpha$  expression is increased in humans indicating a positive correlation with insulin resistance (Hotamisligil et al., 1993). The various proinflammatory cytokines secreted by adipose tissue, including TNF- $\alpha$ , IL-1, and IL-6, all of which have been involved in disrupting insulin signaling (McArdle et al., 2013). As another cytokine, IL-6 plays a crucial role in the progress of insulin resistance in obesity (Fernández-Real & Ricart, 2003). Hypertrophic enlargement of adipocytes is originated from increased production of IL-6 by adipose tissue and so expression of adipose IL-6 shows a positive correlation with insulin resistance both in vivo and in vitro (Qatanani & Lazar, 2007; Sopasakis et al., 2004). On the contrary, adiponectin is an adipose-specific adipokine that produces insulin sensitizing effects. The adiponectin levels decreases in obesity, and adiponectin-treatment increases insulin sensitivity in animal models (Berg et al., 2001; Díez & Iglesias, 2003). Adiponectin-deficient mice showed a stimulated insulin resistance, on the contrary over-expression of adiponectin in mice enhances glucose tolerance and insulin sensitivity (Maeda et al., 2002). Adiponectin reduces the inflammatory response stimulated by TNF- $\alpha$  and adiponectin treatment decreases TNF- $\alpha$  production in macrophages of adipose tissue (Ouchi et al., 2000).



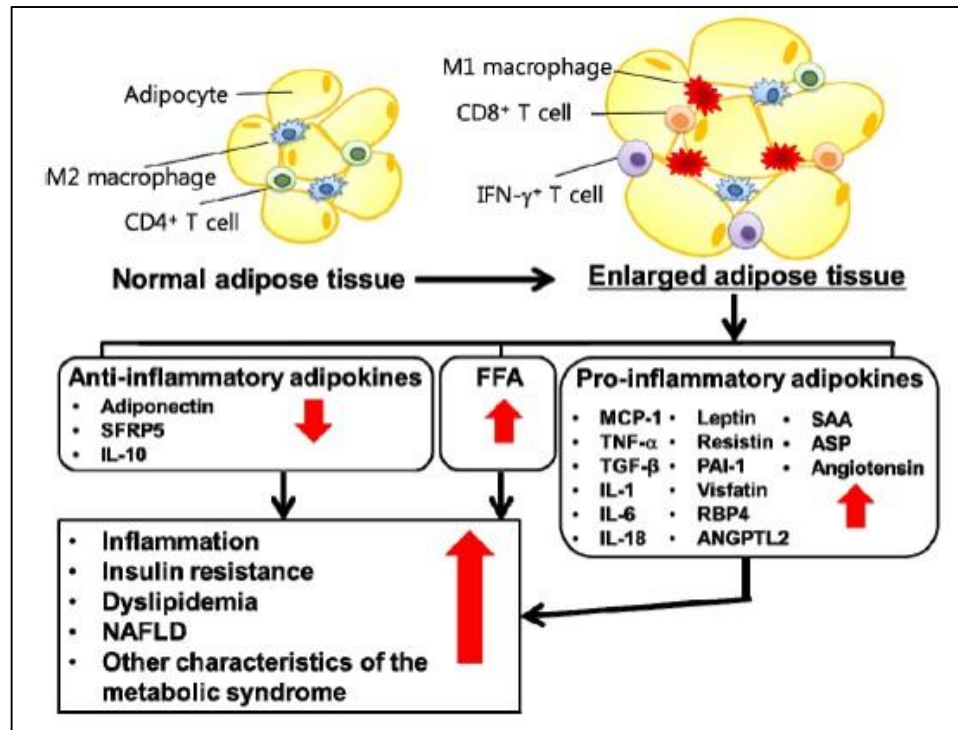


**Figure 8.** Secretion of inflammatory adipokines from adipose tissue in obese state.

### 1.1.5. The Berlin Fat Mouse Inbred (BFMI) Lines as Mouse Models for Obesity

BFMI lines are new animal models having obesity because of hyperphagia and disturbed lipid metabolism (Meyer et al., 2009; Neuschl et al., 2010; Wagener et al., 2006). Without knock-out mutations as a causative effect, the BFMI lines are genetically complex mice and they have spontaneous obesity phenotype. In terms of their polygenic nature underlying obesity phenotypes, the BFMI lines can be used as a prominent model for the investigation of obesity-induced alterations in humans (Wagener et al., 2006). These lines indicate an increment in total body fat coupled with an enlargement of the adipocytes in different adipose tissues resulting in the hypertrophy and lipid accumulation in adipocytes, even though they are fed with a SBD.

## 1.2. Electromagnetic Radiation and Basics of Spectroscopy

“Electromagnetic radiation is considered as two mutually perpendicular electric and magnetic fields, oscillating in single planes at right angles to each other. These fields are in phase and are propagated as a sine wave” (Figure 9) (Stuart, 2004).

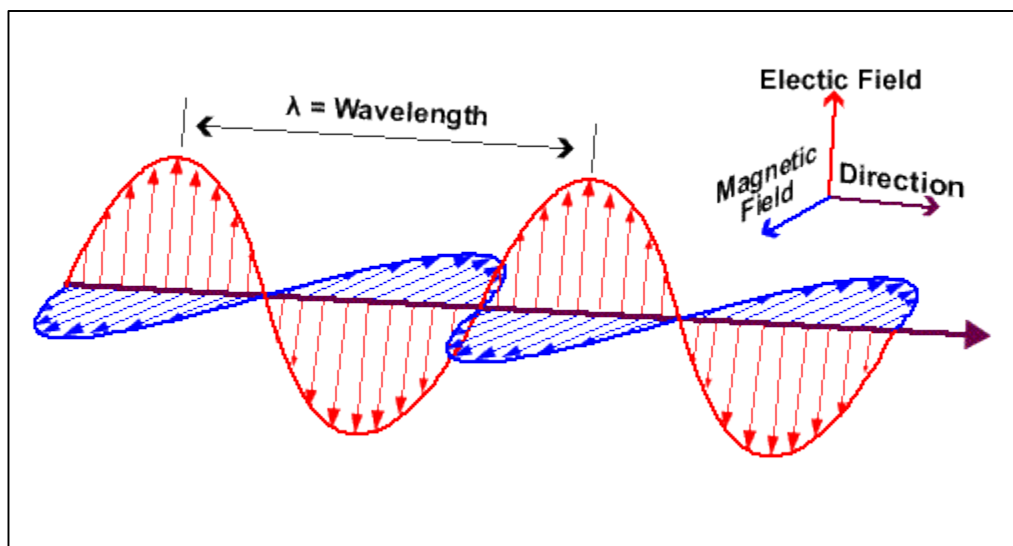


**Figure 9.** An electromagnetic wave

According to Bohr equation, the energy (E) of the electromagnetic wave is formulized as:

$$\Delta E = h \cdot \nu$$

where  $\Delta E$  is the dispersement between the energy states of interest,  $h$  the is Planck's constant with value as  $6.63 \times 10^{-34}$  Joule second and  $\nu$  is the frequency of the applied electromagnetic radiation.

$$c = \lambda \nu$$

where  $\lambda$  is the wavelength of light,  $c$  is the speed of light in vacuum with the value as  $3.0 \times 10^8 \text{ ms}^{-1}$ . These two equations forenamed above are used for the identification of the wavenumber as a spectral unit which is denoted by  $\bar{\nu}$  with a unit  $\text{cm}^{-1}$ .

$$\bar{\nu} = \text{wavenumber} = (1/\lambda) \longrightarrow E = h \cdot \nu = h c / \lambda = h c \bar{\nu}$$

The equations given above, both frequency and wavenumber are directly proportional to energy.

As a consequence of the interaction of electromagnetic radiation with matter, various types of redirections of the radiation can be obtained as emission (the energy releases by the molecule), scattering (the direction of propagation changes) or absorption (the energy transfers to the molecule). If a molecule absorbs the energy of light, it will be excited to a higher energy level. This excited molecule gets a quantum of energy which corresponds to the difference between the energy levels of the molecule. These electronic energy levels obtain from the spatial distributions of the electrons are shown by an energy-level diagram in Figure 10. The lowest electronic level is named by ground state and the others are named by excited states. (Campbell & Dwek, 1984). The vibrational energy levels are shown by thin horizontal lines. While the long arrow illustrates an electronic transition, the short arrow represents a vibrational transition.

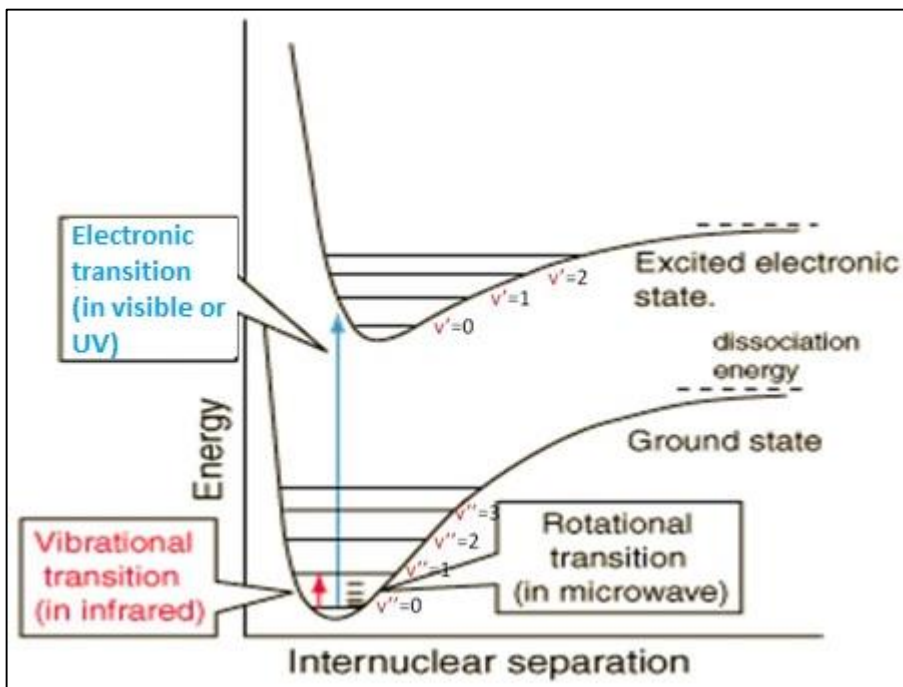


**Figure 10.** Typical energy-level diagram

\* Adopted from [http://www.tau.ac.il/~phchlab/experiments\\_new/LIF/theory.html](http://www.tau.ac.il/~phchlab/experiments_new/LIF/theory.html)

The electronic transition, vibrational, rotational and transitional levels are main molecular energy levels and the total energy ( $E_{total}$ ) can be calculated performing by:

$$E_{total} = E_{transition} + E_{rotation} + E_{vibration} + E_{electronic} + E_{electron\ spin\ orientation} + E_{nuclear\ spin\ orientation}$$

“Each E in the equation represents the appropriate energy as indicated by its subscript. The separations between the neighboring energy levels corresponding to  $E_{rotation}$ ,  $E_{vibration}$  and  $E_{electronic}$  are associated with the microwave, infrared and ultraviolet-visible region of the electromagnetic spectrum, respectively” (Campbell & Dwek, 1984).

Spectroscopy is the study of the interaction of electromagnetic radiation in all its forms with matter which gives a data called spectrum. "A spectrum is a plot of the intensity of energy detected versus the wavelength or frequency of the energy" (Freifelder, 1982). Electromagnetic radiation is the main source of energy used for spectroscopic studies. These spectroscopic studies include irradiation of a sample with several form of electromagnetic radiation. Monitoring of the absorption, emission or scattering of the electromagnetic radiation in the spectrum provides to have information of the atomic and molecular design of samples (Struve & Mills, 1990). In Figure 11, the regions of the electromagnetic spectrum are represented.

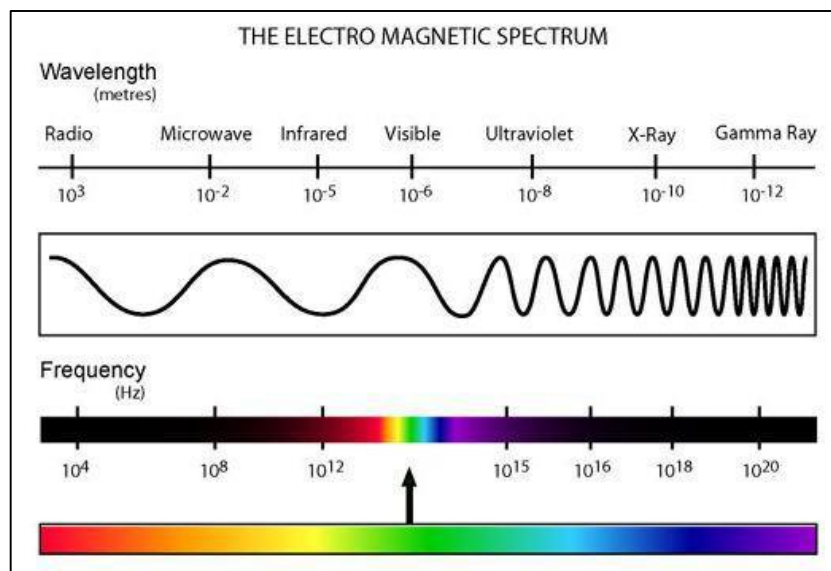


**Figure 11.** The electromagnetic spectrum

### 1.2.1. Basis of Infrared Spectroscopy

The vibration modes in a molecule at the atomic level can be discovered by infrared energy through changing the dipole moment. In the IR energy range, infrared vibrational spectroscopy analyzes photon absorption and transmission which are based on frequencies and intensities. Each chemical bond in a molecule vibrates at a special frequency that is only belonged to itself. Atoms of a molecule (e.g. CH<sub>3</sub>) may have various modes of vibration because of the stretching and bending vibrations of the groups. If a change in the dipole moment of a molecule is occurred by vibration, it will absorb a photon with the same frequency of the incident IR light. Infrared (IR) region of the EM spectrum is divided into three sub regions; (1) the lowest energy far-infrared ( $400\text{--}10\text{cm}^{-1}$ ) is neighbor to microwave spectrum region and can be used for rotational spectroscopy. (2) The mid-infrared ( $4000\text{--}400\text{ cm}^{-1}$ ) can be used to study the fundamental vibrations and associated with rotational-vibrational structure. (3) The higher energy near-IR ( $14000\text{--}4000\text{ cm}^{-1}$ ) can be used to study the harmonic or overtone vibrations (Marcelli et al., 2012).

In IR Spectroscopy, after the energy of infrared region couples with most vibrational transitions, the applied radiation in the infrared region is absorbed by the matter and this interaction results in alterations in chemical bonds of the molecules in the matter leading to vibrations with different modes in the infrared region. That's why infrared spectroscopy enables to determine the transitions between vibrational energy levels of the atoms within a molecule. The vibrations are separated in two groups as stretching and bending and their modes (twisting, scissoring, wagging, rocking) of linear and non-linear vibrations are originating from the differences in the bond angle and length as regards the different movements of various functional groups such as amide, carbonyl etc. (Figure 12) (Campbell & Dwek, 1984; Marcelli et al., 2012). In the system, the potential alterations in the vibrational modes of the molecules can result in a variance in the function, conformation and structure of the functional groups of the molecules.

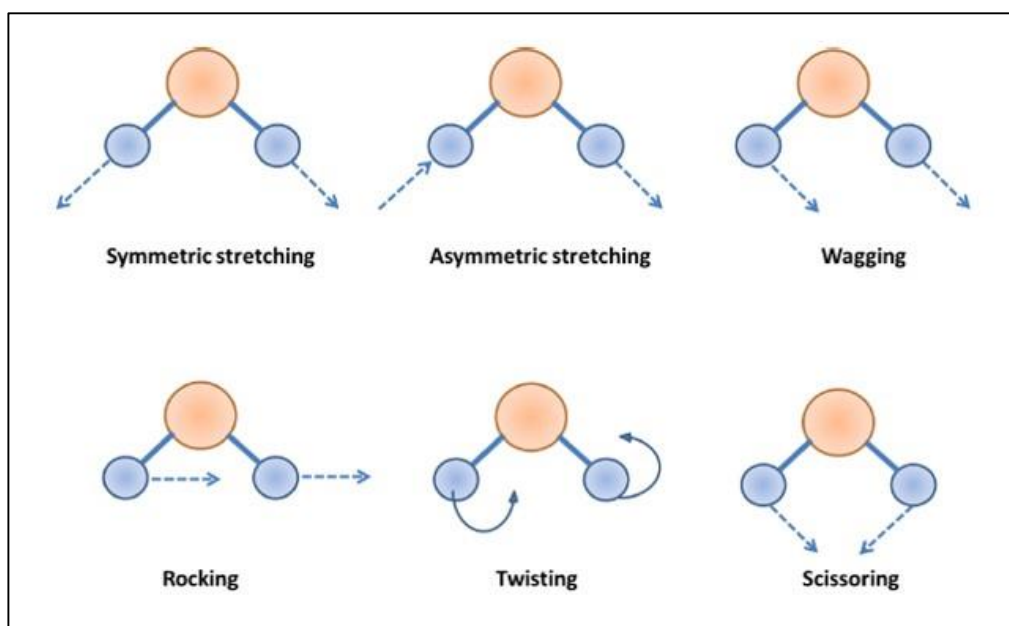


**Figure 12.** Simple layouts of the vibrational modes associated to a molecular dipole moment change detectable in an IR absorption spectrum.

When infrared light is in interaction with molecules, absorptions at specific wavelengths are occurred arising from the vibrations of functional groups. Consequently, a spectrum is obtained that is a plot of absorption as a function of wavenumber denoted in terms of  $\text{cm}^{-1}$ . The absorptions are sensitive to alterations in environment, conformation and chemical structure. Each molecule has a unique combination of atoms, for this reason they generate different infrared spectrum emphasizing the power of infrared spectroscopy in determination of changes in each special molecule (Figure 13) (Marcelli et al., 2012).

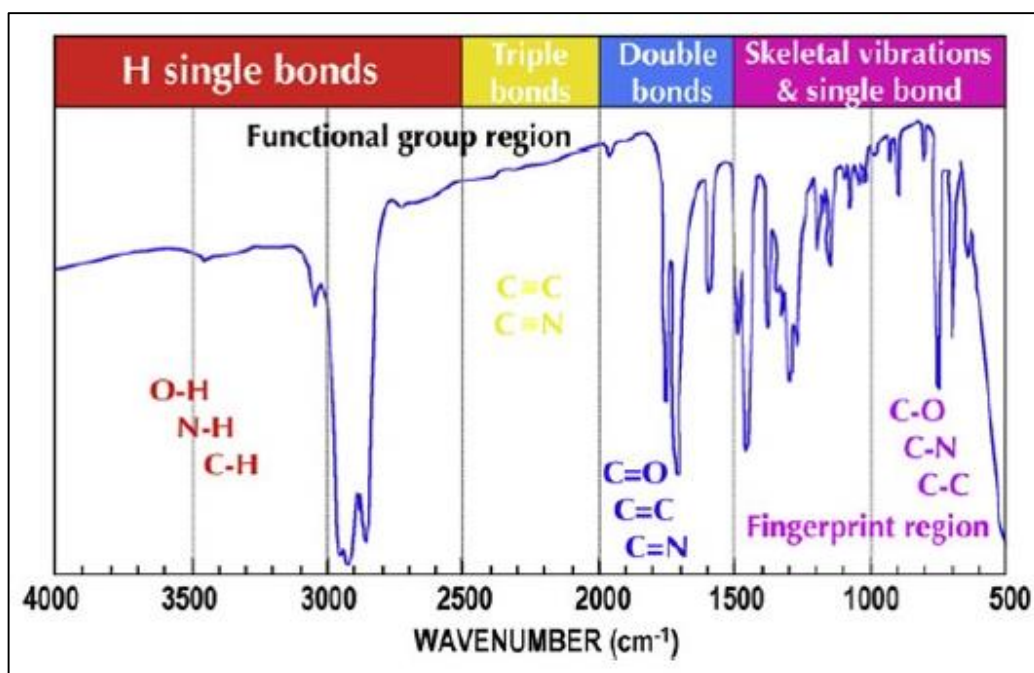


**Figure 13.** A typical mid-IR transmission spectrum showing in a schematic way typical absorptions lines associated to vibrational modes of molecules.

### 1.2.2. Fourier Transform Infrared Spectroscopy (FTIR)

Fourier Transform Infrared Spectroscopy (FTIR) spectrometer is based upon an important instrument called Michelson Interferometer. In a Michelson interferometer adapted for

FTIR, the working principle is based upon the interference of radiation between two beams to produce an *interferogram*, that is a signal formed as a result of the change of path length at a beam splitter (Stuart & Ando, 1997). These two beams with different path length recombine in the beam splitter producing an interference resulting in the interferogram.

This interference is determined by the detector, and then recorded values of distance and frequency are interconverted by Fourier transformation as a mathematical method, finally frequencies are reconstructed individually as an infrared spectrum (Figure 14).

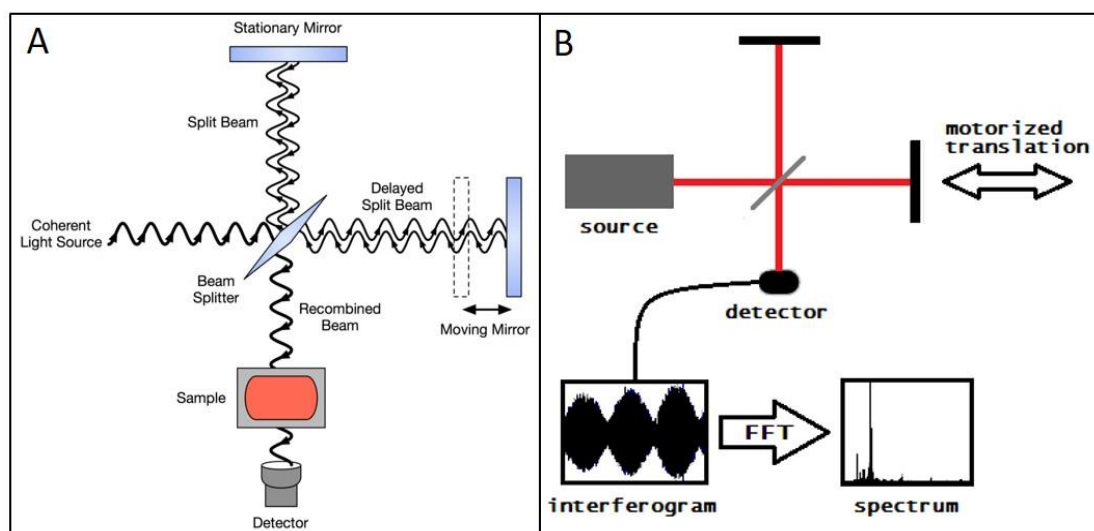


**Figure 14.** A) Schematic diagram of a Michelson interferometer configured for FTIR B) The general system flowchart of FTIR.

The advantages of FTIR spectroscopy can be listed as follows:

- FTIR spectroscopy method is a rapid and sensitive technique and it enhances signal to noise ratio by signal averaging the numbers of scans per sample. The data processing is very easy with the application of computer softwares and quantitative calculations could be obtained (Ci et al., 1999; Manoharan et al., 1993; Rigas et al., 1990; Stuart & Ando, 1997).



- Very small amounts of the samples are adequate for the analysis, furthermore in vivo investigations are also feasible and these samples could be prepared in a short time either in gaseous, liquid, or solid states (Mendelsohn, 1986).
- FTIR spectroscopy can be applied to any kind of material such as inhomogeneous solids, solutions, suspensions, viscous liquids and powders. Kinetic or time-resolved analysis of samples could be used by this technique (Haris & Severcan, 1999; Mantsch, 1984; Mendelsohn, 1986).
- All alterations in functional groups of the biomolecules can be determined in the system within the same spectrum simultaneously. Spectral data can be achieved easily and rapidly. Additionally, qualitative interpretation can be performed by the software allowing the storage of the obtained data and enables user to make some manipulations on the data coupled with quantitative calculations (Ci et al., 1999; Garip et al., 2007; Kneipp et al., 2000; Manoharan et al., 1996; Rigas et al., 1990; Yano et al., 1996).
- FTIR spectroscopy technique is a cheaper in comparison to other techniques particularly ESR, CD, NMR (Diem, 1993).
- FTIR spectroscopy, as a rapid and non-destructive technique, provide qualitative interpretation without any requirement for an external calibration and give information about structure, function and composition of the system (Aksoy et al., 2012; Çakmak et al., 2003; Haris & Severcan, 1999; Melin et al., 2000).

These advantages make FTIR spectroscopy measurements reliable and repeatable. This technique has higher sensitivity in detecting the changes of functional groups belonged to the various components of tissues including proteins, lipids, carbohydrates and nucleic acids (Dogan et al., 2007). Alterations in band frequencies, intensities and bandwidths can be visualized in the spectra and they can give significant structural and compositional information (Bozkurt et al., 2010; Cakmak et al., 2011; Ci et al., 1999; Garip et al., 2010; Toyran et al., 2007; Toyran et al., 2004). Infrared Spectroscopy is sufficient for the identification of pure materials because absorbance peaks which are obtained at specific

wavenumbers are useful for the characterization of these materials. For this reason, obtained IR spectra of the molecules can be used as a fingerprint minutia compared to other molecules. Mid-IR region is the principal region and mid-IR spectroscopy is a precious analytical method in terms of the investigation and characterization of the biological materials (Marcelli et al., 2012). Therefore, IR spectroscopy is a promising technique which provides biochemical information of the biological material (Mourant et al., 2003).

In recent years, FTIR spectroscopy has become a promising method in biology and medicine for diagnosis and characterization of specific molecular alterations between normal and disease states. In the literature, many studies on different kind of diseases including; obesity and diabetes (Bozkurt et al., 2010; Farhan et al., 2011; Josse et al., 2011; Katiyar et al., 2011; Kucuk Baloglu et al., 2015; Sen et al., 2015; Severcan et al., 2000; Severcan et al., 2010), different types of cancers (Bellisola & Sorio, 2012; Gok et al., 2016; Li et al., 2012), the characterization of microorganisms (Garip et al., 2007; Garip et al., 2009), chemical treatments including protective effect of drugs on radiation induction (Cakmak et al., 2012; Cakmak et al., 2011), have been investigated lately.

#### **1.2.2.1. Attenuated Total Reflectance Fourier Transform Infrared (ATR-FTIR) Spectroscopy**

ATR-FTIR spectroscopy bases upon total internal reflection phenomenon resulting in an evanescent wave. “When the infrared beam, which is directed onto an optically dense crystal with a high refractive index, passes through an ATR crystal at a certain angle, it is internally reflected that causes creation of evanescent wave protruding only a few micrometers beyond the surface of ATR crystal” (Aksoy et al., 2012). This evanescent wave reaches a few microns ( $0.5\mu - 5\mu$ ) for both surface of the crystal and into a sample. Since the sample absorbs energy in the convenient spectral region, the evanescent wave attenuates and then this attenuated energy travels to the detector in the infrared spectrometer to form an IR spectrum (Gasper et

al., 2010; Goormaghtigh et al., 1999). The basic requirements for this technique are; the refractive index of the crystal needs to be higher than the refractive index of the sample and the sample needs to be in contact with the crystal directly (Figure 15).

The ATR crystals are made from special matters which possess low solubility in water and high refractive index. Diamond, germanium and silicon are widely used for ATR crystal, however; the mostly used one is diamond zinc selenide (Di/ZnSe) (Kazarian & Chan, 2006). Since these crystals are relatively cost effective than the others and resistant to many chemicals such as acids and alkali, ZnSe is the most sufficient for the utilization in the mid-IR region. The distance which a wave spreads from the surface of the crystal is approximately 1.66  $\mu\text{m}$  for Di/ZnSe ATR crystal.

ATR-FTIR is a rapid, sensitive and low cost effective technique monitoring of different functional groups of molecules in the biological systems. Needing a small sample size and ease of sample preparation make this technique useful for biological studies. Since ATR-FTIR studies are not affected by the sample thickness, the samples could be directly examined without any necessity for preparation processes by placing them on the ATR-crystals apparatus. For example, a solid or an aqueous sample can be directly placed on ATR crystal and then IR spectrum can be obtained in a short span of time. The ordinary scaling criterion is the setting of the of amide I peak maximum absorbance to 1 (Gaigneaux et al., 2006).

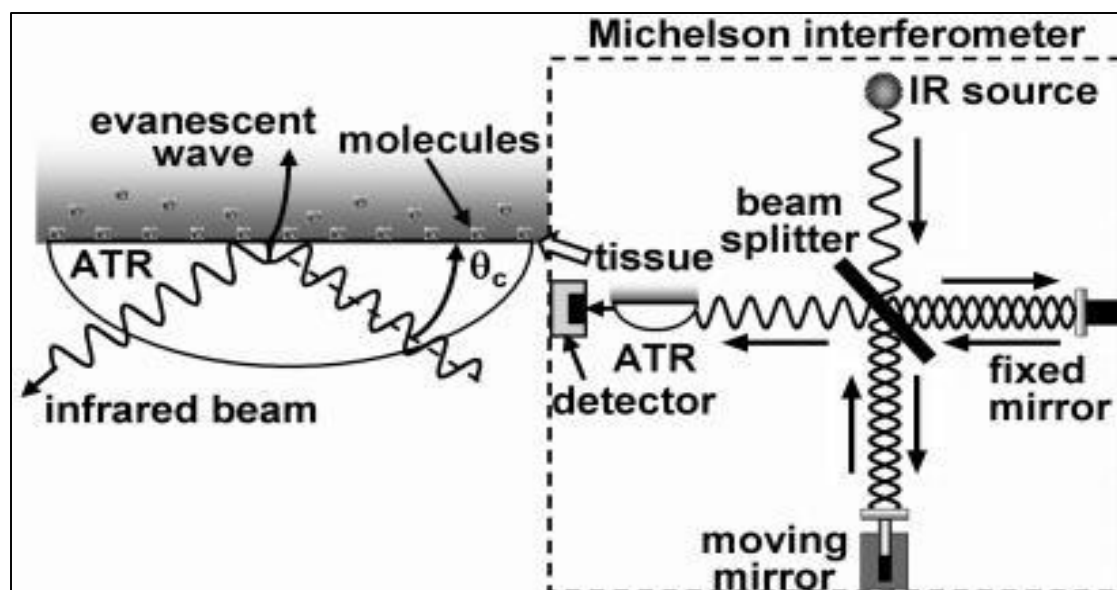


**Figure 15.** A multiple reflection ATR-FTIR system (Wang et al., 2007)

#### 1.2.2.2. Fourier Transform Infrared Microspectroscopy

FTIR microspectroscopy can be defined as a binary combination of an infrared spectroscopy with an optical microscope. This infrared spectrometer coupled with microscope (Figure 16) (Gazi et al., 2006) allow to study with biological samples and to obtain molecular information with a higher spacial resolution (Levin & Bhargava, 2005). This special technique enables to investigate the molecular biochemistry and morphology of biological samples. FTIR microspectroscopy is a non-invasive technique which is different from fluorescence imaging spectroscopy because FTIR imaging do not need staining for creating the image contrast (Hof et al., 2005).

In biological materials, a specific tissue area can be mapped point-by-point in every pixel leading to a chemical map of the sample by using FTIR microspectroscopy. A specific FTIR spectrum is achieved in each single pixel in this chemical map. Regarding to the optical features of the sample, FTIR microspectroscopy can be applied in transmission or reflection mode (Bechtel et al.,. Sample is placed on a microscope slide which is IR-transparent, such as barium fluoride (BaF<sub>2</sub>), calcium fluoride (CaF<sub>2</sub>), ZnSe glass slides in transmission mode.

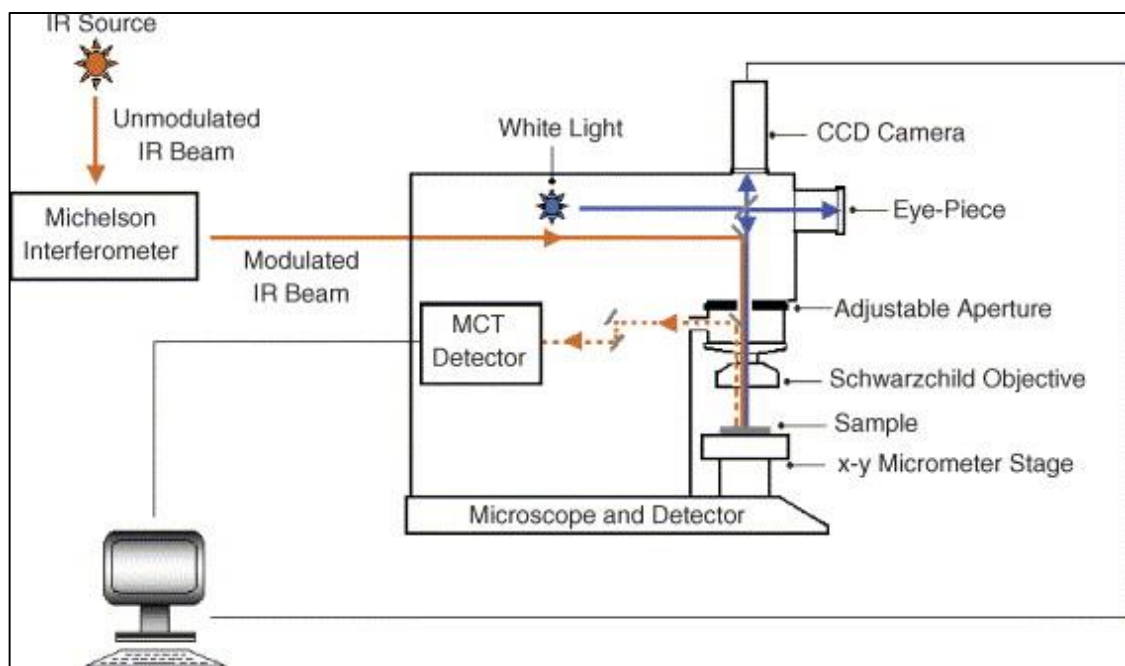


**Figure 16.** Schematic diagram representing the working principle of FTIR microspectroscopy.

The advantages of the FTIR microspectroscopy are given below;

- FTIR microspectroscopy enables the rapid analysis of very small amount samples and its main advantage is allowing the chemical analysis of trace amount of biological materials insitu, without extraction, from microscopic regions of a tissue section (Jackson et al., 1998; Kretlow et al., 2008; LeVine & Wetzel, 1998).
- In contrast with traditional histochemical methods needing a long-standing sample preparation procedure, such as fixation, embedding, sectioning and staining of the tissue, FTIR microspectroscopy do not require any preprocessing or labeling process (Kretlow et al., 2008). On the other hand, the recorded information by FTIR microscopy is represented by false-colour images, that is similar to the images of histological-stained samples (Marcelli et al., 2012).
- FTIR microspectroscopy enables to function as the spatial determination of the distribution biomolecules in tissue entirely with a high resolution. This type

functional group mapping can supply an important favor for finding out spectral data as a distributing of some chromophores in tissue samples can be analyzed (Jackson et al., 1998).

### **1.3. Chemometrics in FTIR Spectroscopy**

Chemometrics can be defined as the applications of statistical and mathematical calculations to obtain the information from the vibrational spectra (Lavine, 2000). Since vibrational spectra have many molecular-based specific spectral peaks, they can provide many information. For this reason, to get these valuable data, the multivariate data analysis can be performed to IR spectra. The multivariate analysis methods can be divided into two groups; unsupervised and supervised chemometric approaches (Brereton, 2003).

The unsupervised chemometric methods do not need for primer information about investigated samples like healthy versus disease meanwhile the supervised chemometric methods required this information. For this reason, the clustering pattern of the samples are achieved randomly (Massart et al., 2003). Among the unsupervised methods, principal component analysis (PCA) and hierarchical cluster analysis (HCA) were performed in this study.

#### **1.3.1. Hierarchical Cluster analysis (HCA)**

HCA is a method for ordering samples in a dendrogram (“tree diagram”), where samples with the highest correlations are grouped together while samples with small correlations are widely separated (Xue et al., 2011). The HCA can be performed to show the grouping of similar data collected from different samples (Wang & Mizaikoff, 2008). A quantitative measure of similarity or dissimilarity can be used by correlation techniques in this classification (Shaps, 1980). The heterogeneity calculations were made by using Euclidian distance and Ward’s algorithm from the average spectra. Euclidean distance was used to

calculate the sample similarities and indicate the complete linkage clustering by Ward's algorithm. This algorithm clusters homogeneous objects as much as possible by combining the spectra that form the smallest variance distance (Bozkurt et al., 2010; Ward, 1963). In cluster analysis, Ward's algorithm together with Euclidian distances to construct the dendograms was previously reported to give one of the best predictions (Lasch et al., 2004).

### **1.3.2. Principal Component Analysis (PCA)**

PCA is based upon the clustering of similar samples within the scores plot gives information about the class separation. An increase in the spatial separation between the two points in a scores plot implies an increase in the dissimilarity between two samples. PCA techniques use a vector space transform to reduce the dimensionality of large data sets so it could be preferred principally for the determination of general relationships between the data sets (Gasper et al., 2010).

PCA can reduce a large scale of spectra consisting of hundreds of absorbance values to a point in a multidimensional space using a linear transformation. The coordinates are the principle components (PC) and the plot obtained is named as the scores plot. Also, each PC identifies the spectral variability among sample and it is actually a linear combination of the whole original variables; namely, of all the wavenumbers (Nakamura et al., 2010). The coefficients of combination are named as loadings, and each wavenumber counterpoises to a loading. These loading plots are the plots of the relationship between original variables and subspace dimensions that are used for interpreting relationships Among variables. The bigger change in the loading plot is, the bigger the effect of the corresponding wavenumber in the interpretation of the data variance (Chen et al., 2015).

#### **1.4. Aim of the Study**

The current study is composed of three main parts which focuses on obesity with different approaches. The first part of this study aimed to characterize and compare visceral (VAT) and subcutaneous (SCAT) adipose tissues in terms of macromolecular content and investigate transdifferentiation between white and brown adipocytes. In accordance with this purpose, Fourier transform infrared (FTIR) microspectroscopy and uncoupling protein 1 (UCP1) immunohistological staining was used to investigate VAT and SCAT of male Berlin fat mice inbred (BFMI) lines, which are spontaneously obese.

The second part of this study, we focused on the triglyceride profile of VAT and also SCAT as a marker of abdominal obesity to distinguish control and obese lines from each other in SCAT and VAT samples and to differentiate our 4 obese lines from each other whether they have insulin resistance or not. To propose triglyceride bands located at 1770-1720  $\text{cm}^{-1}$  spectral region as a more sensitive obesity related biomarker, the diagnostic potential of FTIR spectroscopy was used in SCAT and VAT samples obtained from male control (n=6) and four different obese BFMI mice lines (n=6 per group). FTIR spectroscopy coupled with hierarchical cluster analysis (HCA) and principal component analysis (PCA) was applied to the spectra of triglyceride bands as a diagnostic tool in the discrimination of the samples.

Third part of the study targets to determine gender-based differences in the effect of obesity on VAT and SCAT in obese mice lines. Firstly, the macromolecular characteristics of VAT and SCAT were compared in male and female BFMI mice by FTIR microspectroscopy. In addition, to compare the transdifferentiation of brown and white adipocytes in different genders, UCP1 immunohistological staining was used for both male and female samples. In accordance with this comparative approach, ATR-FTIR spectroscopy coupled with multivariate data analysis was applied to the spectra of some special regions in the discrimination of the male and female samples.



## **CHAPTER II**

### **2. MATERIALS AND METHODS**

#### **2.1. Animal Studies, Feeding and Husbandry Conditions**

The German Animal Welfare Authorities approved whole experimental protocols related to the treatment of animals (approval no. G0171/10). Primary animals of the Berlin Fat Mice lines (BFMI) were purchased from various pet shops in Berlin, Germany. These mice were selected during 58 generations by choosing in terms of their low protein and high fat content with a low body weight. The mice exhibiting a phenotype of high fat content were endorsed as the Berlin Fat Mouse (BFM) line along the selection process. “After 58 generations of selection for high fatness in the BFM line, distinct inbred derivatives (BFMI lines) have been generated by brother-sister mating from randomly chosen founder sib-pairs of the selection line” (Wagener et al., 2006). In this study, 10 week old females and males of BFMI852, BFMI856, BFMI860 and BFMI861 inbred lines, which were selected according to their phenotypic characteristics after six generations of inbreeding, were used. The DBA/J2 mice line was used as the control, which is a commercially acquirable inbred line and usually used as a standard mice exhibiting a wild type-like phenotype. The DBA/2J line indicated the highest weight gain in return for feeding with a high fat diet among 43 inbred strains (Hageman et al., 2010; Svenson et al., 2007). Since the DBA/2J line have a different genetic background with

BFMI lines, the use of this line was preferred in previous studies (Aksu et al., 2007; Hantschel et al., 2011; Reichart et al., 2003; Wagener et al., 2010; Widiker et al., 2010). Consistently, the BFMI lines indicate more significant obesity induced alterations compared to DBA/2J line that is susceptible to obesity.

The mice were kept under conventional conditions with a 12:12 h light/dark cycle at a humidity of 65% and temperature of  $22 \pm 2$  °C. They were separated into groups of two to three mice in macrolon cages with a 350 cm<sup>2</sup> floor space (E. Becker & Co (Ebeco) GmbH, Castrop-Rauxel, Germany) and with dust-free bedding type S80/150 (Rettenmeier Holding AG, Wilburgstetten, Germany). All mice had ad libitum access to water and food. The animals were fed with a rodent standard breeding diet after weaning at the age of 3 weeks. The standard breeding diet (V1534-000, ssniff R/M-H, Ssniff Spezialdiäten GmbH, Soest/Germany) contains 12.8 MJ per kg of metabolisable energy, 58% of which arises from carbohydrates (33% from proteins and 9% from fat). The fat content of standard breeding diet was derived from soy oil (Hantschel et al., 2011). All control and BFMI obese groups have six mice for each. The SCAT and VAT samples were harvested for each mouse. Since the posterior depot of SCAT has simpler anatomy and consisting of a single tissue band, we particularly focused on the posterior depot located at the base of the hind legs (Cinti, 2005). After 10 weeks, the mice were killed by decapitation. The gonadal and subcutaneous adipose tissue were collected immediately and washed with PBS buffer to avoid the blood on the tissue. In our experiment, we used inguinal adipose tissue as a SCAT and gonadal adipose tissue as a VAT. The tissue samples were snap-frozen in liquid nitrogen and stored at -80 °C until experiments.

## **2.2. FTIR Microspectroscopic Studies**

### **2.2.1. Sample Preparation**

SCAT and VAT samples of 6 mice of each line were used in FTIR microspectroscopic studies and 3 sections were prepared for each sample. In sectioning part, adipose tissue samples

were embedded in Cryomatrix Frozen Embedding Medium (Thermo Scientific, USA). 7  $\mu\text{m}$ -thick tissue sections were gained consecutively by using a cryotome (Shandon, USA) at  $-25^{\circ}\text{C}$  both for immunohistological staining and FTIR microspectroscopy studies. These sections were immediately transferred onto IR-transparent  $\text{BaF}_2$  (Barium Fluoride) windows (Spectral Systems, NY, USA). To eliminate the moisture from the sections, the windows with sample were conserved in a desiccator coupled with vacuum pump at cold room for overnight.

### **2.2.2. FTIR Microspectroscopic Data Collection and Analysis**

Perkin Elmer Spectrum Spotlight 400 Imaging System (Perkin Elmer Instruments, Boston, MA, USA) was used to obtain FTIR images, the system included a fast-scanning FTIR spectrometer coupled with a liquid nitrogen cooled mercury-cadmium-telluride (MCT) focal plane array detector located in an image focal plane of an IR microscope.

Spectral images of samples were collected at a spectral resolution of  $8\text{ cm}^{-1}$  in the wavenumber region between  $4000$  and  $750\text{ cm}^{-1}$  in the transmission mode. The IR detector pixel size was  $6.25 \times 6.25\text{ }\mu\text{m}$  and 4 spectra were collected for each pixel. Despite the fact that SCAT and VAT are highly homogeneous tissues, three different areas in each tissue section were randomly selected to collect IR maps. As an example, these three IR maps for one sample are presented in Appendix A. FTIR microscope gathers IR images providing an IR spectrum from each pixel by scanning the selected areas pixel by pixel. The size of the spot or pixel was determined by the size of the microscope aperture. Due to the size of the collected FTIR maps was  $700 \times 700\text{ }\mu\text{m}$ , totally 12544 spectra were achieved from each selected area for each section. Firstly, the average of 12544 spectra was collected from each area and then the average spectrum of these three similar average spectra of selected areas was used for each sample for calculation of the spectral parameters. The background spectrum was collected from empty IR window and subtracted from spectra of tissue sample automatically by Spotlight Auto-image software (Perkin Elmer Instruments, Boston, MA, USA). The main parameter affecting the results of cellular

alterations in FTIR microspectroscopic studies, is sample thickness of tissues. In order to prevent the possible errors that occur due to differences in section thickness which can result in concentration-related alterations in the spectral absorbance values, the band area ratios were used in the analysis of FTIR Microspectroscopy (Bi et al., 2005; Boskey et al., 2006; West et al., 2004). Spectral maps were analyzed by using ISYS software (Spectral Dimensions, Olney, MD, USA). The spectral regions for the calculation of band areas are presented in Table 1.

**Table 1.** The spectral regions and baseline points for particular infrared bands used in calculation of band area ratios.

| <b>Infrared band</b>                     | <b>Integrated spectral region (cm<sup>-1</sup>)</b> | <b>Baseline points (cm<sup>-1</sup>)</b> |
|--|---|--|
| Olefinic=CH                              | 3020-2992   | 3100-2740                                |
| CH <sub>3</sub> antisymmetric stretching | 2976-2948   | 3100-2740                                |
| CH <sub>2</sub> antisymmetric stretching | 2940-2916   | 3100-2740                                |
| CH <sub>3</sub> symmetric stretching     | 2880-2864   | 3100-2740                                |
| CH <sub>2</sub> symmetric stretching     | 2864-2844   | 3100-2740                                |
| C-H region                               | 2980-2830   | 3100-2740                                |
| Carbonyl (C = O) stretching              | 1764-1724   | 1850-1500                                |
| Amide I                                  | 1672-1636   | 1850-1500                                |
| Amide II                                 | 1560-1536   | 1850-1500                                |

To detect the alterations in the structure of lipids, the integrated area under the specific lipid bands (CH<sub>2</sub> antisymmetric stretching, olefinic and carbonyl stretching bands) were divided individually by the area under the whole C-H region. Since C-H region contains vibrations of the fatty acyl chains of membrane lipids, it is sensitive to determine the whole lipid content of a system (Kneipp et al., 2002; Wang et al., 2005). The C-H region also includes a band originating from proteins (CH<sub>3</sub> symmetric stretching band). However, C-H region can be regarded as lipid region because this protein band is very weak (Bozkurt

et al., 2010; Cakmak et al., 2011; Garip et al., 2009). To investigate the ratio of the carbonyl groups and unsaturated lipids to total lipid content, the area of the carbonyl (C=O) ester band and olefinic band were divided by the area of the C-H region respectively (Cakmak et al., 2012; Kucuk Baloglu et al., 2015). The data about lipid acyl chain length was obtained from the ratio of the area of the CH<sub>2</sub> antisymmetric stretching band to the area of the C-H region and CH<sub>3</sub> antisymmetric stretching band respectively (Wang et al., 2005). The lipid to protein ratio was obtained by calculating the ratio of the area of the C-H region to the area under the amide I band (Cakmak et al., 2012, 2011). Since amide I and amide II profiles depend on the protein structural composition, the band area ratios of amide I/ amide II and amide I/ amide I + amide II were also calculated.

### **2.3. Immunohistological Staining**

The SCAT and VAT of BFMI lines and control DBA/J2 line have been used for UCP1 immunohistological staining in order to distinguish brown and white adipose tissues for observing the transdifferentiation. “For staining “EXPOSE rabbit specific AP (red) detection IHC Kit” (Abcam, USA) and Biotin goat anti rabbit antibody (Vector Lab. Inc., USA) were used. Immunohistological staining was applied as described in the kit procedure. After drying for overnight in desiccator, slides were treated with acetone at -20°C and waited for 10 minutes at -20°C and then washed 3 times in buffer (PBS). Then, we applied Protein Block and incubated the slides for 10 minutes at room temperature to block nonspecific background staining and the slides were washed 3 times in buffer again. In next step, we applied primary antibody (Biotin goat anti rabbit antibody (Vector Lab. Inc., USA)) and incubated the slides according to manufacturer's protocol and washed 3 times in buffer. After that, AP conjugate was applied and the slides were incubated for 30 minutes at room temperature and rinsed 4 times in buffer. The 200 µl of enhancer was applied to the slides and the slides were incubated for 4 minutes at room temperature. We mixed equal volume of Naphthol Phosphate and Fast Red just before using, and then applied 200 µl of this mixture onto the slides with Enhancer. The recommended

incubation time was 8 minutes at room temperature. Then, the slides were rinsed 4 times in buffer followed by Hematoxylin staining as a counter-staining. For counter-staining, Hematoxylin was added to cover the slides which were then incubated for 1 minute and they were washed 7-8 times in tap water. Stained slides were made permanent by Eukitt® quick-hardening mounting medium (Sigma-Aldrich, USA) and they were quantified by observing with a light microscope under 40X magnification” (Kucuk Baloglu et al., 2015).

## **2.4. ATR-FTIR Spectroscopic Studies**

IR spectra of SCAT and VAT were acquired by using a Universal ATR accessory (Perkin Elmer Inc., Norwalk, CT, USA) that is integrated to a Perkin Elmer Spectrum 100 FTIR spectrometer (Perkin-Elmer Inc., Boston, MA, USA). In ATR-FTIR spectroscopy technique, to remove the atmospheric CO<sub>2</sub> and H<sub>2</sub>O absorption bands of environmental air, a background spectrum was taken before collecting the sample spectra and then this spectrum was mathematically subtracted from sample spectra. This process was repeated automatically by the software for each sample spectra. Subsequent to subtraction process, a small amount (5 mg) of sample was directly placed on the Diamond/ ZnSe crystal platform and scanned without any drying process in the 4000 to 650 cm<sup>-1</sup> spectral region at room temperature, where 50 scans were collected at a resolution of 4 cm<sup>-1</sup> for each spectrum. The spectrum was independently collected 3 times for each sample from randomly chosen fragments. This process was used to ensure about the alterations in the absorbance values which was nearly same and secondly to reduce possible experimental errors which might be affected from intra-sample variability. Average spectra of these 3 replicates were used for further analysis and data manipulations were performed via Spectrum 100 software (Perkin-Elmer).

## **2.5. Hierarchical Cluster Analysis (HCA)**

HCA describes the similarities between the spectra of interested samples by using classification algorithms and distance calculation. Previous to HCA and also PCA analysis, to more effectively comparing the spectra, spectral data was subjected to some preprocessing procedures. Firstly, second derivative spectra, a widely used preprocessing step in spectral analysis, were obtained and used to minimize baseline variability and background effects in the spectra (Brown et al., 2000; Giese & French, 1955; Mariey et al., 2001; Mark et al., 2007; Rieppo et al., 2012; Susi & Byler, 1983; Whitbeck, 1981). Secondly, vector normalization process was used to eliminate the differences arising from the thickness variations of samples (Mariey et al., 2001). For the detection of spectral differences between the control and different obese groups, vector normalized and second derivative spectra in the particular ranges were used as an input data. The level of heterogeneity was calculated by OPUS 5.5 software program from the average spectra. These results were represented in the figure as a dendrogram which indicates clustering in 2 dimensions by graphical means. Calculations of spectral distances were done between pairs of spectra by the use of Pearson's correlation coefficients. The dimension of similarity is the heterogeneity, where decreasing heterogeneity corresponds to decreasing dissimilarity.

The heterogeneity calculations were performed by using Euclidian distance and Ward's algorithm from the average spectra. Euclidean distance was used for the calculation of the sample similarities and to show the whole linkage clustering by Ward's algorithm. The Ward's algorithm enables to cluster homogeneous samples as much as possible by collecting the spectra that construct the smallest distance in variance (Severcan et al., 2010; Ward, 1963). Ward's algorithm together with Euclidian distances in cluster analysis is an appropriate way to form the dendograms providing one of the best predictions (Lasch et al., 2004).

Sensitivity and specificity, which can be obtained from HCA method, are common parameters in clinical studies. The sensitivity evaluates the incidence of real positives which are correctly identified, for example the percentage of obese mice identified as having the disease. Additionally, the specificity evaluates the incidence of negatives which are correctly identified, for example the percentage of control mice identified as not having the disease (Table 2) (Fung et al., 1997; Severcan et al., 2010; van Rhijn, van der Poel, & van der Kwast, 2009).

**Table 2.** Definitions for sensitivity and specificity during hierarchical cluster analysis based on FTIR data.

**Cluster analysis results based on FTIR data**

|                | <b>Positive</b> | <b>Negative</b> |   |
|----------------|-----------------|-----------------|---|
| <b>Obese</b>   | A               | B               | <b>Sensitivity = <math>A / (A+B)</math></b> |
| <b>Control</b> | C               | D               | <b>Specificity = <math>D / (C+D)</math></b> |

***Positive and negative values:***

A: Number of obese animals clustered in obese group (true positive)

B: Number of obese animals clustered in control group (false negative)

C: Number of control animals clustered in obese group (false positive)

D: Number of control animals clustered in control group (true negative)



## **2.6. Principle Component Analysis (PCA)**

PCA is a well-known statistical procedure that reduces the dimensionality of a multivariate data set, while conserving the variation already exist in the original predictor variables (Li et al., 2008). Therefore, by using this technique, a large scale of spectra composing of hundreds of absorbance values was reduced to one point in a multidimensional space using a linear transformation. The PCA is enable to provide two types of data; (1) scores plots of class separation and (2) loadings plots to define the main contributory variables (e. g. wavenumbers) which confirm the discriminatory wavenumbers in the IR spectrum (Cox, 2005; Nakamura et al., 2010). In PCA, the coordinates are represented as principle components (PC) and the plot acquired is termed as the scores plot. These PCs describe the spectral variability between samples in decreasing rank (Nakamura et al., 2010). To be more precise, the first principle component (PC1), is the primary axis of the coordinate system showing the maximum variance of the data set. The second principle component (PC2) is the secondary axis indicating the next highest variance of the data set (Bhih & Johnson, 2015). The loading plots are capable to determine the frequencies that show the most important variation in the PC terms. These plots indicate the relationship between original variables and subspace dimensions to interpret relationships between variables.

Unscrambler X software packages (v. 10.0.1, Camo Software, Oslo, Norway) was used for vector normalized and 2nd derivative spectra in particular regions. The average spectra for each sample was represented by one point in the PCA scores plot.

## **2.7. Statistics**

The results were represented as ‘mean  $\pm$  standard error of mean (SE)’. The alterations in variance were analyzed by using one-way ANOVA test. As a post-hoc test, Tukey’s test was used and each group’s results were compared with each other. The p values less than

or equal to 0.05 were considered as statistically significant (such as  $*p \leq 0,05$ ;  $**p \leq 0,01$ ;  $***p \leq 0,001$ ). The degree of significance was denoted by \* for the comparison of control DBA/J2 line with BFMI lines, by # for the comparison of BFMI852 with other BFMI lines, by ‡ for the comparison of BFMI856 with other BFMI lines and by † for the comparison of BFMI860 with other BFMI lines.

## CHAPTER III

### 3. RESULTS AND DISCUSSION

#### **Part 1: FTIR imaging of structural changes in visceral and subcutaneous adiposity and transdifferentiation from brown to white adipocyte**

This part of the study targets to characterize and also compare VAT and SCAT according to macromolecular content and identify the possible transdifferentiation from brown to white adipocytes. For this purpose, FTIR microspectroscopy and UCP1 immunohistological staining were performed to investigate VAT and SCAT of spontaneously obese male BFMI lines. Biological specimens include biochemical components such as carbohydrates, proteins, lipids and nucleic acids. These biochemical molecules possess their specific vibrational fingerprints individually (Dogan et al., 2007; Gasper et al., 2009; Levin & Bhargava, 2005). Depending on this phenomenon, FTIR microspectroscopy is capable to acquire visible images of the investigated tissue. In these images, each pixel consists of a spectrum arising from vibrational fingerprints. The representative FTIR spectra obtained from control and obese groups of SCAT in the 4000–750  $\text{cm}^{-1}$  region are presented in Figure 17. The detailed spectral band assignments of mouse adipose tissue are shown in Table 3 (Dogan et al., 2013; Kneipp et al., 2000; Dieter & Heinz, 2009).

To determine obesity related changes in the concentration and composition of biochemical molecules, the area ratios of some specific functional groups of lipids and proteins were calculated. In the band area ratio calculations, the wavenumber limits with baseline points utilized for each vibrational region are presented in Table 1.

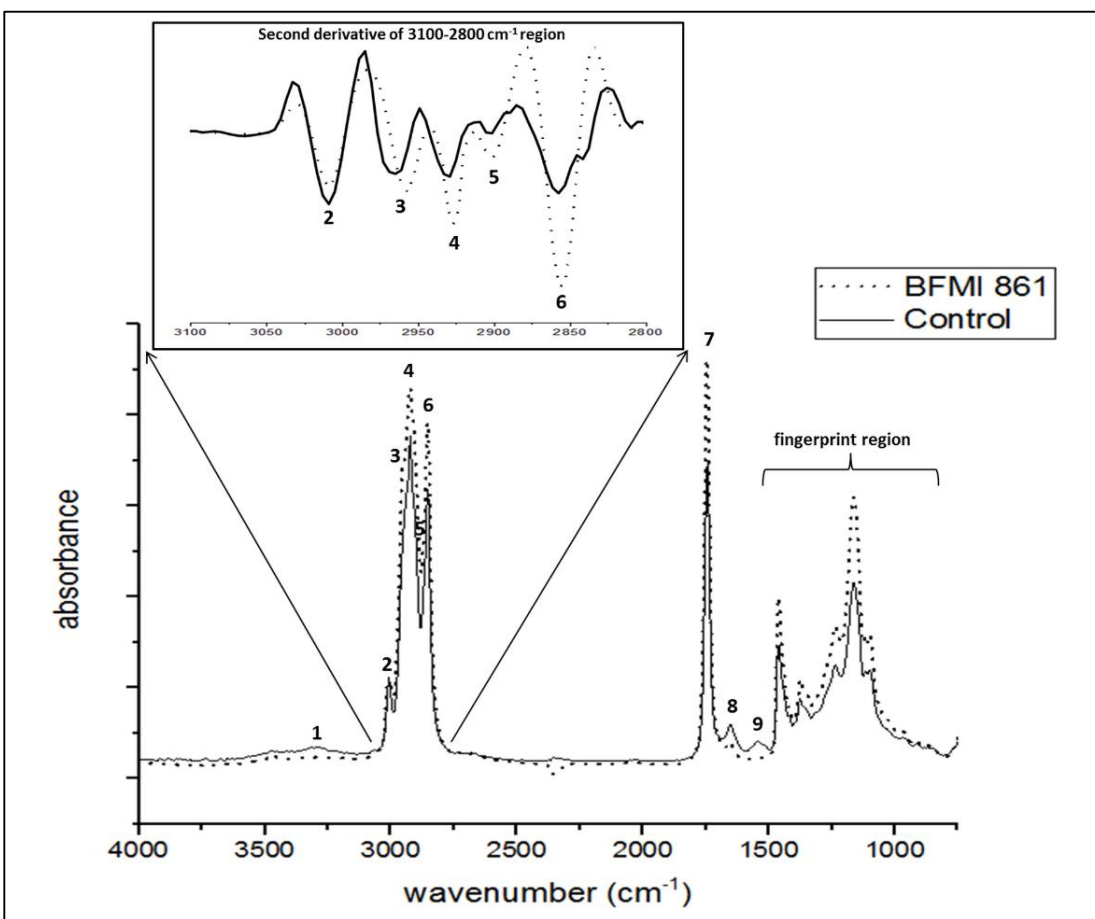


**Figure 17.** Representative FTIR spectra of IF adipose tissue of male control DBA/J2 and obese BFMI861 lines in the 4000-750 cm<sup>-1</sup> region.

**Table 3.** General band assignment of FTIR spectrum of an adipose tissue(Dogan et al., 2013; Kneipp et al., 2000; Dieter & Heinz, 2009).

| <b>Band No</b> | <b>Wavenumber (cm-1)</b> | <b>Definition of the spectral assignment</b>   |
|----------------|--------------------------|--|
| 1              | 3290                     | N–H and O–H stretching: Mainly N–H stretching (amide A) of proteins with the little contribution from O–H stretching of polysaccharides, carbohydrates and water |
| 2              | 3005                     | Olefinic=CH stretching vibration: unsaturated lipids, cholesterol esters   |
| 3              | 2957                     | CH <sub>3</sub> anti-symmetric stretching: lipids, protein side chains, with some contribution from carbohydrates and nucleic acids                              |
| 4              | 2924                     | CH <sub>2</sub> anti-symmetric stretching: mainly lipids, with some contribution from proteins, carbohydrates, nucleic acids                                     |
| 5              | 2875                     | CH <sub>3</sub> symmetric stretching: mainly protein side chains, with some contribution from lipids, carbohydrates and nucleic acids                            |
| 6              | 2855                     | CH <sub>2</sub> symmetric stretching: mainly lipids, with some contribution from proteins, carbohydrates, nucleic acids  |
| 7              | 1744                     | Carbonyl C=O stretch: triglycerides  |
| 8              | 1654                     | Amide I (protein C=O stretching)   |
| 9              | 1545                     | Amide II (protein N-H bend, C-N stretch)   |

The representative spectral maps of lipid/protein,  $\text{CH}_2/\text{CH}_3$  antisymmetric, olefinic/lipid, carbonyl/lipid, amide I/ amide II ratios of SCAT and VAT of the control and obese lines are shown in Figures 18-22. The spectral maps are presented as color-coded images which are consisted of a spectrum in each pixel. The maps were colored based on the calculated ratio values, where red color indicates the highest ratio and blue color indicates the lowest ratio as shown on the color scales in related figures.

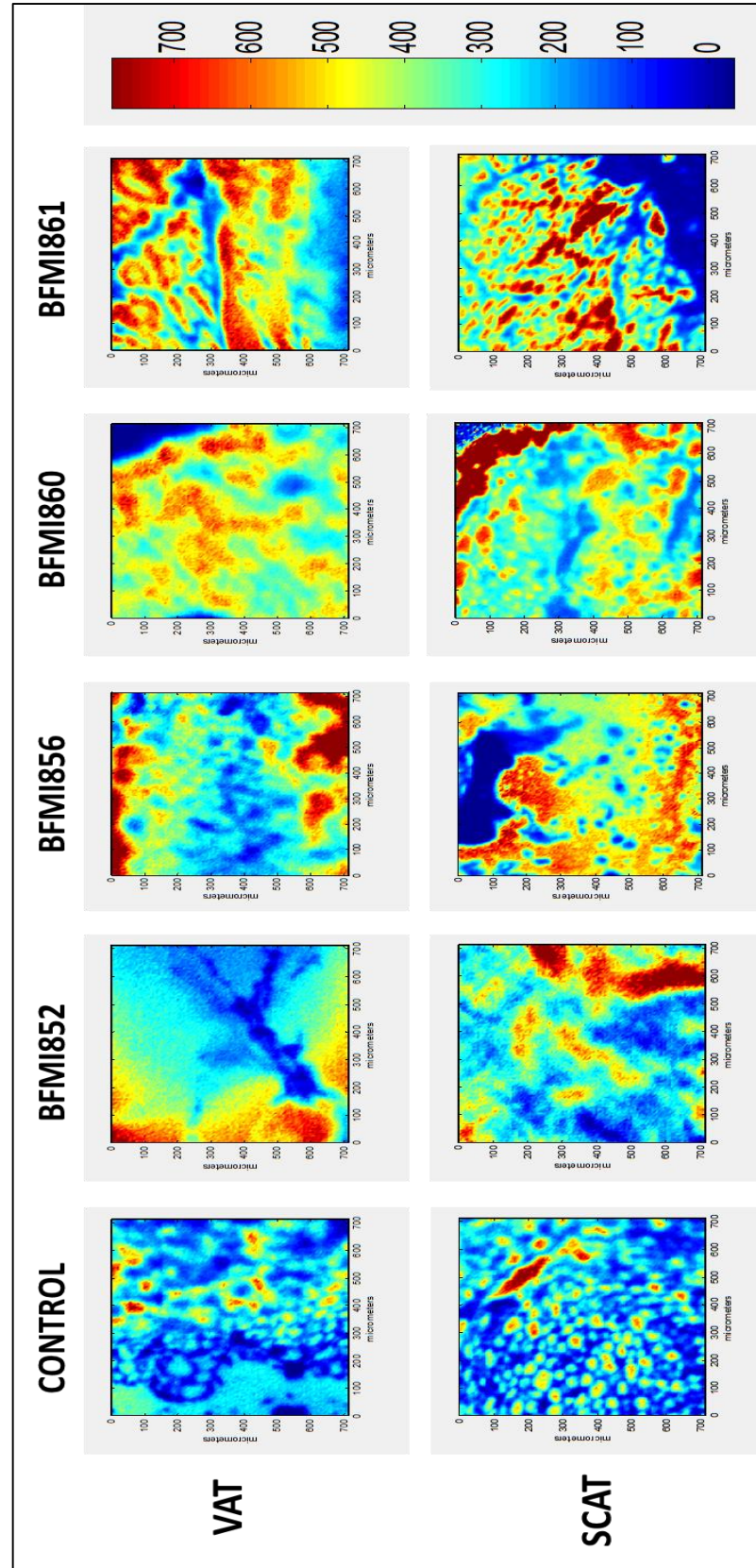


**Figure 18.** Representative images of the lipid/protein ratio in SCAT and VAT of the control and BFMi lines.

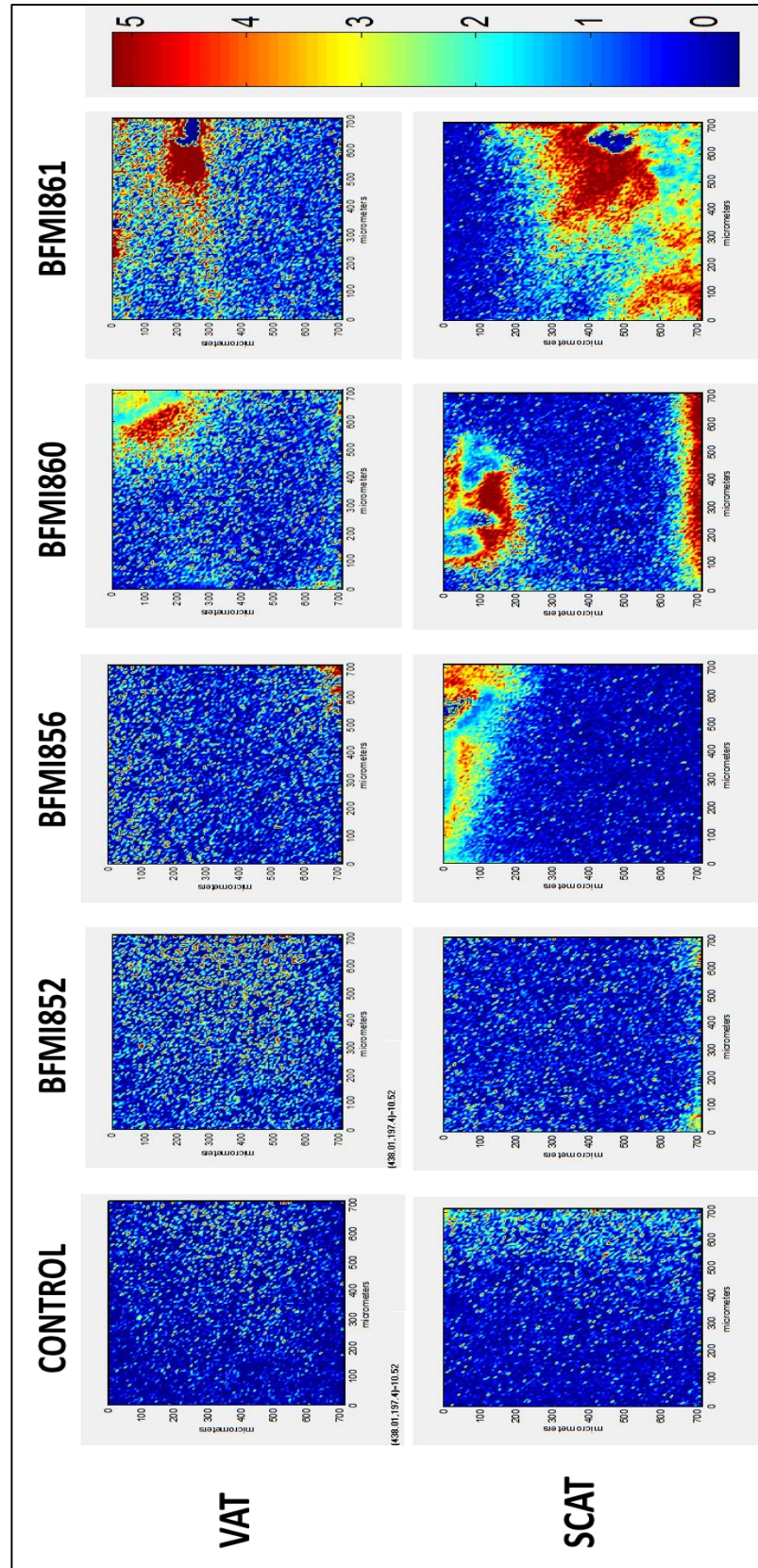


**Figure 19.** Representative images of the CH<sub>2</sub>/CH<sub>3</sub> antisymmetric ratio in SCAT and VAT of the control and BFM lines.



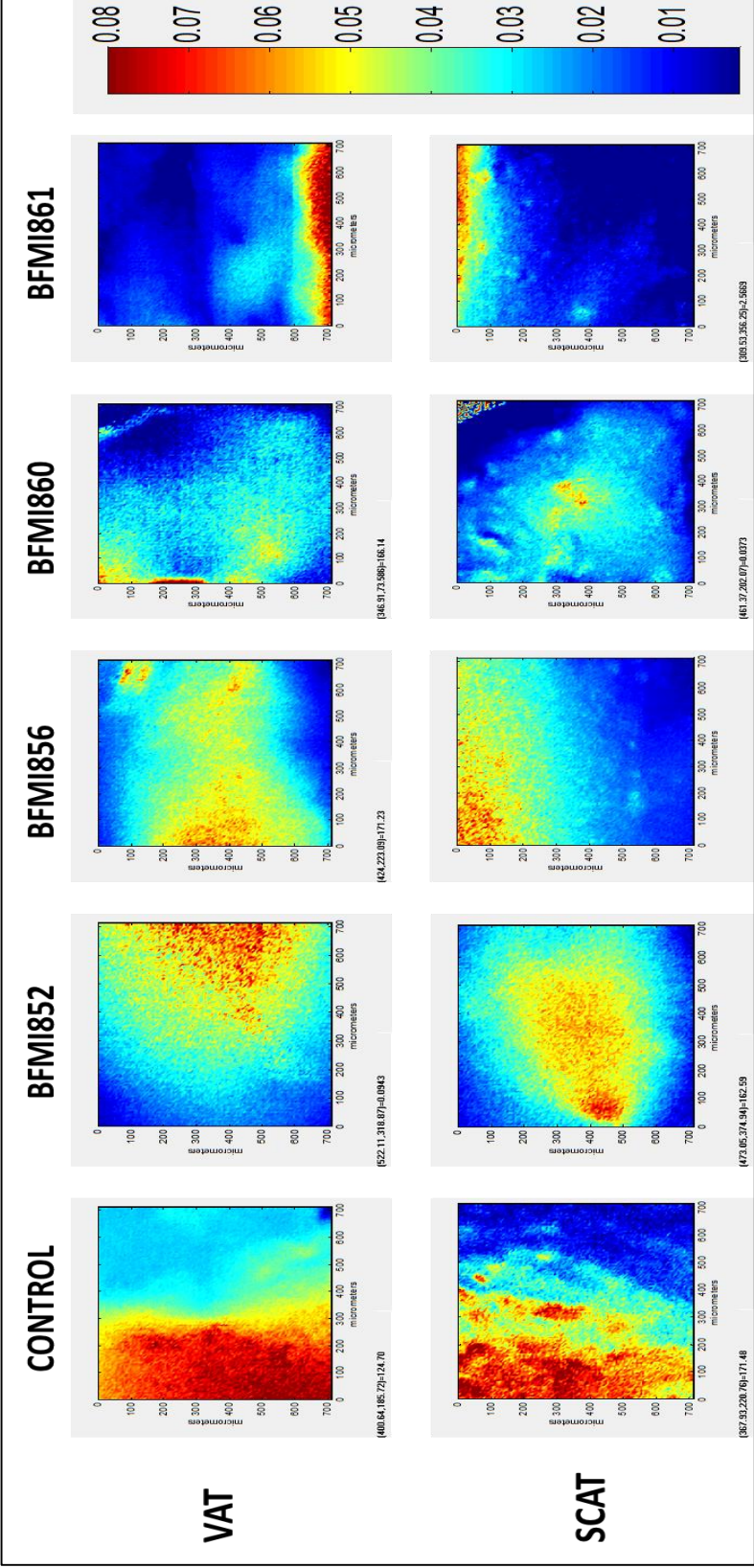


**Figure 20.** Representative images of the olefinic/protein ratio in SCAT and VAT of control and BFM lines.

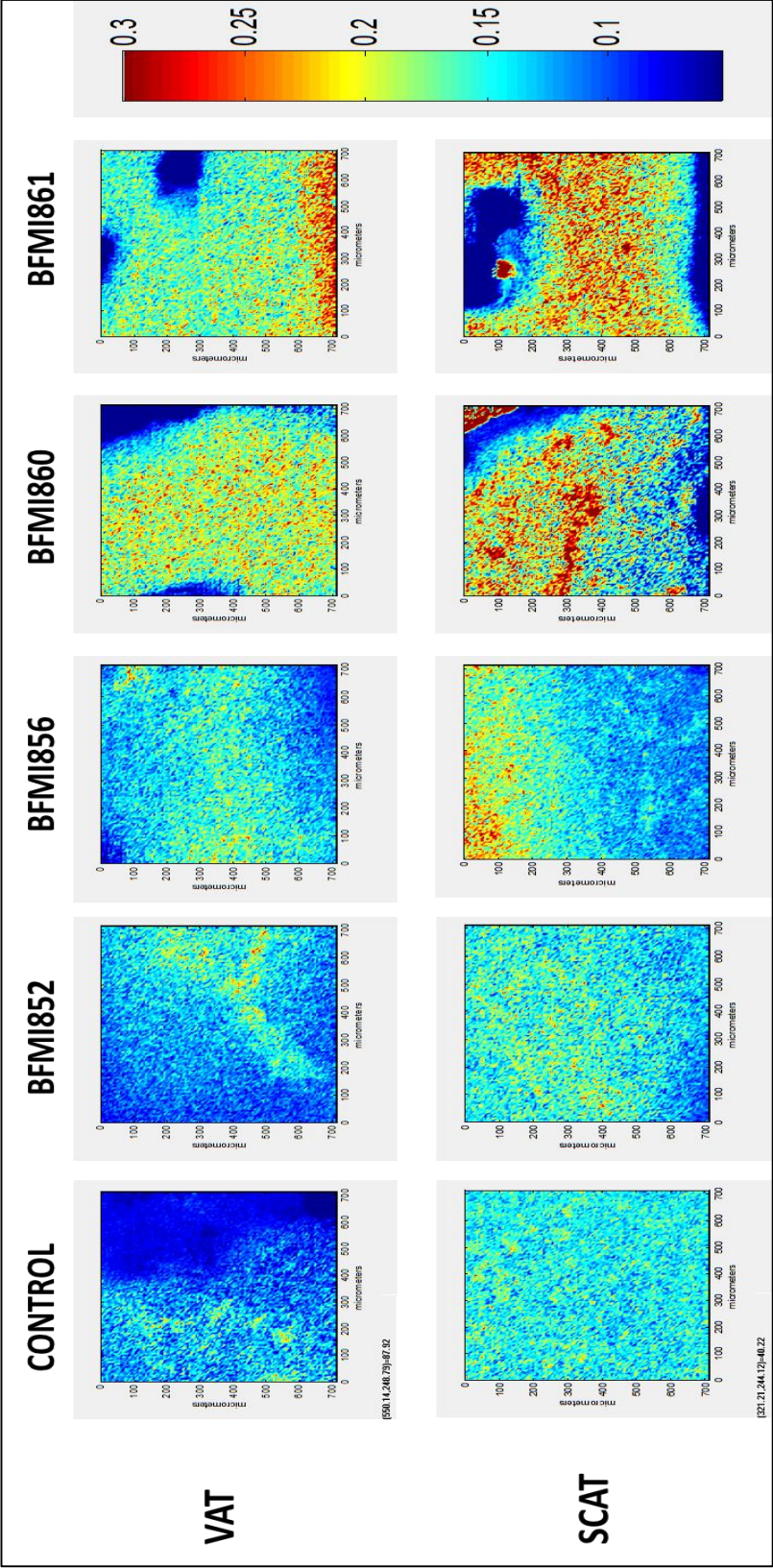


**Figure 21.** Representative images of the carbonyl/lipid in SCAT and VAT of the control and BFMI lines.



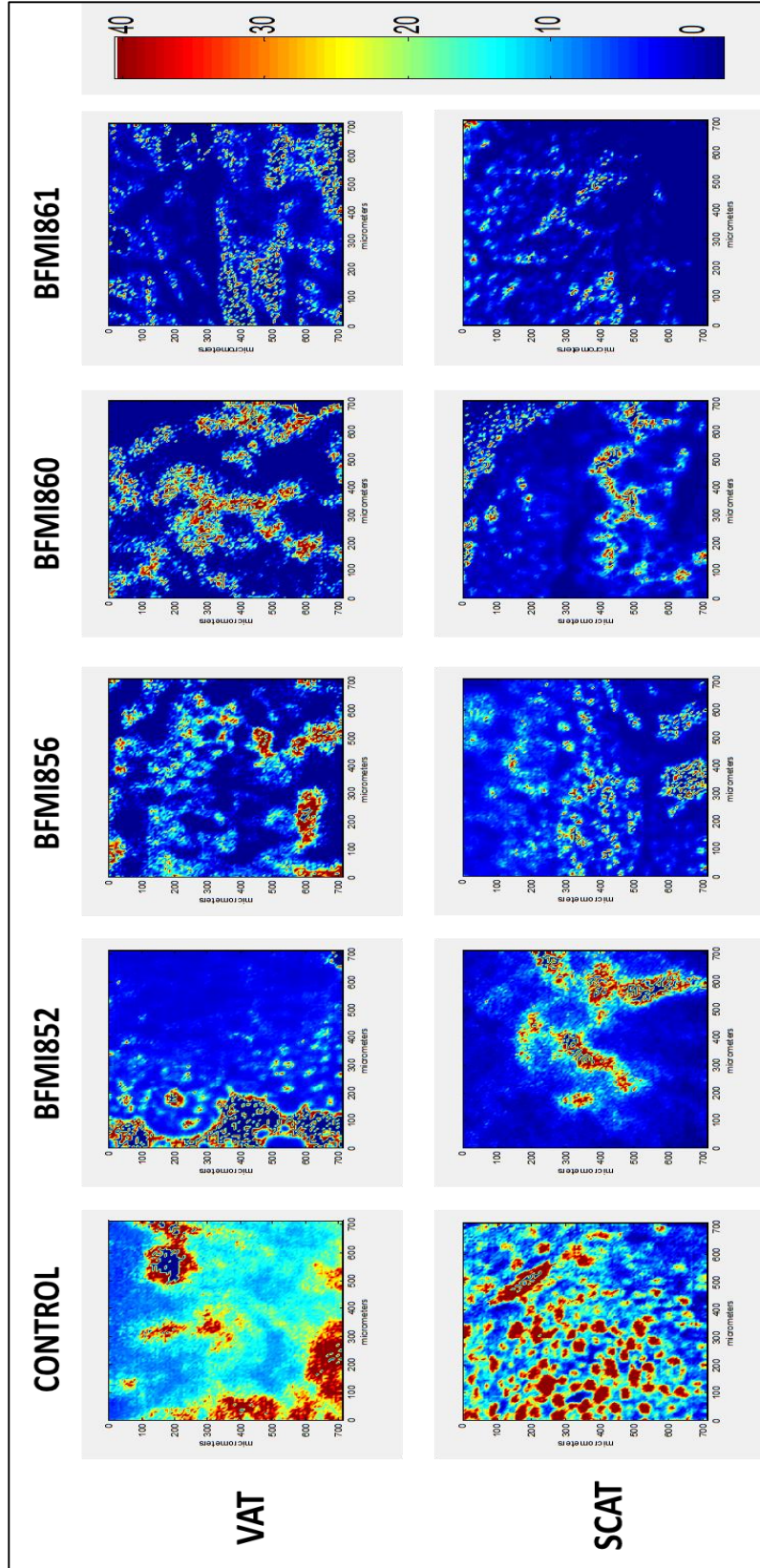


**Figure 22.** Representative images of the amide I/amide II in SCAT and VAT of the control and BFMi lines.

The lipid/protein ratio is a fundamental parameter in molecular asymmetry (Ozek et al., 2010). This ratio can be obtained by proportioning of the particular area of the C-H region to the area of the amide I band. Since the C-H region includes significant vibrations of the fatty acyl chains of membrane lipids, it is a critical marker for the lipid context (Bozkurt et al., 2010; Kneipp et al., 2000; Wang et al., 2005). The Amide I band provides information about concentration and conformation of total protein (Cakmak et al., 2012; Ishida & Griffiths, 1993). To get qualitative data about lipid structure of SCAT and VAT, unsaturated/saturated lipid and carbonyl/lipid ratio were also calculated. Unsaturated/saturated lipid ratio was calculated by proportioning of the particular area of the olefinic band as an unsaturated lipid to that of CH<sub>2</sub> antisymmetric band as a saturated lipid. Similarly, the carbonyl/lipid ratio was calculated by proportioning of the particular area of carbonyl band to that of C-H region. On the other hand, the ratio of areas of the CH<sub>2</sub> antisymmetric band to that of the CH<sub>3</sub> antisymmetric band was calculated in order to detect alterations of lipid acyl chain length. Moreover, CH<sub>2</sub> symmetric/CH<sub>2</sub> antisymmetric and the amide I/ amide I + amide II ratios were calculated to get more information about lipid and protein amounts, respectively. Figure 23 represented the comparison of all these ratios above in terms of bar graphs for the control and 4 different obese lines. Obviously seen from the figure, the ratios of the lipid/protein, carbonyl/lipid, CH<sub>2</sub> symmetric/CH<sub>2</sub> antisymmetric and CH<sub>2</sub>/CH<sub>3</sub> antisymmetric increased; while ratios of the olefinic/lipid and amide I/ amide I + amide II decreased for obese lines in comparison to the control line.

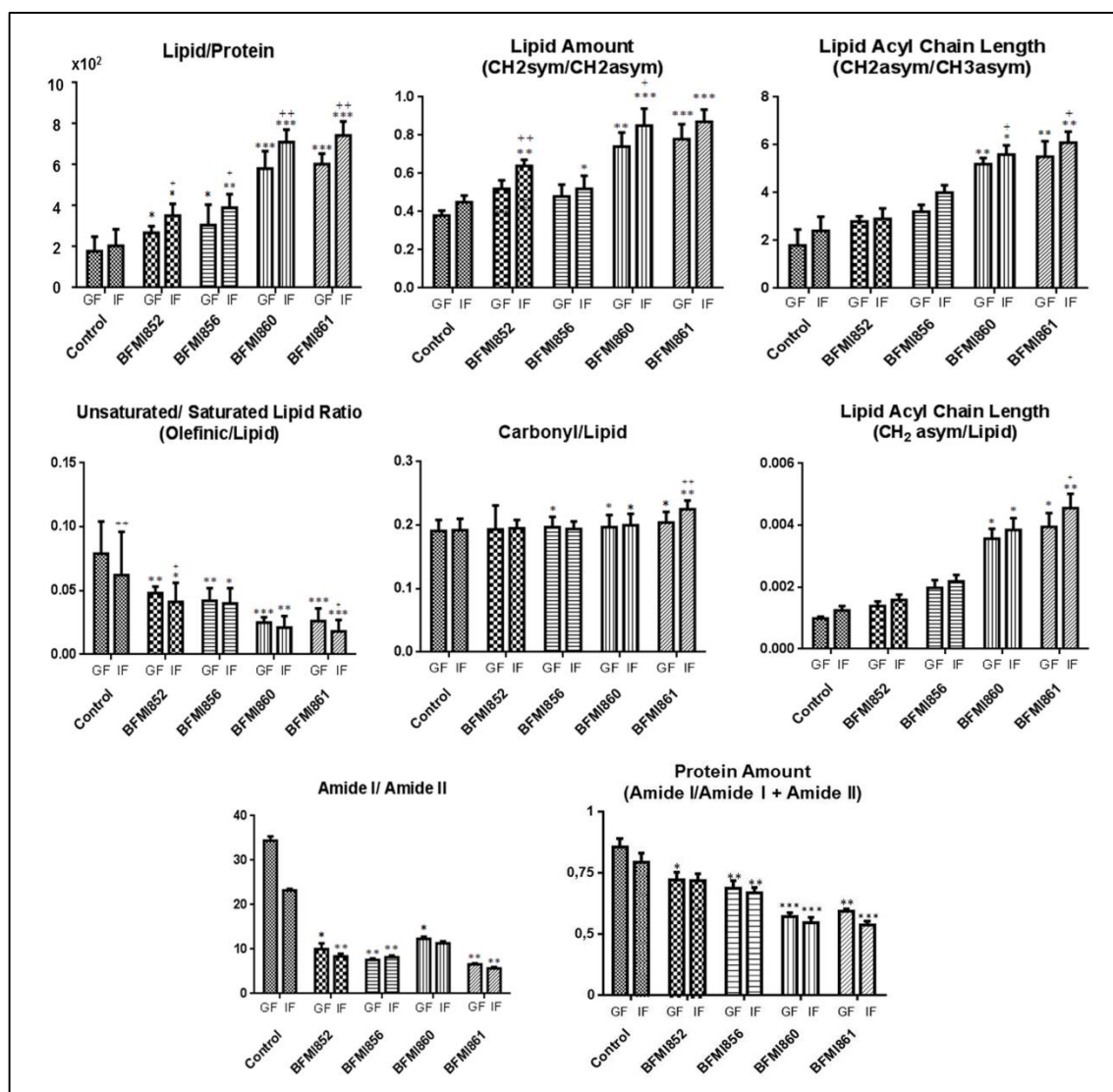


**Figure 23.** The bar graphs of the lipid/protein, CH<sub>2</sub> symmetric/CH<sub>2</sub> antisymmetric, CH<sub>2</sub>/CH<sub>3</sub> antisymmetric, olefinic/lipid, carbonyl/lipid, CH<sub>2</sub> antisymmetric/lipid, amide I/ amide II, amide I/ amide I + amide II ratios of control (DBA/J2) and 4 different obese (BFMI) male mice lines. (GF: VAT; IF: SCAT).

The lipid/protein ratio provides information about alterations in lipid context compared to protein context. As it was expected, an increased lipid/protein ratio was achieved in all obese groups in comparison to the control group. The significant increase in the lipid content ( $\text{CH}_2$  symmetric/ $\text{CH}_2$  antisymmetric ratio) and/or from the significant decrease in protein content (amide I/ amide I + amide II) that we observed in obese lines can be the most probably reason of remarkable increase in the lipid/protein ratio in the obese lines in comparison to the control line (Bozkurt et al., 2010). The enlargement of VAT and SCAT mass in the body is the main reason of obesity and this process usually eventuates in disturbed glucose and lipid metabolism (Bays et al., 2008). Since SCAT is more prone to store the lipids rather than VAT, the increment in the lipid/protein ratio was more significant in SCAT rather than VAT (Ibrahim, 2010). However, the SCAT has limited storage capacity because of the definite cell size increment. Therefore, VAT is also a storage site for the excess lipids. Since VAT is more active than SCAT, which is a passive storage depot, and more sensitive to lipolysis, it mainly affects lipid and glucose metabolism (Bonora et al., 1992). The lipolysis of triglycerides from VAT ends up with the release of FFAs into liver by portal vein. Therefore, excess deposition of lipids in VAT can be more harmful than SCAT (Björntorp, 1990).

On the other hand, the increase of lipid/protein ratio in obese groups may also be derived from a lower protein content. The alterations in band area values of amide I give information about total protein content (Gasper et al., 2009). A significant decrease in the band area value of the amide I was obtained in obese groups indicating a decrease of protein content (Table 4). This consequence was also supported by the significant decrease of amide I/ amide I + amide II ratio (Figure 22). In order to achieve more information about alterations in protein structure and composition, the band area ratio of amide I/ amide II was also calculated and a lower ratio was obtained in obese lines compared to a control group consistently. Due to the fact that amide I and II bands are based on the protein structure, this decrease in obese lines indicates some changes in the protein conformation (Cakmak et al., 2011; Schmidt et al., 2007; Yu et al., 2008). Moreover, there was a considerable shifting in the wavenumber of amide I band to higher values in the all

obese groups compared to the control group which supports the changes in structural composition of protein (Aksoy et al., 2012; Cakmak et al., 2006; Haris & Severcan, 1999; Severcan & Haris, 2012). As a result, the decrease in the area of amide I band and amide I/amide II band area ratios and the shifting of the amide I band to higher wavenumber values can be interpreted as a consequence of the changes in protein expression and this situation causes obesity related alterations in protein structure and conformation in SCAT and VAT (Bozkurt et al., 2010).

**Table 4.** The band area and band position values of the amide I band in male control (DBA/2J) and obese (BFMI lines) mice gonadal and inguinal adipose tissues.

|   |          | Control      | BFMI852       | BFMI856        | BFMI860        | BFMI861        |
|---|----------|--------------|---------------|----------------|----------------|----------------|
| <b>Amide I area value</b>   | Gonadal  | 0.83±0.01    | 0.63±0.04*    | 0.42±0.03*     | 0.38±0.02**    | 0.37±0.03**    |
|   | Inguinal | 0.73±0.04    | 0.57±0.05     | 0.56±0.02      | 0.33±0.04**    | 0.29±0.01**    |
| <b>Amide I band position</b>  | Gonadal  | 1652.56±0.30 | 1653.50±0.13* | 1654.53±0.51*  | 1655.31±0.25** | 1656.65±0.60** |
|   | Inguinal | 1652.93±0.93 | 1653.31±0.42* | 1654.57±0.18** | 1656.85±0.29** | 1656.94±0.28** |
| <i>“The values are the mean ± standard error of the mean for each group. Comparison was performed by one-way ANOVA and Tukey’s test was used as a post test. The degree of significance was denoted with * for the comparison of control DBA/J2 strain with other BFMI lines. P values less than or equal to 0.05 were considered as statistically significant; *p ≤ 0,05; **p ≤ 0,01; ***p ≤ 0,001.”</i> |          |              |               |                |                |                |

As an index of double bonds, the olefinic/lipid ratio provides information about the relative amount of unsaturated lipids in the total lipid composition (Cakmak et al., 2012; Kneipp et al., 2000). A significant decrease in olefinic/lipid ratio indicating a decrease in unsaturated lipid content was observed in all obese lines compared to the control group. The level of unsaturation was also lower in SCAT rather than in VAT for all groups. The alterations in unsaturation lipid context can affect stabilization, structure and function of

membrane adversely (Yeagle, 2004). Polyunsaturated fatty acids (PUFAs) are vulnerable to free radical attack. These attacks cause to lipid peroxidation reactions, leading to alterations in unsaturated/saturated lipid design of the membranes. On the other hand, a drop in level of unsaturation in the membrane can cause the tightly packing of fatty acids leading to an increase in phase transition temperature, hence leads to a decrease in membrane fluidity (Yeagle, 2004). More rigid membrane structure can be correlated with insulin resistance it can cause some limitations for the correct insulin-receptor binding (Russo, 2009). As stated in literature, VAT accumulation has an effect on the mechanism of insulin resistance (Gastaldelli et al., 2002). In other words, extreme accumulation of VAT is associated with reduced insulin sensitivity. The decreased FFA reesterification, and increased resistance of lipolysis to the inhibitory effect of insulin can be also make contribution to this association in both VAT and SCAT (Albu et al., 1999; Brochu et al., 2000; Meek et al., 1999; Zierath et al., 1998).

The  $\text{CH}_2$  antisymmetric /  $\text{CH}_3$  antisymmetric stretching ratio was calculated to detect the qualitative alterations in lipid acyl chain length. In this ratio, the higher indicates the presence of longer chained lipids (Derenne et al., 2014; Gasper et al., 2009; Kumar et al., 2014; Smiley & Richmond, 1999; Wang et al., 2005). Although all obese BFMI lines showed an increase in this ratio, these increments were only significant in 860 and 861 lines. SCAT showed more increase than VAT in all BFMI lines. To provide supportive information about variations in lipid acyl chain length, an additional ratio was also calculated by proportioning the area of the  $\text{CH}_2$  antisymmetric stretching band to the C-H region. This ratio gave higher values in obese lines compared to the control supporting relative alterations towards longer lipid acyl chains (Antoine et al., 2010; Cakmak et al., 2012). The increase of  $\text{CH}_2$  antisymmetric /  $\text{CH}_3$  antisymmetric stretching ratio in all obese groups implies that the synthesis of longer lipid hydrocarbon acyl chain was occurred qualitatively in biological membranes (Cakmak et al., 2012; Wang et al., 2005). These alterations in lipid hydrocarbon chain length can cause variations in bilayer thickness leading to disturbing effect on the permeability and thermodynamic stability of the lipid



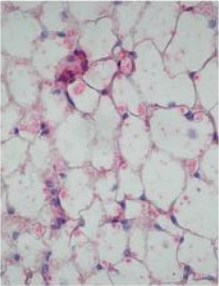
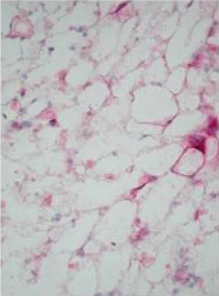
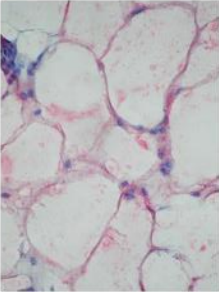
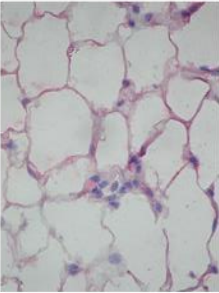
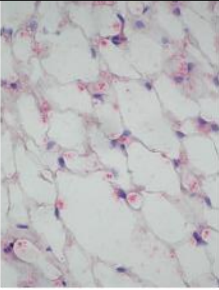
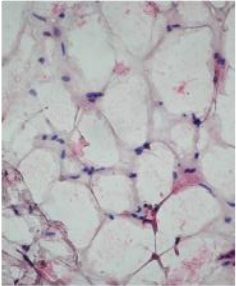
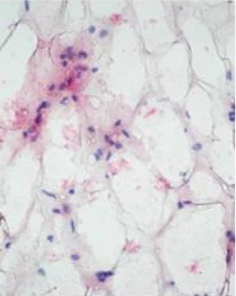
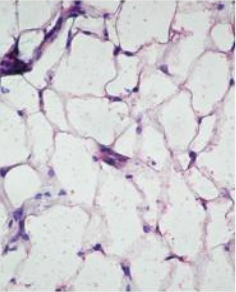
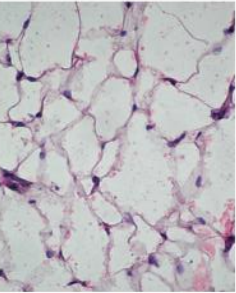
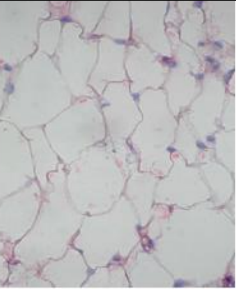
bilayer of membranes. In immunohistological staining results, impaired membrane appearance was obtained in adipocytes of obese lines consistently.

Carbonyl/lipid ratio indicates the levels of triglycerides and cholesterol esters in the system (Nara et al., 2002; Ozek et al., 2010; Voortman et al., 2002). Although all obese BFMI lines indicate an increase in this ratio, these increases were only significant in 860 and 861 lines, especially in SCAT, implying an increased concentration of the ester groups belonging to triglycerides in adipose tissues of the obese lines (Cakmak et al., 2003; Nara et al., 2002). SCAT, an inguinal adipose tissue, was found to have a higher carbonyl/lipid ratio than VAT as a gonadal adipose tissue. In accordance with these results, it has been reported that larger adipocytes which consists of SCAT, synthesize more triglycerides than smaller adipocytes composed of VAT (Edens et al., 1993; Farnier et al., 2003). The accumulation of triglycerides and other lipids in adipose tissue is highly correlated with the symptoms of insulin resistance (Pan et al., 1997; Phillips et al., 1996). The excess lipolysis of triglycerides causes the release of FFA excessively, and these FFAs especially from VAT are released into liver through portal vein. This process has a critical role in the development of insulin resistance (Hotamisligil et al., 1995). On the other hand, the inhibitory effect of FFAs on insulin sensitivity result in the increased lipolysis in adipocytes because insulin is the main regulator of HSL which is an enzyme controlling the triglyceride hydrolysis (Ruan et al., 2002). Adipocytes accumulate large amounts of lipids in order for the rapid release of lipids upon stimulation, so that other organs can use lipids as an energy source when it is necessary. However, extreme deposition of lipids in adipose tissue, especially in the VAT depot, is closely associated with enhanced risk of insulin resistance, cardiovascular disease and cancer (Cohen & LeRoith, 2012; Hossain et al., 2007).

In immunohistological staining studies, it was aimed to discriminate BAT and WAT from each other and to investigate the transdifferentiation of these tissues. Figure 24 represents the general microscope images of UCP1 stained VAT and SCAT sections of the control and obese lines under 40X magnification. When control and obese mice lines were

compared with each other, three main results became prominent; increased cell size, decreased UCP1 protein content, and impaired membrane surface. In the images, UCP1 proteins have a reddish-pink color appearance. As it is seen in the figure 24, the adipocytes in obese lines had less amounts of UCP1 proteins compared to the control line. The comparison of brown and white adipocytes amounts in the control and obese lines revealed that the brown adipocytes gave place to white adipocytes in all obese lines. This replacement namely transdifferentiation was obtained especially in BFMI860 and 861 lines and was more significant in SCAT. This process may be clarified by two explanations, the first one is by an increase of number and size of white adipocytes. The increase of WAT mass activates an inflammatory process in metabolically active regions. This activation generates a powerful increase of hormone-like molecules, proinflammatory cytokines, and other inflammatory components, described as “adipokines” in circulating mechanism (Lago et al., 2007; Pan et al., 1997; Wozniak et al., 2009). This complicated physiological process causes an enhanced level of glucocorticoids, leads to the development and differentiation of preadipocytes, and so an augmentation of WAT mass (Bourlier et al., 2008; Purnell et al., 2009). The second explanation is the probability of the transdifferentiation of brown adipocytes to white adipocytes. Consistently, the lower amount of UCP1 proteins in obese groups was observed in immunohistological staining results, implying a reduced amount of brown adipocytes especially in SCAT. Brown and white adipocytes enable to transform each other, when it is required so this physiological cohabitation is maintained through reversible transdifferentiation (Cinti, 2009). This ability is important because BAT can provide a resistance to obesity and so this brown-phenotype exhibits an anti-obesity effect (Cinti, 2009). As stated in literature, obesity-prone mice possess fewer BAT than obesity-resistant mice (Almind et al., 2007). Since the visceral adipocytes have smaller size and have different resistance to death compared to subcutaneous adipocytes, it was speculated that visceral white adipocytes were brown adipocytes previously (Cinti, 2009).

Since brown adipocytes have a crucial role in glucose metabolism and insulin sensitivity, these features make BAT a target for the treatment of obesity and diabetes (Townsend & Tseng, 2012). A recent rodent study using BAT transplantation from donor mice to recipient mice achieved to increase BAT mass in mice and so they demonstrated upgraded glucose tolerance, enhanced insulin sensitivity and decreased body weight with reduced fat mass (Stanford et al., 2013). These type of BAT transplantation studies with successful treatment results were reported in the literature (Gunawardana & Piston, 2012; Liu et al., 2013). These all data showed that the BAT has a critical role in obesity and other metabolic diseases.

|      | CONTROL  | BFMI852   | BFMI856  | BFMI860   | BFMI861   |
|------|--|---|--|---|---|
| VAT  | <br>17.2 %  | <br>9.6 %  | <br>6.2 %  | <br>3.5 %  | <br>3.1 %  |
| SCAT | <br>12.7 % | <br>6.3 % | <br>5.6 % | <br>2.9 % | <br>2.1 % |

**Figure 24.** Microscopic images of immunohistological UCP1 staining results of SCAT and VAT belong to the control and obese lines under 40X magnification. The percentage values of UCP1 protein were calculated by ImageJ 1.50e.

Decreased amount of protein was obtained from area value calculation of the amide I band and the area ratios of amide I/ amide I + amide II bands in obese lines indicates possible alterations in obesity-related protein expression. The immunohistological staining results supported FTIR results with a decreased amount of UCP1 proteins in obese lines. Several studies reported that expression of proteins including leptin, TNF- $\alpha$ , IL-6 and adiponectin can increase and decrease in term of different conditions in WAT (Hotamisligil et al., 1995; Makki et al., 2013; Qatanani & Lazar, 2007). Since these proteins were released into the circulatory system after the secretion from adipocytes, they were quantified in circulation (Piya et al., 2013). However, only adiponectin is expressed only from white adipocytes among these proteins. The other proteins are also expressed from other tissues and circulating cells such as hypothalamus, hepatocytes, macrophages (Makki et al., 2013; Piya et al., 2013).

Therefore, the levels of adiponectin can be used to obtain information about the alterations in protein amount in adipose tissues. Consistently, it is known that the adiponectin levels in the plasma and adipose tissue decreased in obese people (Hosogai et al., 2007; Ryo et al., 2004). When taken together with the decrease amount of UCP1 protein, decreased adiponectin expression levels most probably cause a decrease in the amount of total protein in SCAT and VAT in harmony with FTIR results.

## **Part 2: Triglyceride Dependent Differentiation of Obesity in Adipose Tissues by FTIR Spectroscopy Coupled with Chemometrics**

Although the prevalence of obesity in the world is increasing day by day, there is no a very accurate method for the diagnosis of obesity. Body mass index (BMI) and waist circumference (WC) are commonly calculated to estimate whether a person has a healthy weight or not. However, as conventional methods, they are inadequate to identify obesity. For this reason, a practical and accurate method is essential to detect biomarkers of obesity and obesity related metabolic diseases. Since obesity is a metabolic disease leading to elevated levels of triglycerides in the blood circulation resulting in the accumulation of them in adipose tissue, the triglyceride profile could be a key point during the diagnosis of obesity (Koyama et al., 1997). The recent studies have showed that triglycerides are strong predictors of the amount of VAT therefore they could be markers to estimate visceral adiposity (Huang et al., 2015). Consistently, in a previous study, a significant increase in the carbonyl/lipid ratio which indicates the levels of triglycerides and cholesterol esters was observed within the SCAT and VAT in obese BFMI lines, suggesting an increased concentration of the triglycerides (Nara et al., 2002; Voortman et al., 2002). In addition, the storage of triglycerides and lipids within adipose tissue is positively correlated with the insulin resistance (Pan et al., 1997; Phillips et al., 1996). In the light of this information, we focused on spectral differences in triglyceride region located at  $1770\text{-}1720\text{ cm}^{-1}$  which can be a key point in internal diagnosis of abdominal obesity with or without insulin resistance. In current part, the aim was to explore a rapid diagnosis method by detecting triglyceride bands as a more sensitive biomarker of obesity and obesity-related insulin resistance.

In accordance with this diagnostic approach, ATR-FTIR spectroscopy was preferred as a rapid and low cost effective technique and the multivariate data analysis, namely HCA and PCA were performed to differentiate the control and obese groups based on spectral differences in the triglyceride region located at  $1770\text{-}1720\text{ cm}^{-1}$ . Since the PCA and HCA

use different algorithms and base upon the similarities and dissimilarities of individuals of the different groups, we performed these techniques as rapid and reliable analysis methods in diagnostic studies. Firstly, PCA was used to investigate the possible clustering of samples and to detect IR spectral bands that can distinguish the control and obese individuals. According to PCA results, the most significant difference in loading plots of control and obese groups was obtained from the 1770–1720  $\text{cm}^{-1}$  region assigned to triglyceride band (Figure 25A and 25B). This result stated that the triglyceride region has a crucial contribution in the discrimination of the control and obese groups for SCAT and VAT.

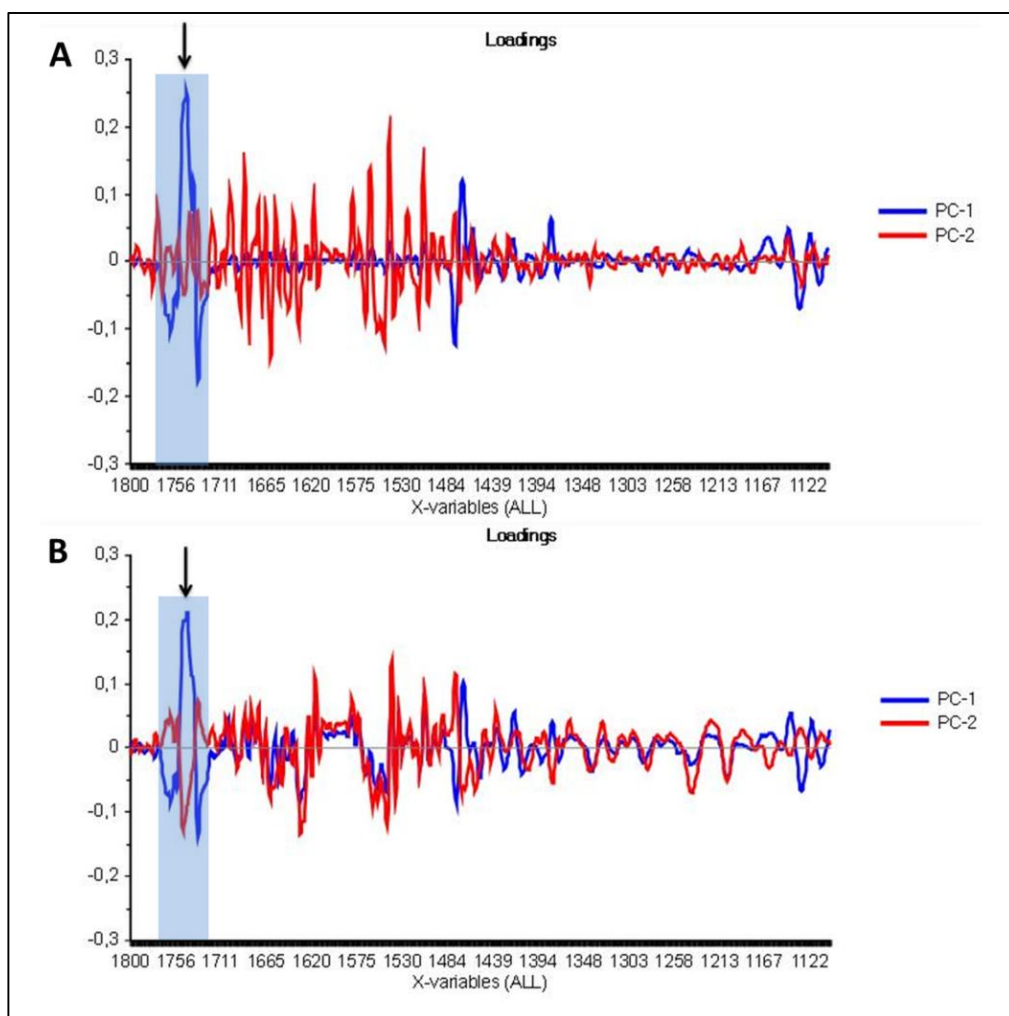


**Figure 25.** PCA loading plots for VAT (A) and SCAT (B) of control and obese groups in the 1800–1000  $\text{cm}^{-1}$  spectral region. The triglyceride region is shown by arrow.



The comparative spectra of the control and obese lines in the 1800-1000  $\text{cm}^{-1}$  range and also the broaden panel zooms in the triglyceride region in the 1770-1720  $\text{cm}^{-1}$  spectral region are shown in Figure 26. To show intensity differences between the control and obese groups in the triglyceride band, the spectra were min max normalized with respect to the amide A band located at 3300  $\text{cm}^{-1}$ . Consistently, the apparent spectral differences between the control and obese lines were obtained in the triglyceride region. In addition, the spectra of BFMI852 and 856 lines were quite similar and the intensity values were higher than the control group slightly. However, BFMI860 and 861 lines showed a significant increase compared to the control group in terms of the intensity values (Figure 26).

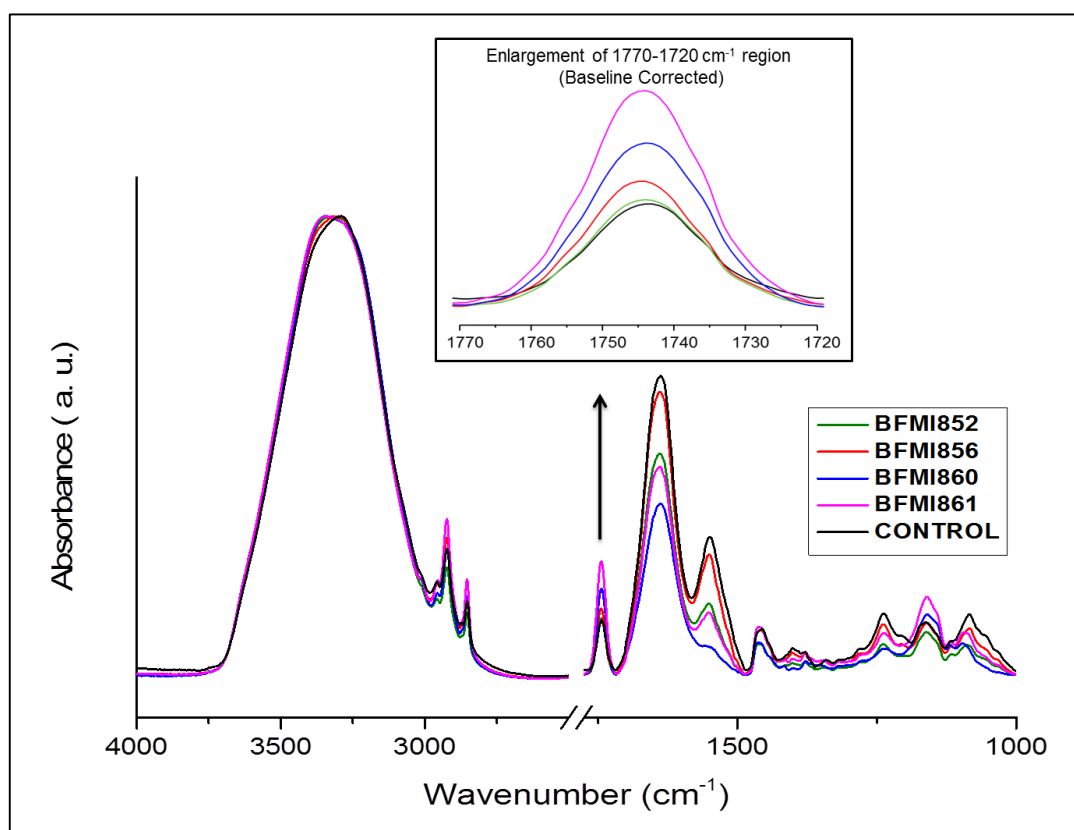


**Figure 26.** Representative ATR-FTIR spectra of the control and obese lines in the 1800–1000  $\text{cm}^{-1}$  spectral region and enlarged panel of baseline corrected version of the triglyceride region (1770-1720  $\text{cm}^{-1}$ ). The spectra were normalized to the band located at 3300  $\text{cm}^{-1}$ .

To investigate the amount of triglycerides in more detail, the band area values were calculated for control and obese lines in SCAT and VAT, which are shown in Table 5. As seen from the table, a higher triglyceride content was obtained in the BFMI852 and 856 lines compared to the control group. In addition, the BFMI860 and 861 lines indicated a more significantly higher triglyceride content in comparison to control group implying the higher triglyceride content especially in SCAT. When the obese lines were compared, BFMI860 and 861 lines showed a significant increase in the content of triglycerides than that of BFMI852 and 856 lines. On the other hand, to find out associations between VAT and SCAT, Pearson correlation coefficient of the triglyceride band area values of these adipose tissues was calculated and a strong positive correlation ( $r = 0.984$ ,  $p < 0.0001$ ) was achieved as shown in Figure 27.

**Table 5.** The alterations in band area values of the triglyceride band for the control and obese lines in SCAT and VAT.

|   | <b>Control</b> | <b>BFMI852</b> | <b>BFMI856</b> | <b>BFMI860</b>   | <b>BFMI861</b>     |
|---|----------------|----------------|----------------|------------------|--------------------|
| <b>SCAT</b>   | 0,81±0.04      | 1,49±0.09**    | 1,50±0.15**    | 2,07±0.08***,†,‡ | 2,16±0.15***,†,‡,§ |
| <b>VAT</b>  | 0,70±0.02      | 1,23±0.10*     | 1,29±0,22*     | 1,92±0.08***,†,‡ | 1,98±0.04***,†,‡,§ |
| <p>“The values are the mean ± standard error of the mean for each group. Comparison was performed by one-way ANOVA and Tukey’s test was used as a post hoc test. The degree of significance was denoted with asterisks (*) for the comparison of the control group with other BFMI lines, with daggers (†) for the comparison of BFMI852 with other BFMI lines, with double daggers (‡) for the comparison of BFMI856 with other BFMI lines, and with gamma (γ) for the comparison of BFMI860 with other BFMI lines. P values less than or equal to 0.05 were considered as statistically significant; *P &lt; 0.05; **P &lt; 0.01; ***P &lt; 0.001.”</p> |                |                |                |                  |                    |

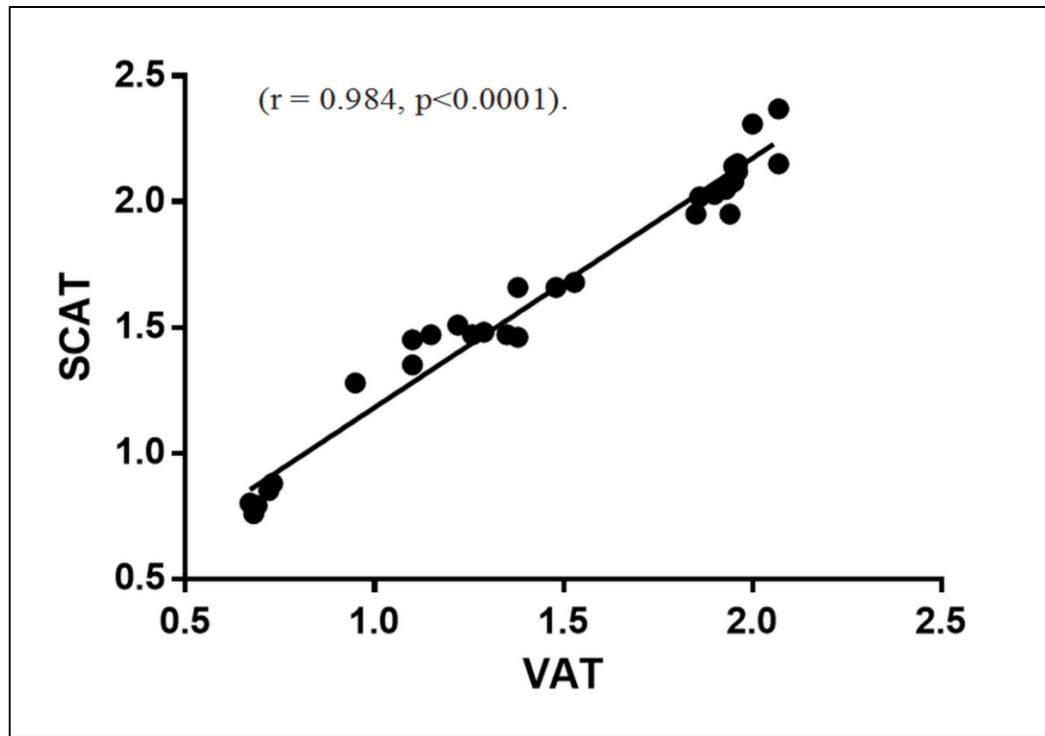


**Figure 27.** Correlation between VAT and SCAT. Spearman correlation coefficient ( $r$ ) and  $p$  value are provided on each panel. Calculations were performed using GraphPad (Prism version 6).

The correlation between SCAT and VAT can be important in harvesting of tissue samples for bariatric operations and biopsies because the location of SCAT which is just beneath skin, is more accessible than VAT. The bariatric operations enable to obtain large amounts of adipose tissue from human SCAT and VAT (Hagman et al., 2012; van Beek et al., 2014). New biopsy needle techniques are also used for sampling of SCAT with minimal discomfort by a percutaneous approach (Alderete et al., 2014). SCAT regions that are more easily accessible by transcutaneous biopsy make this tissue more practical compared to VAT for clinical studies with humans (Bigornia et al., 2012). It has been reported that Near-infrared (NIR) spectroscopy was performed to scan and measure the SCAT content non-invasively in human studies (Azizian et al., 2008; Bashkatov et al., 2005; Conway et al., 1984). In addition, a new method of in vivo lipid content determination in the SCAT

from the ear of humans or animals was developed via NIR spectroscopy (Hormoz Azizian et al., 2003).

Since the qualitative changes in several human adipose tissue stores are affected simultaneously by the whole body metabolic dysfunctions, SCAT correlate with VAT strongly in terms of the symptoms of obesity (Bigornia et al., 2012). SCAT is divided into two layers anatomically, i.e. superficial SCAT (sSCAT) and deep SCAT (dSCAT) in the abdominal region. The dSCAT located under Scarpa's fascia is more related to VAT than to sSCAT in terms of lobular organization and adipocyte size. These two types of SCAT and VAT have similar structure of vessel density and the amount of fibrosis. Both type of these tissues are related to triglycerides and HDL cholesterol in women and men (Fox et al., 2007; Tordjman et al., 2012). As stated in literature, dSCAT is associated with insulin resistance as well as VAT (Bigornia et al., 2012; Smith et al., 2001; Tulloch-Reid et al., 2004). It is known that the storage of triglycerides within adipose tissue is positively associated with the obesity related insulin resistance therefore SCAT is strongly correlated with VAT with respect to the symptoms of obesity related insulin resistance. Also, both SCAT and VAT are associated with chronic inflammation so they have similarly positive correlation with C-reactive protein, fibrinogen, tumor necrosis factor receptor-2, intercellular adhesion molecule-1, interleukin-6, and P-selectin (Pou et al., 2007). The inflammatory level of SCAT arised from the macrophage accumulation is strongly associated with the level of inflammation in VAT (Bigornia et al., 2012).

The hierarchical clustering can be performed coupled with FTIR spectroscopy to organize FTIR spectra set into clusters depending upon spectral differences. In the current study, HCA used these differences in the triglyceride region as an input data. To explore discrimination power between all obese lines, HCA was performed for 4 lines in the 1770-1720  $\text{cm}^{-1}$  region. As a result, BFMI 860 and 861 lines were completely separated from BFMI 852 and 856 lines for SCAT and VAT (Figure 28). Hence, the BFMI 860 and 861 lines were regarded as one group and the BFMI 852 and 856 lines as another group. The sensitivity and specificity values were calculated and achieved as 100% for both adipose

tissues. Moreover, PCA results revealed an apparent differentiation of these obese lines from each other in score plots. As seen from the figure 28, the BFMI 860-861 lines and BFMI 852-856 lines were distinguished from each other successfully for both SCAT and VAT.

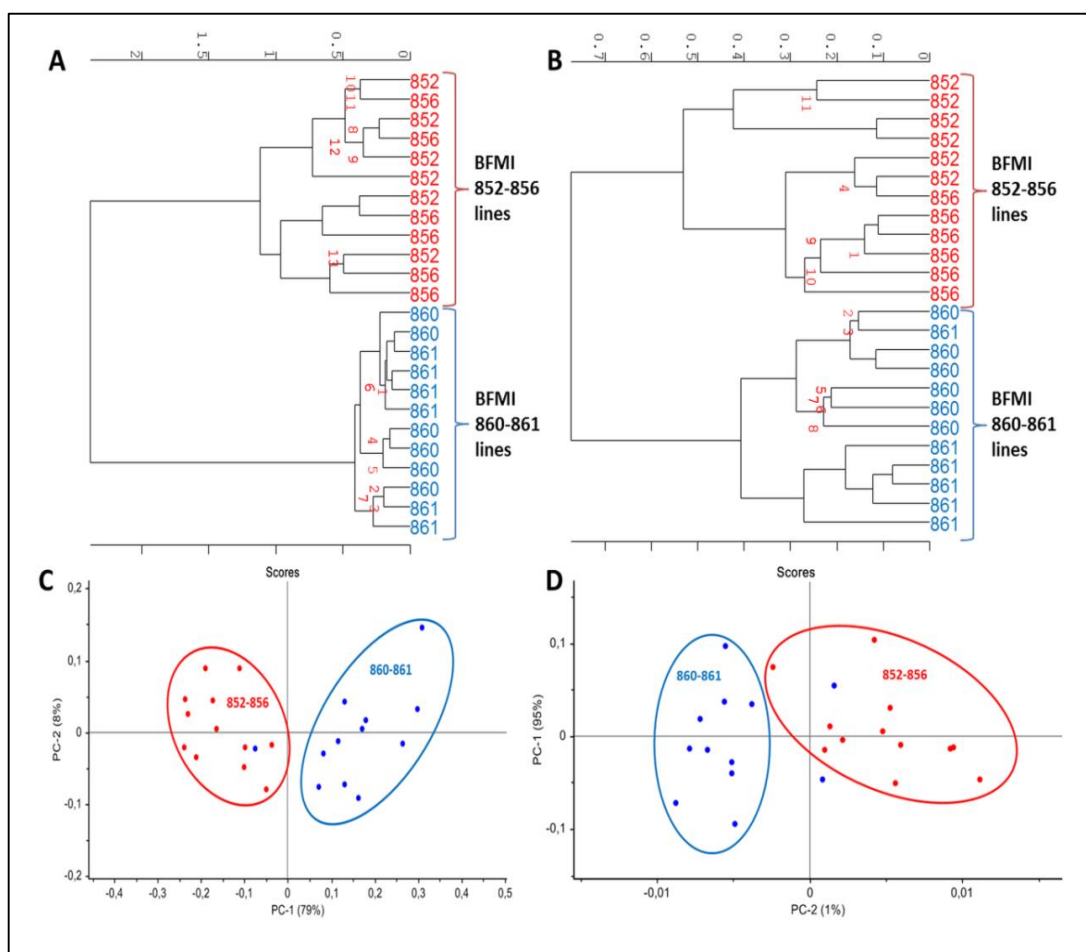


**Figure 28.** Hierarchical clustering of BFMI lines (852, 856, 860, 861) in SCAT (A) and VAT (B) in the 1770-1720  $\text{cm}^{-1}$  spectral region. PC1 versus PC2 scores plot of the second derivative vector normalized spectra in the same range of BFMI lines in SCAT (C) and VAT (D). Obese group (BFMI852-856) (red), obesity related insulin resistant group (BFMI860-861) (blue).

In the light of all the results, grouping of the BFMI860 and 861 lines together in HCA and PCA results may be an evidence that these lines show similar symptoms that are different from the others (BFMI 852 and 856). Consistently, it was concluded that BFMI 860-861 lines indicate more triglyceride accumulation when compared to that of BFMI 852-856 lines because they may be more affected from the obesity. Supporting this hypothesis, in previous part, a significant increase in the carbonyl/lipid ratio was reported within the SCAT and VAT of the BFMI860 and BFMI861 lines indicating an enhanced concentration of ester groups belonging to triglycerides (Kucuk Baloglu et al., 2015). An FTIR spectroscopic study reported that the BFMI860 and 861 lines showed significantly higher amounts of triglyceride compared to the control groups in muscle tissues implying an impaired insulin sensitivity and these results were also confirmed by HPLC-ELSD studies (Sen et al., 2015). Another HPLC-ELSD study revealed that a higher triglyceride concentration was obtained in BFMI860-861 lines in comparison to the BFMI852-856 lines in VAT (Baser, 2013). It was reported that the BFMI860 line indicated symptoms of the metabolic syndrome and insulin resistance in consequence of intraperitoneal glucose tolerance (ipGTT) and intraperitoneal insulin tolerance (ipITT) tests and biochemical tests for blood glucose, insulin, leptin, and adiponectin (Hantschel et al., 2011). Additionally, as stated in literature, the BFMI861 line can be used as an animal model for type 2 diabetes and insulin resistance (Wagener et al., 2006). From all this information, the BFMI852 and BFMI856 lines were combined into one group that will be denominated as obese group and the BFMI860 and BFMI861 lines were combined into another group that will be denominated as obesity related insulin resistant group in the rest of the study.

In the current study, since the purpose was to distinguish the control, obese and obesity related insulin resistant groups by using ATR-FTIR spectroscopy, the spectral data were coupled with chemometrics as a diagnostic tool in both SCAT and VAT. Coherently, in HCA results, a successful differentiation between the control and two different obese groups in the  $1770\text{-}1720\text{ cm}^{-1}$  region was obtained as shown in Figure 29A and 29B. If the obese and obesity related insulin resistant groups were considered together, the HCA results showed that all obese groups were successfully differentiated from the control

group for both SCAT and VAT. As a result, the sensitivity and specificity values were obtained as 100% for both adipose tissues in the triglyceride region. In cluster analysis, the higher heterogeneity points the existence of higher differences between groups. SCAT indicated the highest heterogeneity value of 5 in differentiation of the control and different obese samples. Whereas, a lower heterogeneity value of 2 was obtained in the differentiation of the control and different obese samples of VAT. These results implied that SCAT was more dramatically affected from obesity compared to VAT. This may be the reason that the SCAT is the prior storage place for lipids. The adipocytes in SCAT store FFAs primarily and the excess FFAs and glycerol are accumulated as triglycerides into SCAT (Freedland, 2004). Since the accumulation capacity of SCAT is limited because of the hypertrophy, the excess lipids can also be stored in the VAT (Hardy et al., 2012a). Increased SCAT and VAT mass is the main reason of obesity leading to damaged lipid and glucose metabolism (Bays et al., 2008). Consistently, the VAT also showed significant heterogeneity values in HCA. The extreme deposition and so catabolism of triglycerides in VAT result in the excess release of FFAs into the hepatic portal vein (Björntorp, 1990). The excessive releasing of FFAs from VAT into the circulation causes the increased dispense of FFAs to the liver and muscle leading to insulin resistance (Boden & Shulman, 2002).

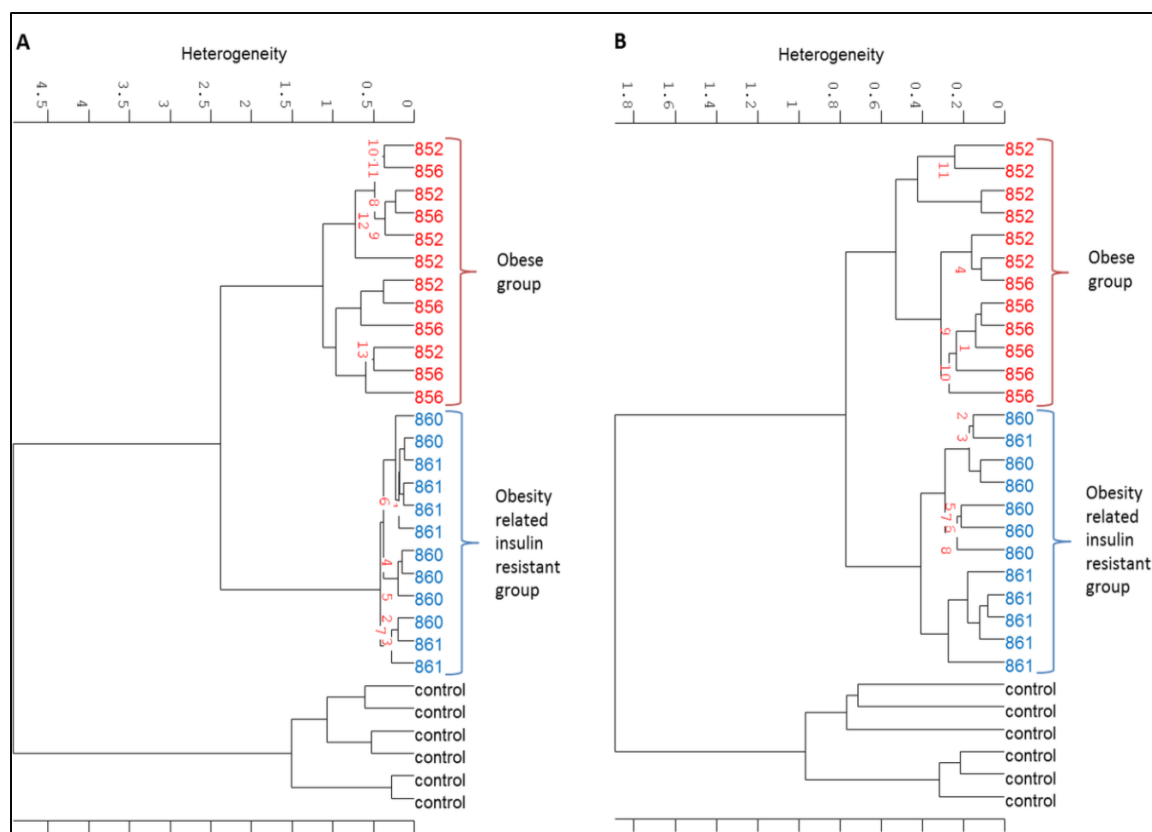


**Figure 29.** Hierarchical clustering of control, obese and obesity related insulin resistant groups in SCAT (A) and VAT (B) in the 1770-1720  $\text{cm}^{-1}$  spectral region. Control group (black), obese group (BFMI852-856) (red), obesity related insulin resistant group (BFMI860-861) (blue).

To explore whether obese and obesity related insulin resistant groups were distinguished individually from the control group, the PCA method was also used for all groups. PCA loading plots in the 1770–1720  $\text{cm}^{-1}$  spectral region for SCAT and VAT samples indicated a high difference between PC1 and PC2 implying a successful differentiation in this region (Figure 30A and 30B). These loadings in composition of SCAT and VAT for all groups were essentially attributed to lipids. The considerable differences between loadings were obtained from C=O stretching of lipids located in 1747 and 1743  $\text{cm}^{-1}$  and the stretching of C=O groups for other lipids like triglycerides located in 1736  $\text{cm}^{-1}$  (Fabian et al., 1995; Holman, 2013; Sukuta & Bruch, 1999). In harmony with these findings, a successful



discrimination of all investigated groups was achieved in a single 2D plot. As shown in Figure 30C and 30D, the PC1 versus PC2 scores plot for the triglyceride region also confirmed the existence of differentiation between the control, obese and obesity related insulin resistant groups in both SCAT and VAT.

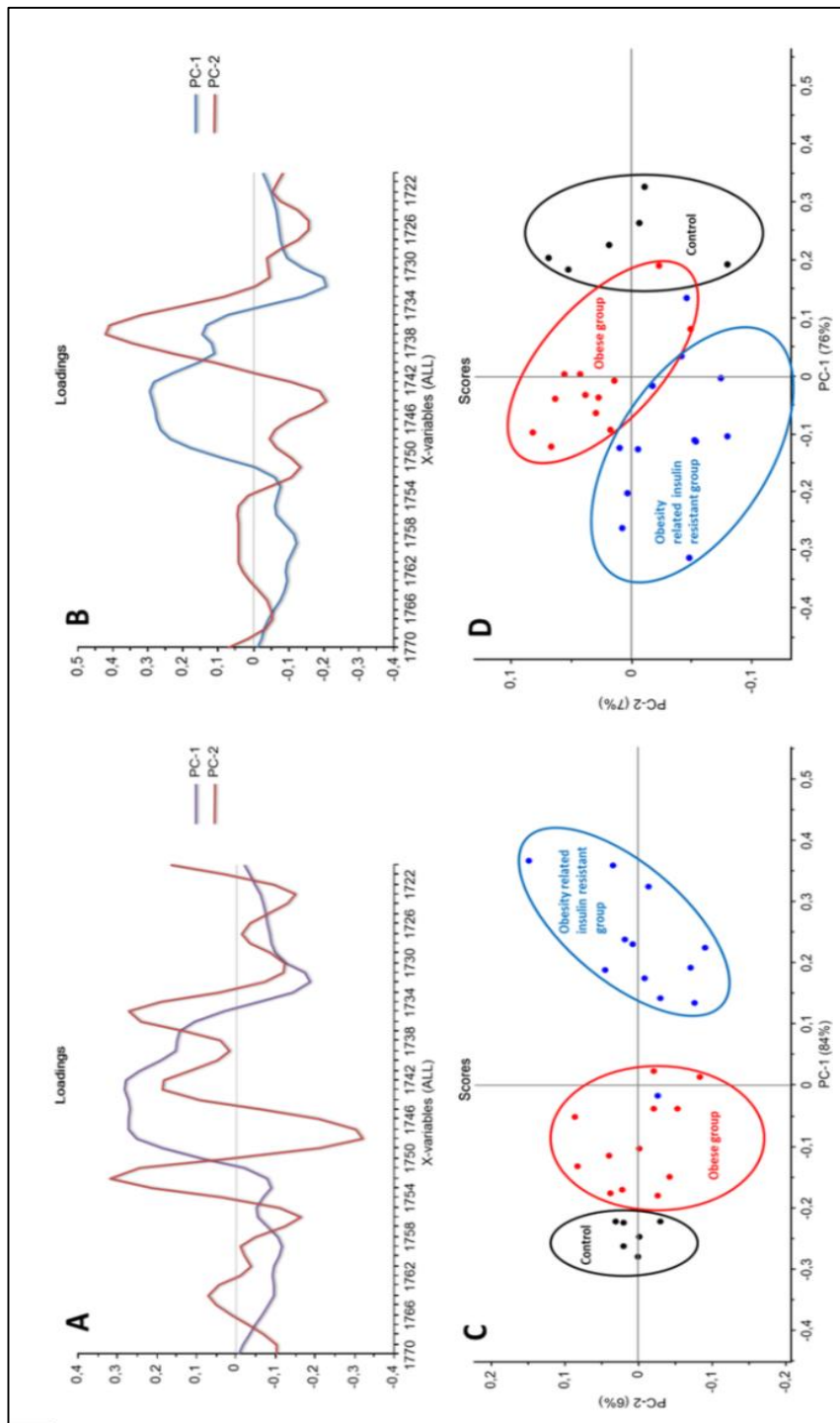


**Figure 30.** PCA loading plots of control, obese and obesity related insulin resistant groups for SCAT (A) and VAT (B) samples in the 1770–1720 cm<sup>-1</sup> spectral region. PC1 versus PC2 scores plot of the second derivative vector normalized spectra in the same range of SCAT (C) and VAT (D). Control group (black), obese group (BFMI852–856) (red), obesity related insulin resistant group (BFMI860–861) (blue).

Since the number of samples used in the PCA was small, the leave-one-out type cross validation was also performed for PCA results. The cross-validation is a powerful general technique when there is not enough data available to divide into training and test sets (Garip et al., 2016; Seni & Elder, 2010). The score plots obtained from the calibration set and the cross validation set were compared so that prediction errors were kept at a minimum level. Since the calibration and cross validation results were very close to each other, we can conclude that the PCA model was reliable. Figure 31 and 32 represent the PCA results obtained from the calibration set and the scores corresponding to leave-one out cross validation for SCAT and VAT, respectively.

In summary, our multivariate analysis results revealed the potential of infrared spectroscopy in differentiation of all obese groups namely obesity related insulin resistant group (BFMI 860-861) and obese group (BFMI 852-856) from control group. Furthermore, the obesity related insulin resistant and obese groups were also distinguished from each other with high sensitivity and specificity values. All of these results supported the powerful differentiation of control, obesity related insulin resistant and obese groups in both SCAT and VAT.

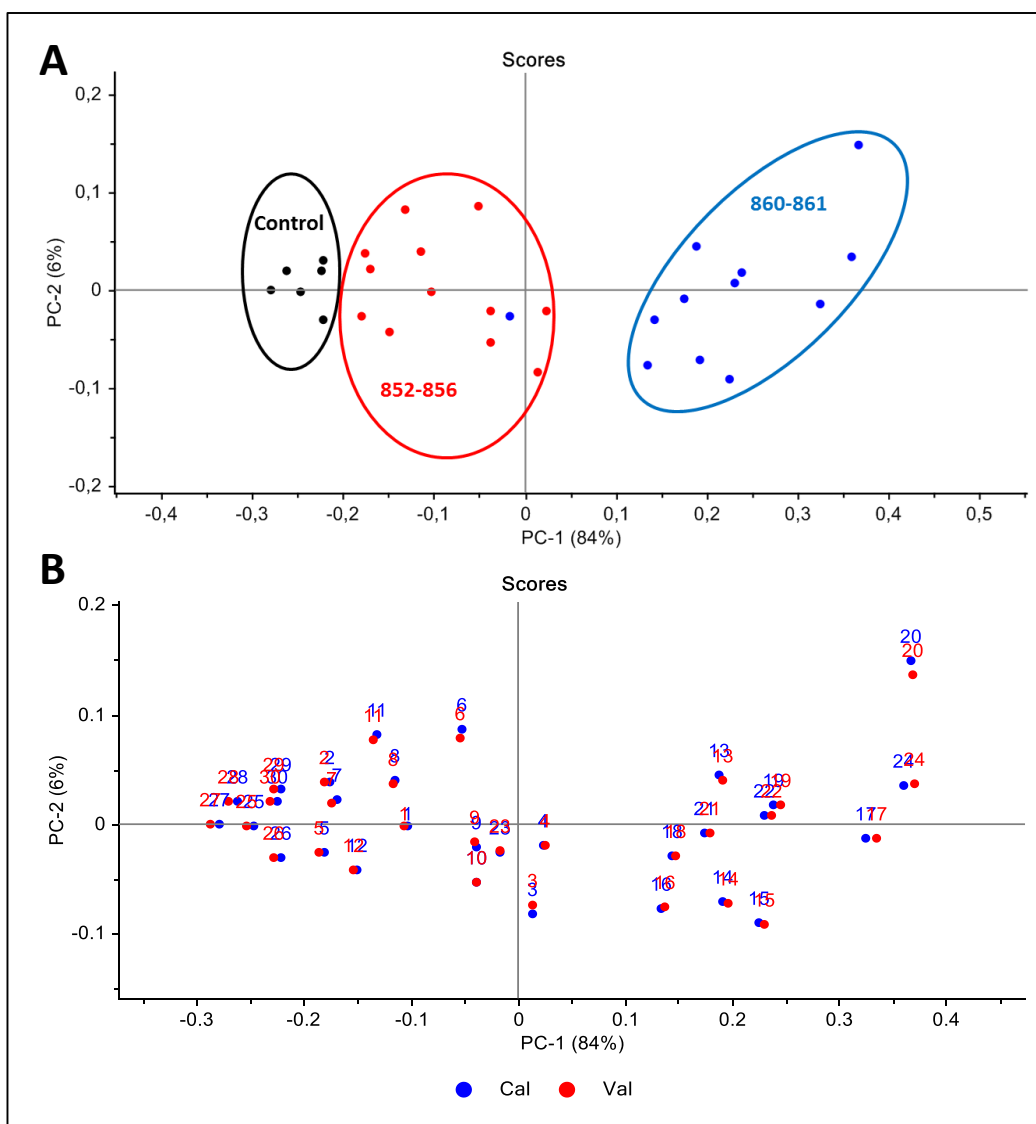


**Figure 31.** PC1 versus PC2 score plots of control, obese and obesity related insulin resistant groups for SCAT (A) samples in the 1770–1720  $\text{cm}^{-1}$  spectral region. Leave-one-out cross validation for SCAT (B) in the same region. Control group (black), obese group (BFMI852-856) (red), obesity related insulin resistant group (BFMI860-861) (blue).

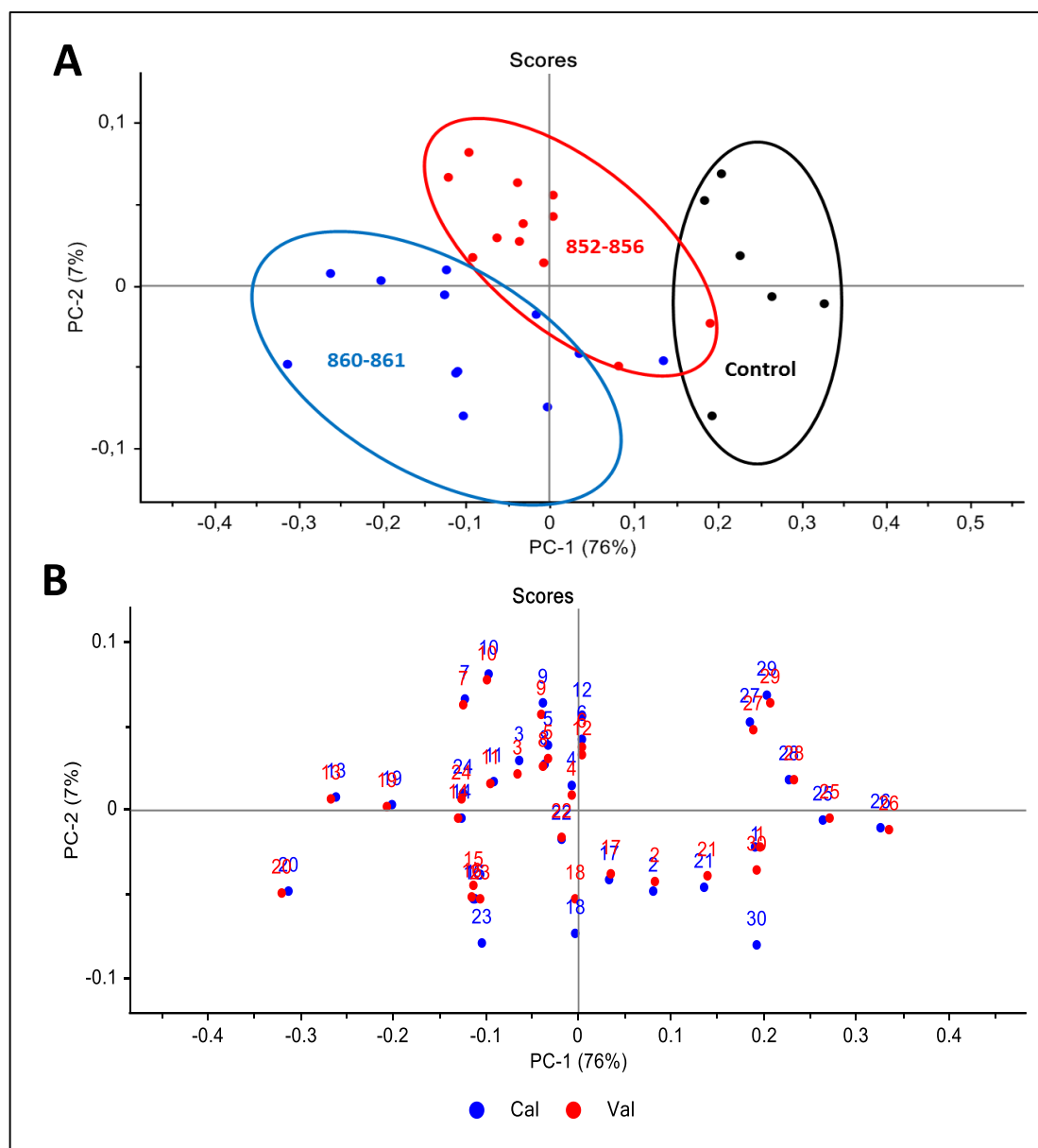


**Figure 32.** PC1 versus PC2 score plots of control, obese and obesity related insulin resistant groups for VAT (A) samples in the 1770–1720  $\text{cm}^{-1}$  spectral region. Leave-one-out cross validation for VAT (B) in the same region. Control group (black), obese group (BFMI852-856) (red), obesity related insulin resistant group (BFMI860-861) (blue).

### **Part 3: Investigation of gender-based differences in the effect of obesity on adipose tissue.**

Biological sex has importance for the evaluation of obesity and obesity related metabolic diseases, because of gender-based distribution, molecular content and pathophysiology of lipids and other biomolecules. This part of the study targets to detect gender-based differences in the effect of obesity on VAT and SCAT in obese mice lines. With this comparative approach, ATR-FTIR spectroscopy coupled with multivariate data analysis was applied to spectra of some special regions in differentiation of the male and female samples. Moreover, the biomolecular characteristics of VAT and SCAT were compared in male and female BFMI mice by FTIR microspectroscopy. Moreover, UCP1 immunohistological staining was used for both male and female samples to compare the amount of brown and white adipocytes in different genders.

Different functional groups in a biomolecule cause characteristic absorbance bands in an FTIR spectrum of the sample of interest (Cakmak et al., 2006; Diem, 1993; Mantsch, 1984). Figure 33 and 34 shows the representative spectra of VAT and SCAT samples of male and female mice in the 4000-650  $\text{cm}^{-1}$  spectral region. As seen from these figures, the spectra of adipose tissue samples show alterations in several bands originating from different functional groups of lipids, proteins, and carbohydrates. In order to indicate the differences visually in detail, the spectra were represented in two separate regions, namely the 3025-2800  $\text{cm}^{-1}$  (C-H region) and the 1800-1000  $\text{cm}^{-1}$  (fingerprint region). Figure 35 and 36 shows the representative infrared spectra of VAT and SCAT samples of male and female mice in the 3050-2800  $\text{cm}^{-1}$  and 1800-1000  $\text{cm}^{-1}$  regions, respectively. The spectra were baseline corrected and normalized with respect to the amide A band for visual demonstration. The main bands are labelled in the figures and detailed band assignments are given in Table 6 (Bortolotto et al., 2005; Bozkurt et al., 2012; Canello et al., 1998; Kneipp et al., 2002; Marcelli et al., 2012; Movasaghi et al., 2008).

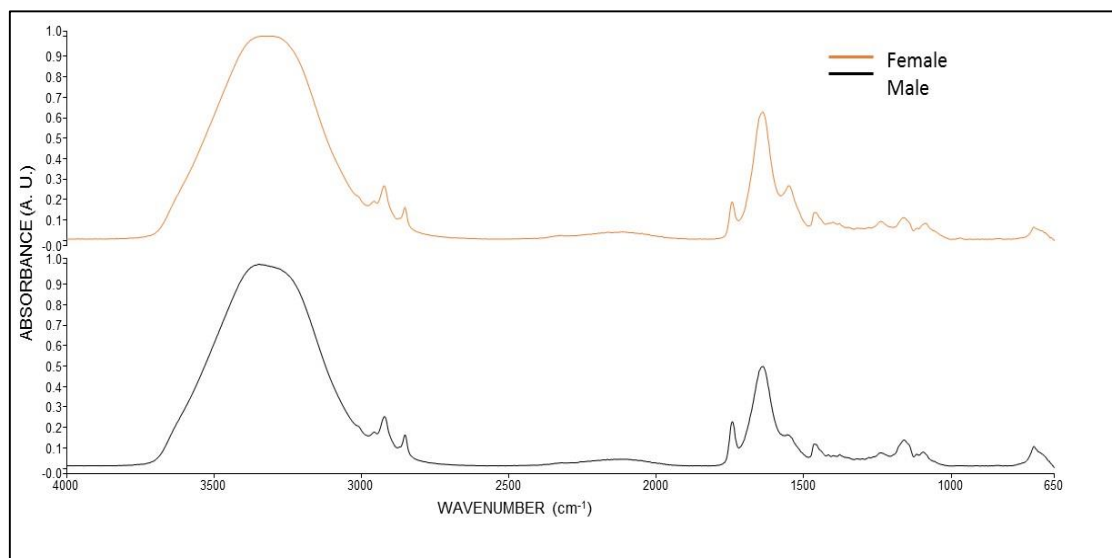


**Figure 33.** The representative FTIR spectra of male and female VAT samples (BFMI860) in the 4000-650  $\text{cm}^{-1}$  region.

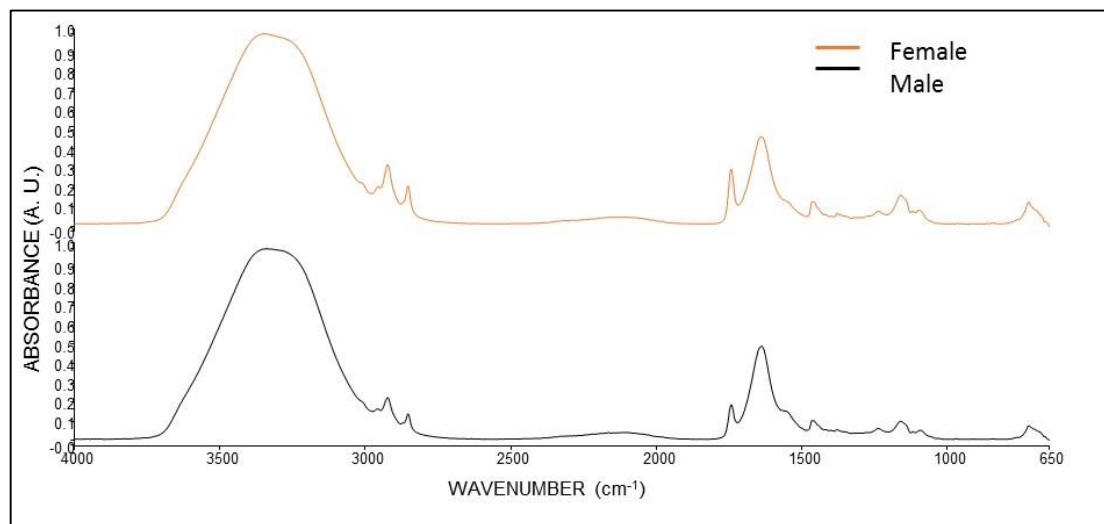


**Figure 34.** The representative FTIR spectra of male and female SCAT samples (BFMI860) in 4000-650  $\text{cm}^{-1}$  region.

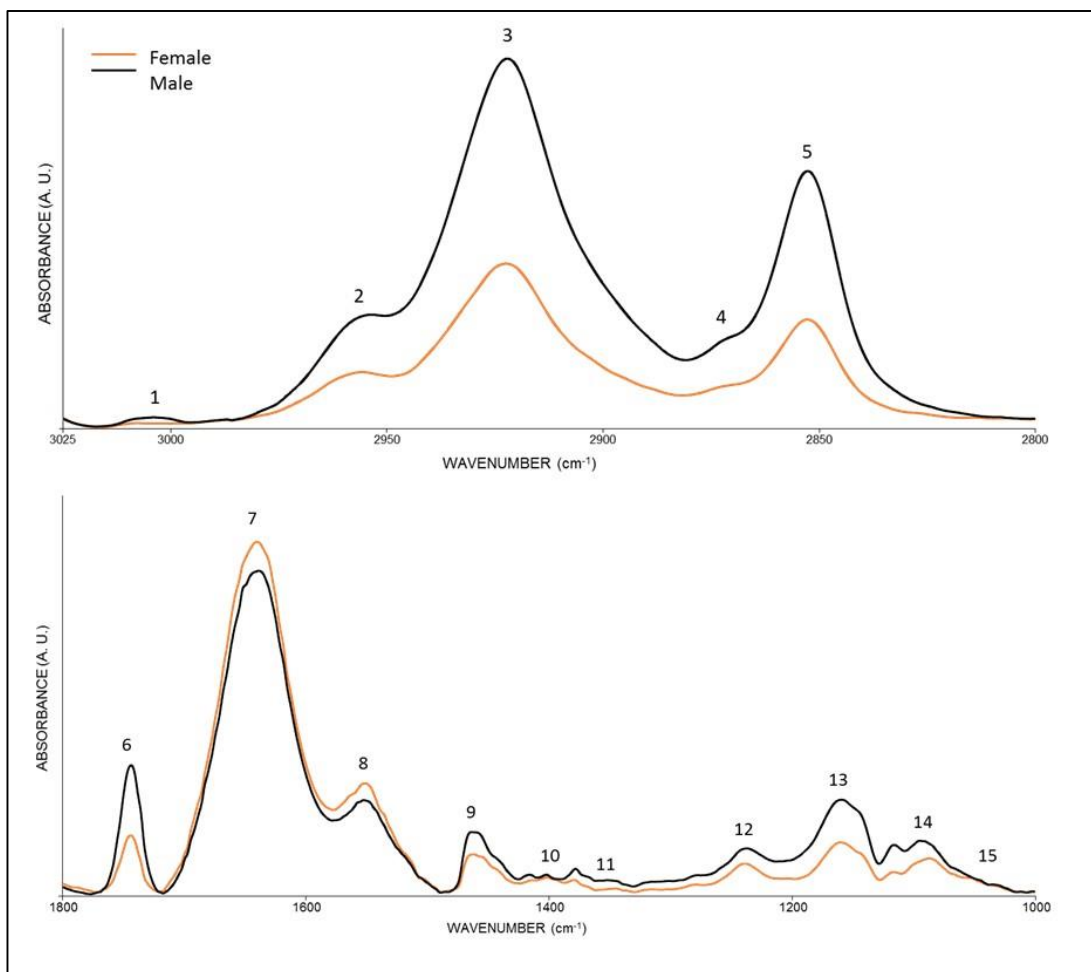


**Figure 35.** Representative infrared spectra of VAT samples of male and female mice in the 3050-2800  $\text{cm}^{-1}$  and 1800-1000  $\text{cm}^{-1}$  regions. (The spectra were baseline corrected and normalized with respect to the Amide A band for visual demonstration).



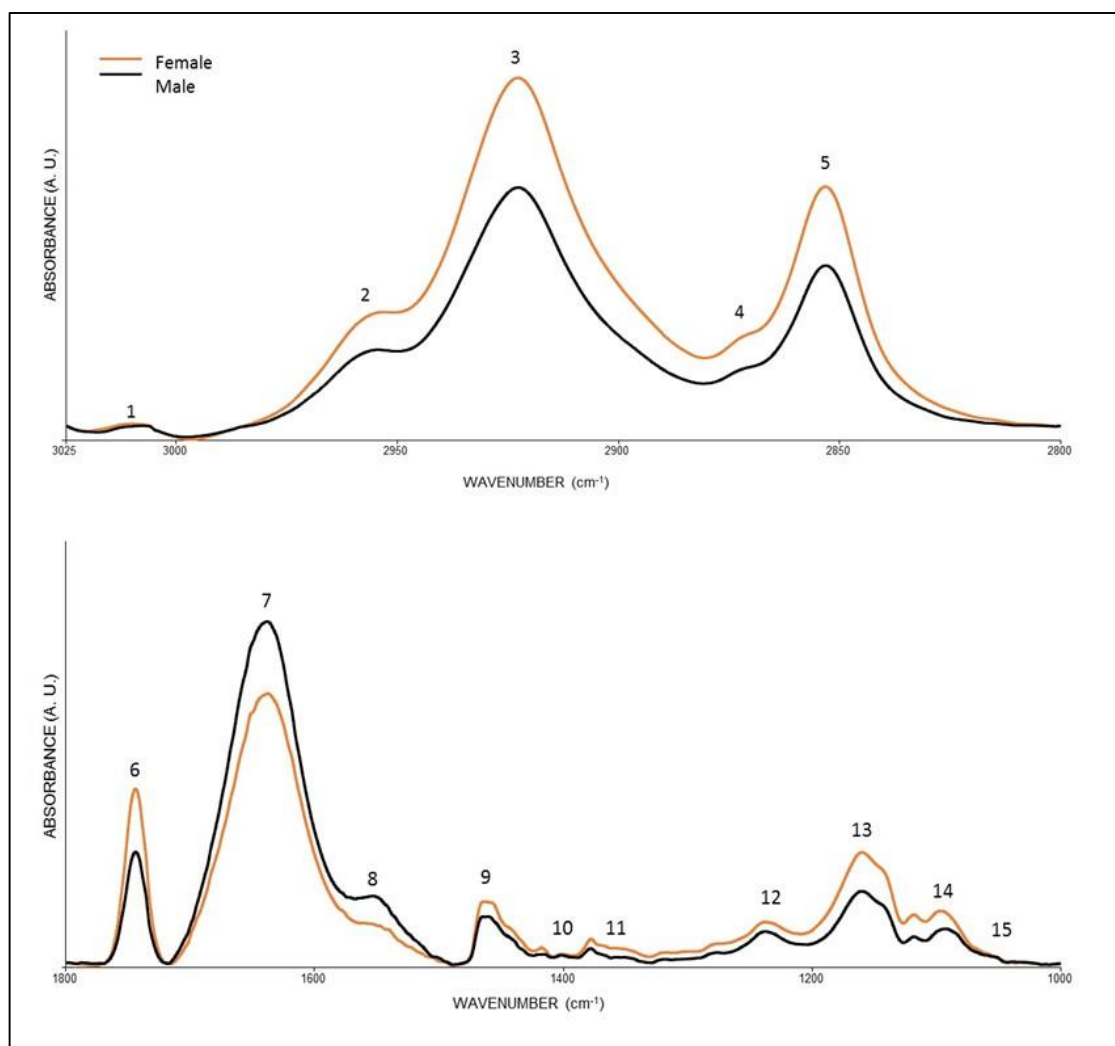


**Figure 36.** Representative infrared spectra of SCAT samples of male and female mice in the 3050-2800  $\text{cm}^{-1}$  and 1800-1000  $\text{cm}^{-1}$  regions. (The spectra were baseline corrected and normalized with respect to the Amide A band for visual demonstration).

**Table 6.** General band assignment of FTIR spectrum of adipose tissues based on literature.

| Band No | Definition of the spectral assignment |   |
|---------|---------------------------------------|---|
| 1       | 3005                                  | Olefinic=CH stretching vibration: unsaturated lipids, cholesterol esters  |
| 2       | 2957                                  | CH <sub>3</sub> anti-symmetric stretching: lipids, protein side chains, with some contribution from carbohydrates and nucleic acids   |
| 3       | 2924                                  | CH <sub>2</sub> anti-symmetric stretching: mainly lipids, with some contribution from proteins, carbohydrates, nucleic acids  |
| 4       | 2875                                  | CH <sub>3</sub> symmetric stretching: protein side chains, lipids, with some contribution from carbohydrates and nucleic acids  |
| 5       | 2855                                  | CH <sub>2</sub> symmetric stretching: mainly lipids, with some contribution from proteins, carbohydrates, nucleic acids   |
| 6       | 1744                                  | Ester C=O stretch: triglycerides  |
| 7       | 1654                                  | Amide I (protein C=O stretching)  |
| 8       | 1545                                  | Amide II (protein N-H bend, C-N stretch)  |
| 9       | 1456                                  | CH <sub>2</sub> bending: lipids   |
| 10      | 1400                                  | COO <sup>-</sup> symmetric stretching: fatty acids  |
| 11      | 1343                                  | CH <sub>2</sub> side chain vibrations of collagen   |
| 12      | 1237                                  | Sulfate stretch from proteoglycans, collagen amide III vibration with significant mixing with CH <sub>2</sub> wagging vibration from the glycine backbone and proline sidechain |
| 13      | 1160                                  | CO-O-C anti-symmetric stretching: phospholipids, triglycerides and cholesterol esters   |
| 14      | 1083                                  | PO <sub>2</sub> <sup>-</sup> symmetric stretching: nucleic acids and phospholipids. C-O stretch: glycogen, polysaccharides, glycolipids   |
| 15      | 1052                                  | C-O stretching: polysaccharides (glycogen)  |

As can be seen from the figures given above, the male and female samples contain different vibrational modes especially in the C-H region ( $3025\text{--}2800\text{ cm}^{-1}$ ) and the fingerprint region ( $1800\text{--}1000\text{ cm}^{-1}$ ). To determine whether or not there is a discrimination between male and female samples, firstly PCA was performed to male and female spectra in the whole IR spectral region. The loading plots of the second derivative vector normalized spectra in the whole range of VAT and SCAT are given in figures 37 and 38, respectively.

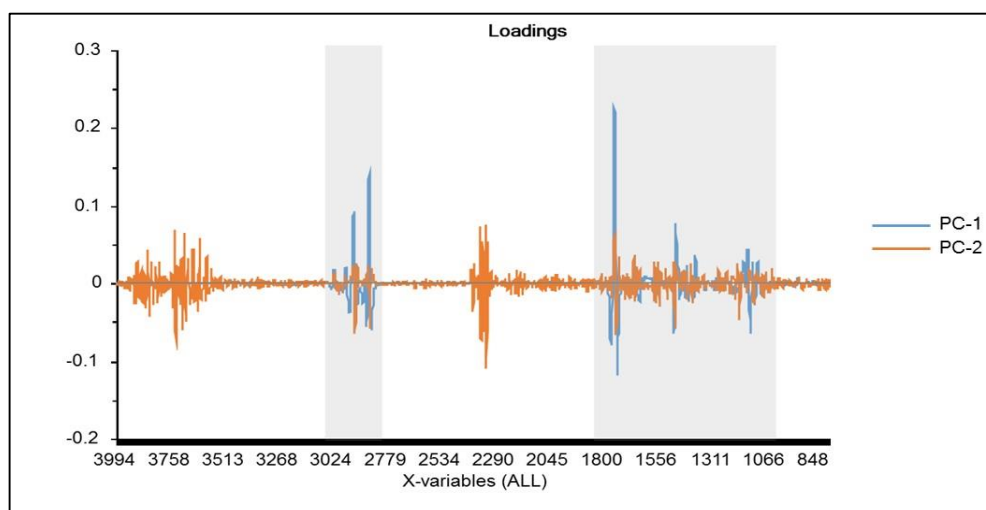


**Figure 37.** PC1 versus PC2 scores plot of the second derivative vector normalized spectra in the whole range of VAT.

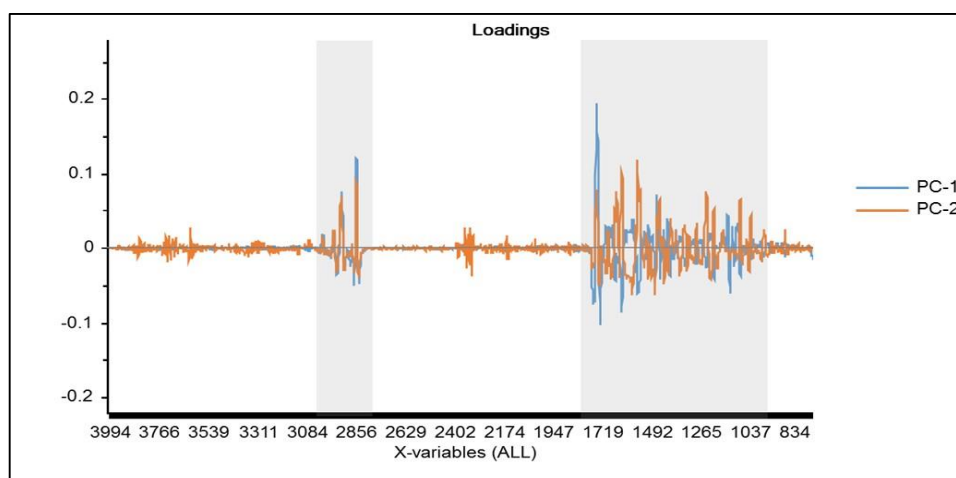


**Figure 38.** PC1 versus PC2 scores plot of the second derivative vector normalized spectra in the whole range of SCAT.

In consistence with previous results, the loading plots obtained from male and female groups spectra indicated that the most dramatic changes in the loading values belong to the 3025-2800  $\text{cm}^{-1}$  (C-H) and the 1800-1000  $\text{cm}^{-1}$  (fingerprint) regions in both types of adipose tissues. These results revealed that the C-H region and fingerprint region have important contribution in the discrimination of the male and female groups for SCAT and VAT. Thereupon, to provide the separation of male and female groups, we also applied PCA to these spectra in the C-H and the fingerprint regions. Consistently, PCA score plots revealed an apparent differentiation of these groups from each other. As seen from figure 39 and 40, the male and female groups were distinguished from each other successfully in C-H region and fingerprint region for VAT. Similarly, the score plot results of the male and female groups with a successful discrimination in C-H region and fingerprint region for VAT were represented in figure 41 and 42, respectively.

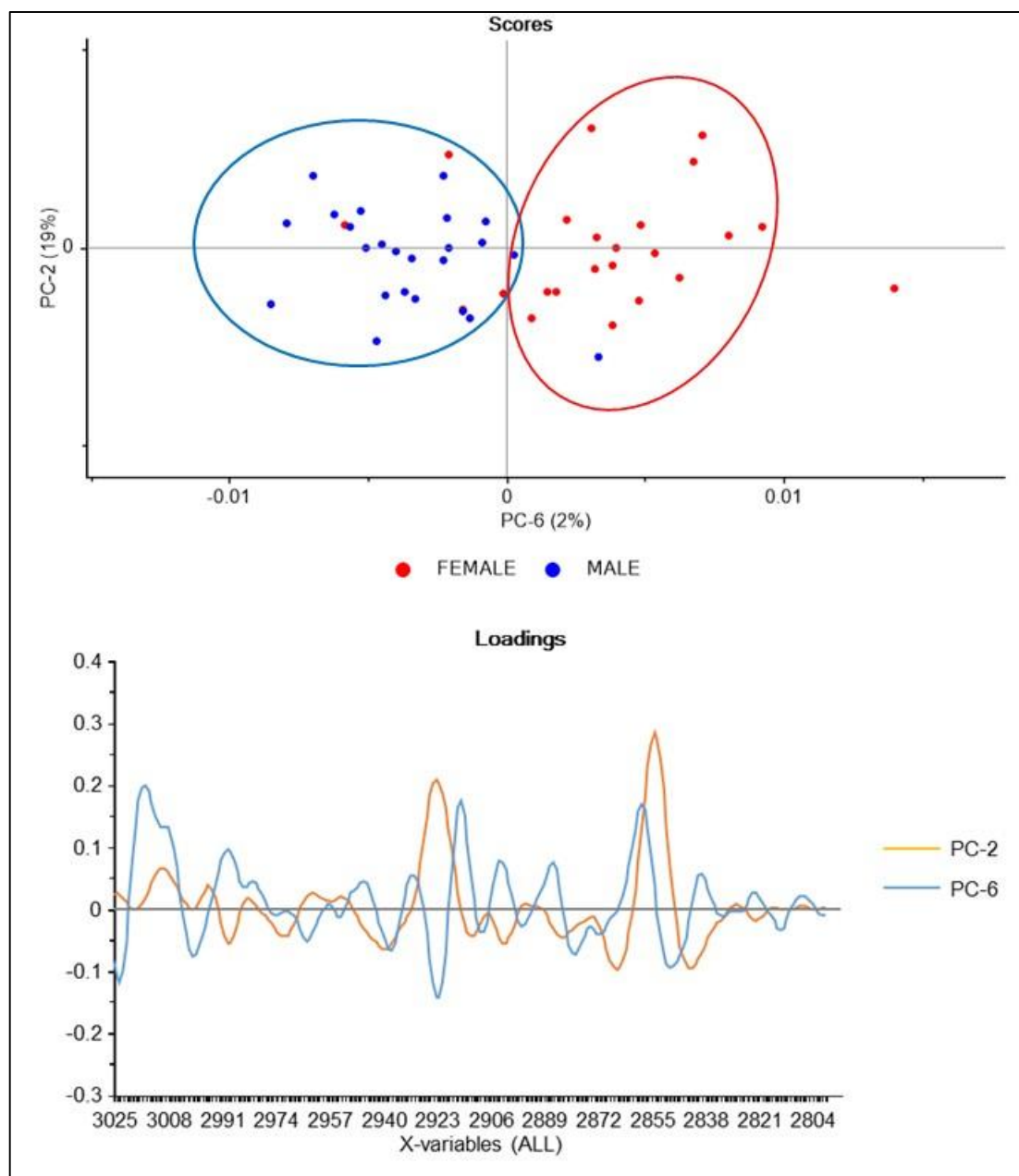


**Figure 39.** PCA loading plots of male and female groups for VAT samples in the C-H region (3025–2800  $\text{cm}^{-1}$ ) (above). PC2 versus PC6 scores plot of the second derivative vector normalized spectra in the same range of VAT (below).

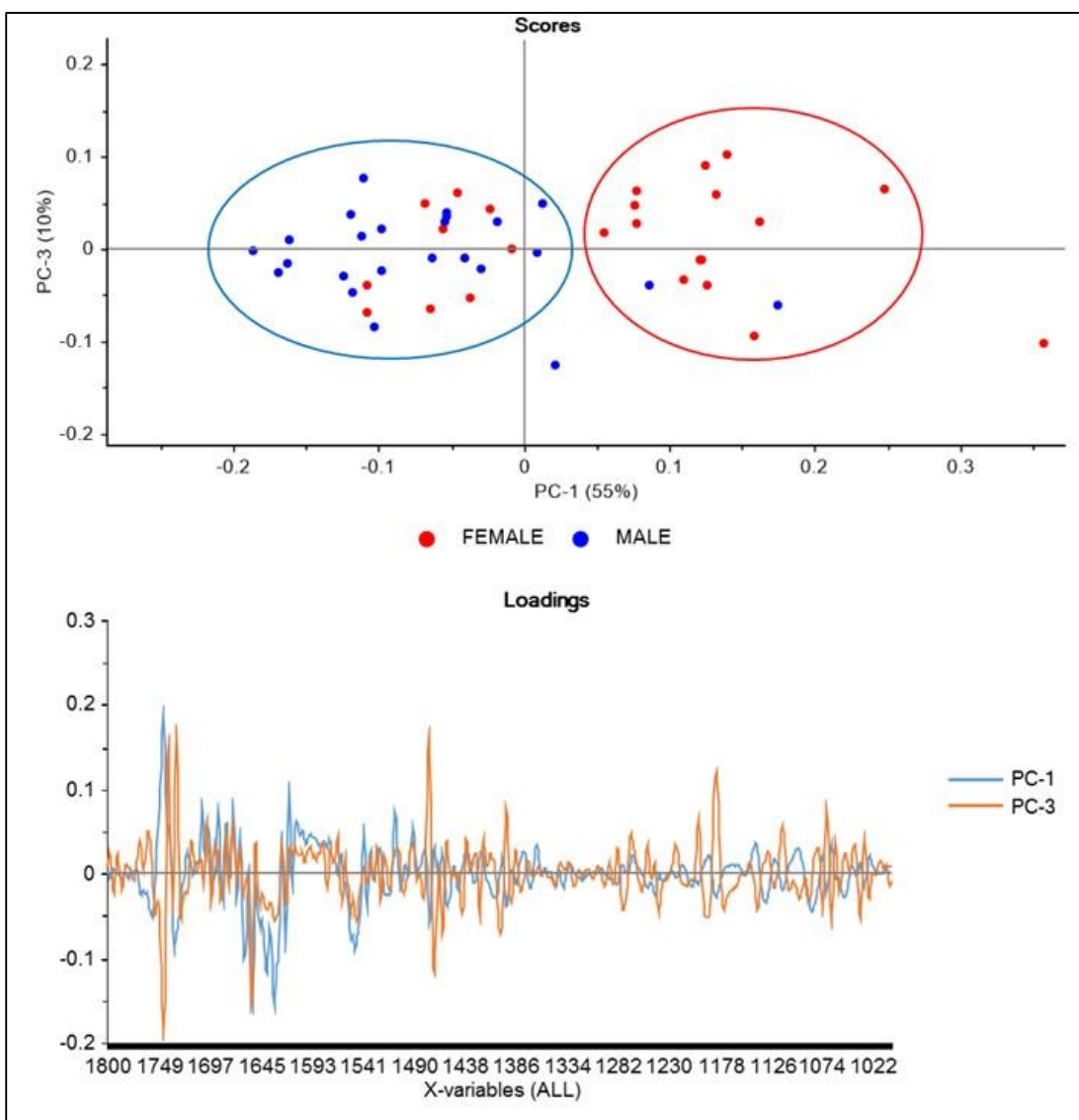


**Figure 40.** PCA loading plots of male and female groups for VAT samples in the fingerprint region (1800–1000  $\text{cm}^{-1}$ ) (above). PC1 versus PC3 scores plot of the second derivative vector normalized spectra in the same range of VAT (below).

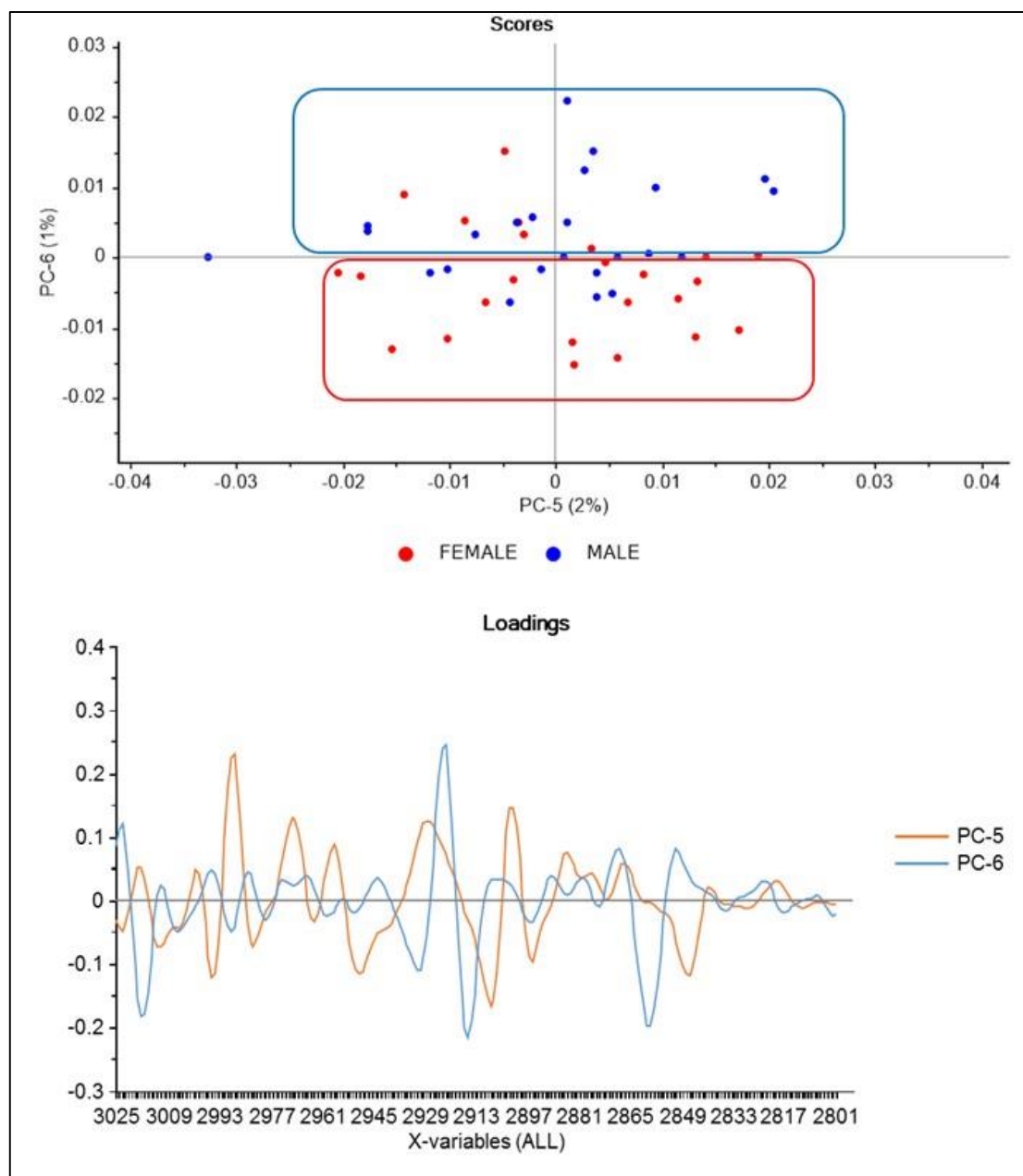


**Figure 41.** PCA loading plots of male and female groups for SCAT samples in the C-H region (3025–2800  $\text{cm}^{-1}$ ) (above). PC5 versus PC6 scores plot of the second derivative vector normalized spectra in the same range of SCAT (below).

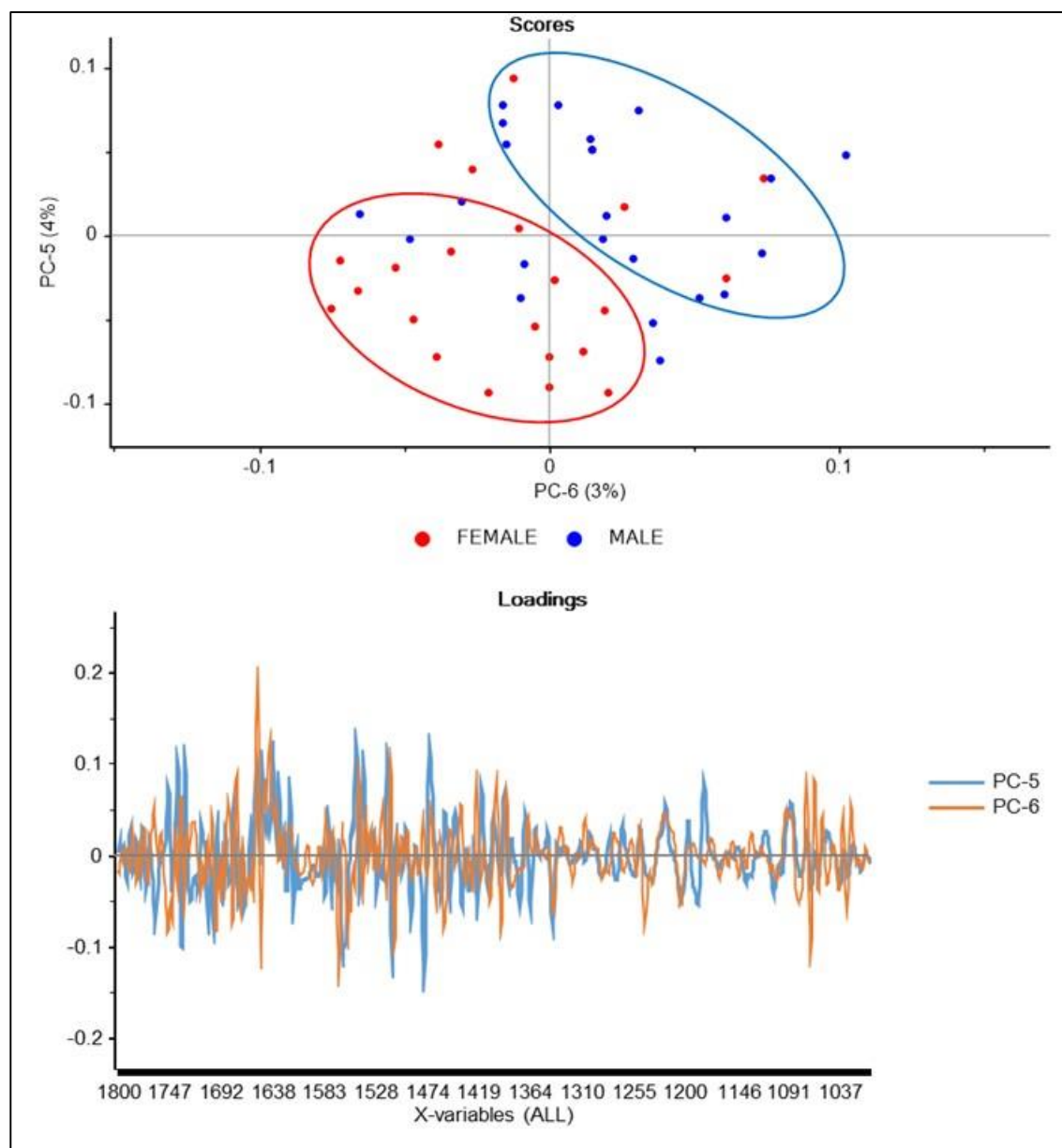


**Figure 42.** PCA loading plots of male and female groups for SCAT samples in the fingerprint region (1800–1000 cm<sup>-1</sup>) (above). PC5 versus PC6 scores plot of the second derivative vector normalized spectra in the same range of SCAT (below).



To confirm the separation of the male and female groups from each other, HCA was also performed to the male and female spectra in C-H region and fingerprint region. Coherently, in HCA results, a successful differentiation between the male and female obese groups in the C-H region and fingerprint region was obtained in VAT and SCAT as shown in Figure 43 and 44, respectively. The sensitivity and specificity values were obtained as shown in table 7. The HCA results showed that all biological gender groups were successfully differentiated from each other for both SCAT and VAT with higher values in the C-H region and fingerprint region.

**Table 7.** Definitions and obtained values for sensitivity and specificity during HCA based on male and female spectral data in VAT and SCAT.

**Cluster analysis results based on FTIR data**

|                | Positive | Negative |                               |
|----------------|----------|----------|-------------------------------|
| <b>Obese</b>   | A        | B        | <b>Sensitivity = A/ (A+B)</b> |
| <b>Control</b> | C        | D        | <b>Specificity = D/ (C+D)</b> |

***Positive and negative values:***

A: “Number of male animals clustered in male group (true positive)”

B: “Number of male animals clustered in female group (false negative)”

C: “Number of female animals clustered in male group (false positive)”

D: “Number of female animals clustered in female group (true negative)”

|      |                    | Sensitivity (%) | Specificity (%) |
|------|--------------------|-----------------|-----------------|
|      | C-H Region         | 88              | 79              |
| VAT  | Fingerprint Region | 92              | 83              |
|      | C-H Region         | 83              | 88              |
| SCAT | Fingerprint Region | 71              | 96              |

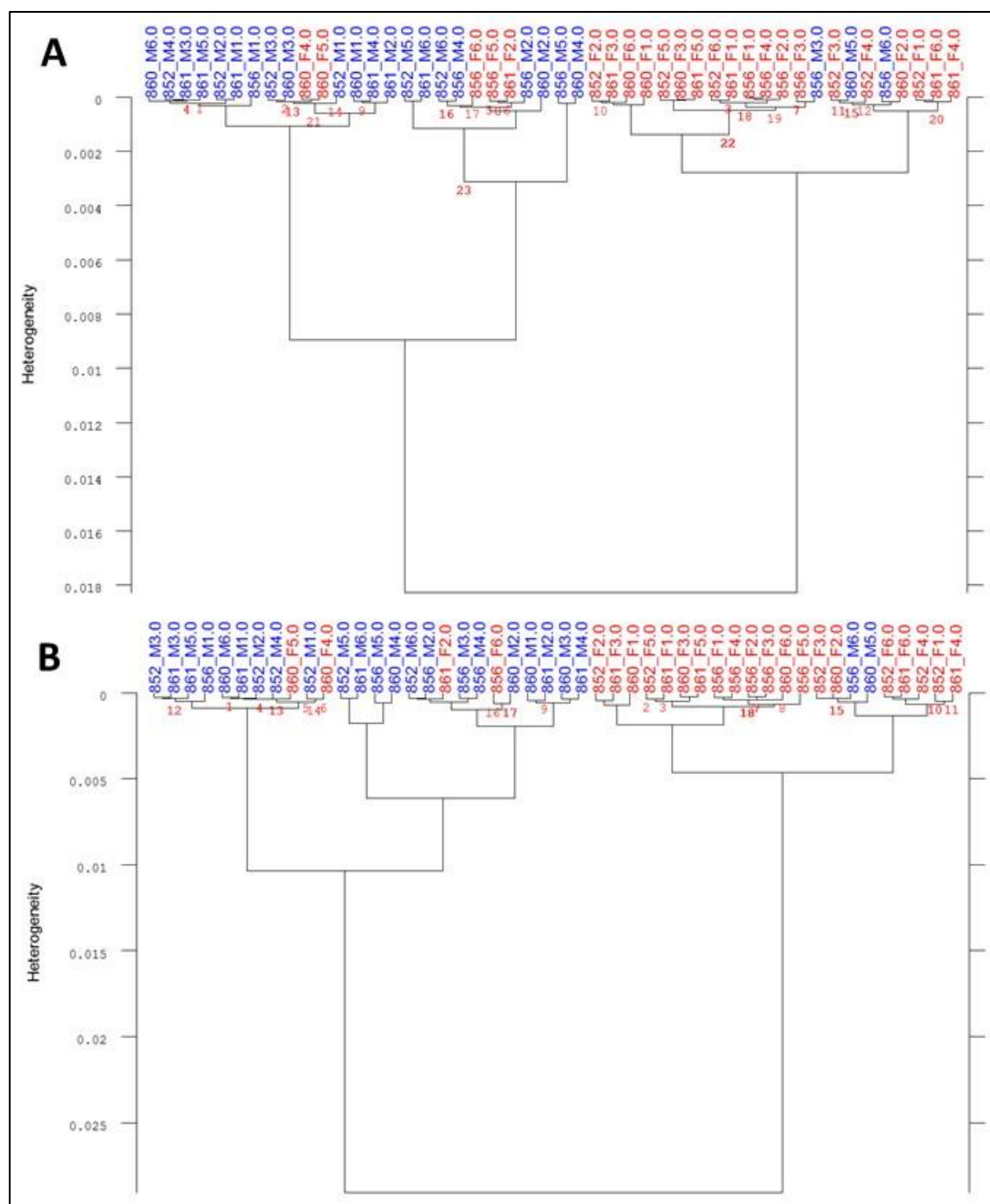


**Figure 43.** Hierarchical clustering of the male and female groups in the C-H region (A) and the fingerprint region (B) belonging to the VAT samples. Male group (blue), female group (red).

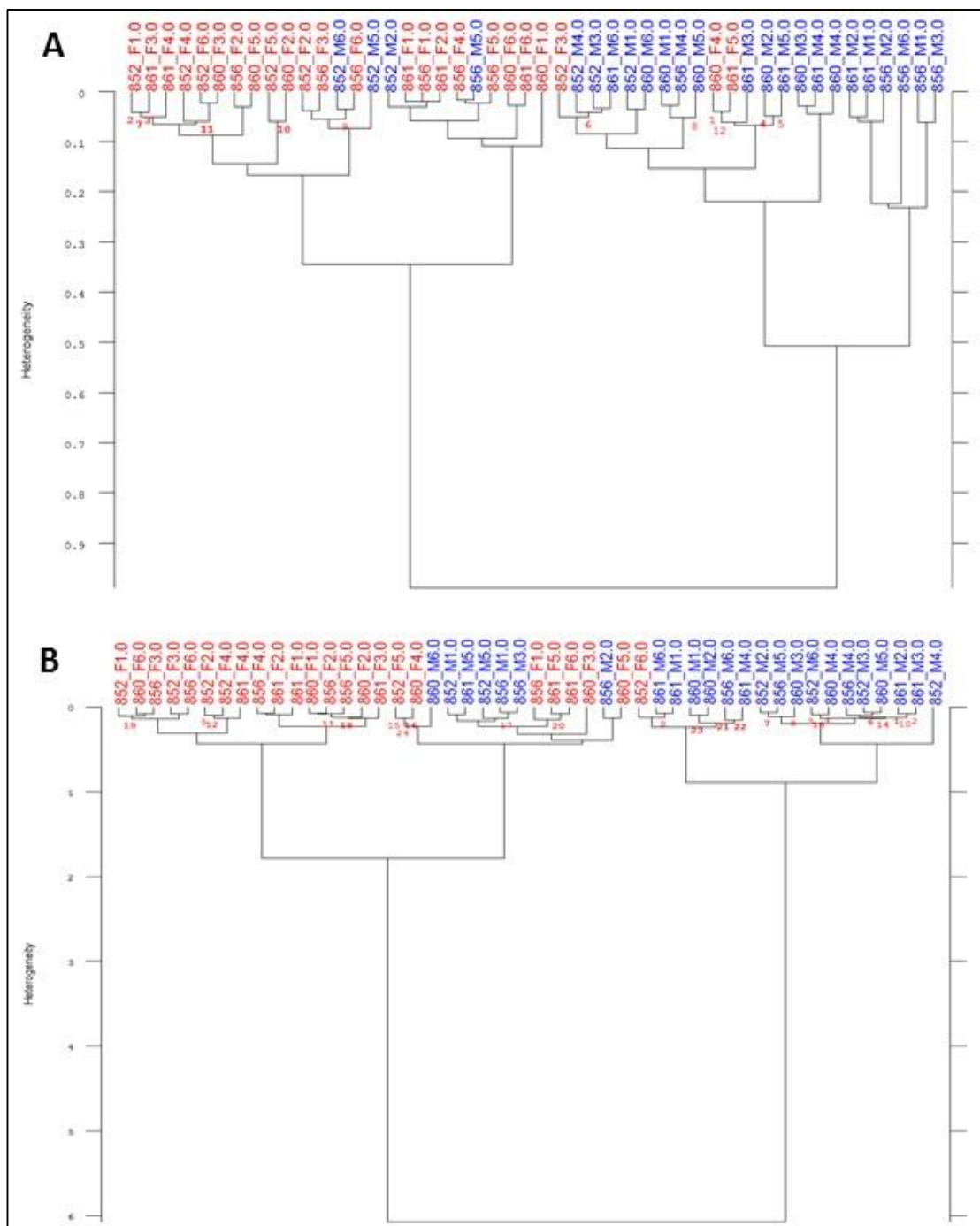


**Figure 44.** Hierarchical clustering of the male and female groups in the C-H region (A) and the fingerprint region (B) belonging to the SCAT samples. Male group (blue), female group (red).

In the light of all the information given above, it can be concluded that the C-H region and fingerprint region have unique spectral alterations in the differentiation of male and female groups. In order to obtain more detailed information about these differences, FTIR microspectroscopy studies were performed on particular bands located at these regions. The area ratios of some specific functional groups in the C-H region and fingerprint region were calculated to determine obesity related alterations in different gender groups according to concentration and composition of biochemical molecules. In the band area ratio calculations, the wavenumber limits with baseline points utilized for each vibrational region are presented in Table 1. The representative spectral maps of lipid (C-H region)/protein (amide I), olefinic/lipid (C-H region), carbonyl/lipid (C-H region), amide I/ amide II ratios of SCAT and VAT of male and female groups are represented in Figure 45-52. The maps were colored based on the calculated ratio values, where red color indicates to the highest ratio and blue color indicates to the lowest ratio as shown on the color scales in related figures.

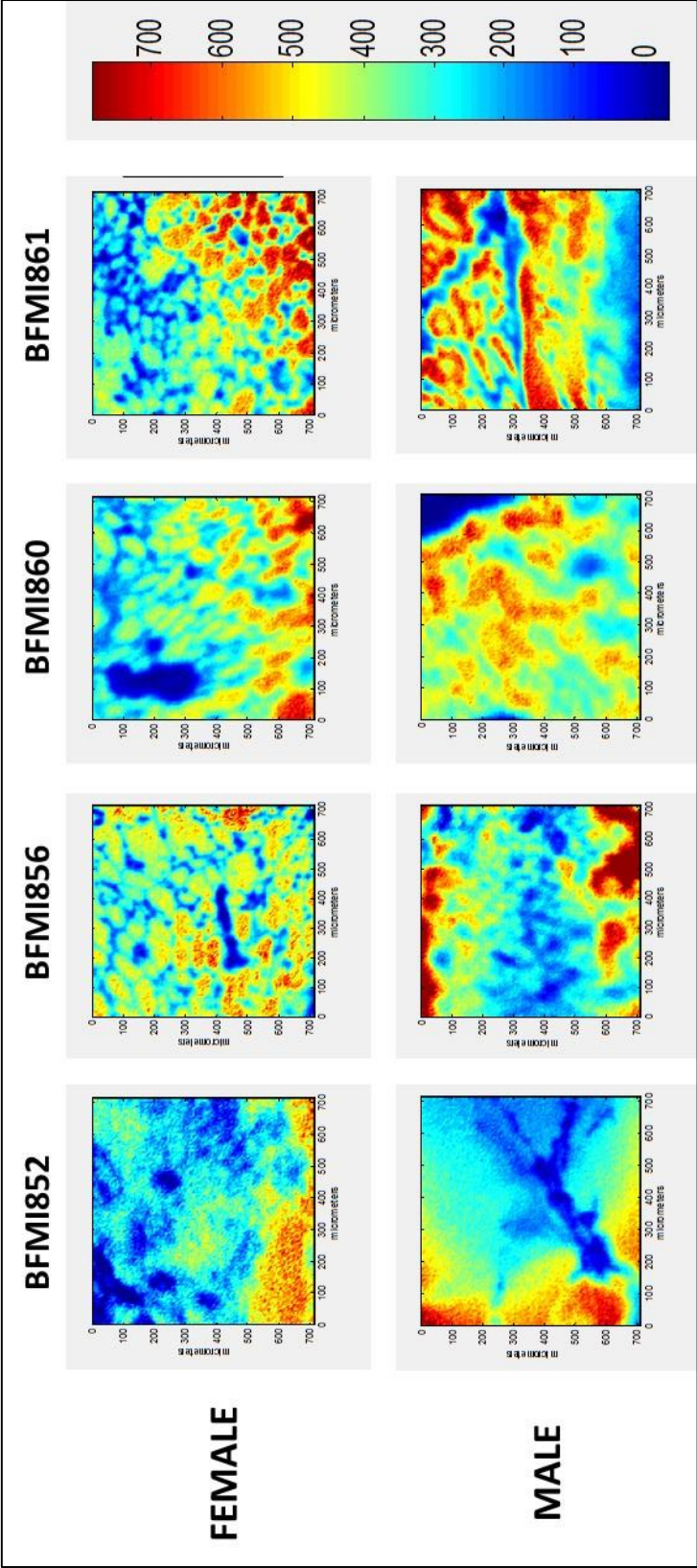


**Figure 45.** Representative images of the lipid/protein ratio in VAT of male and female groups.

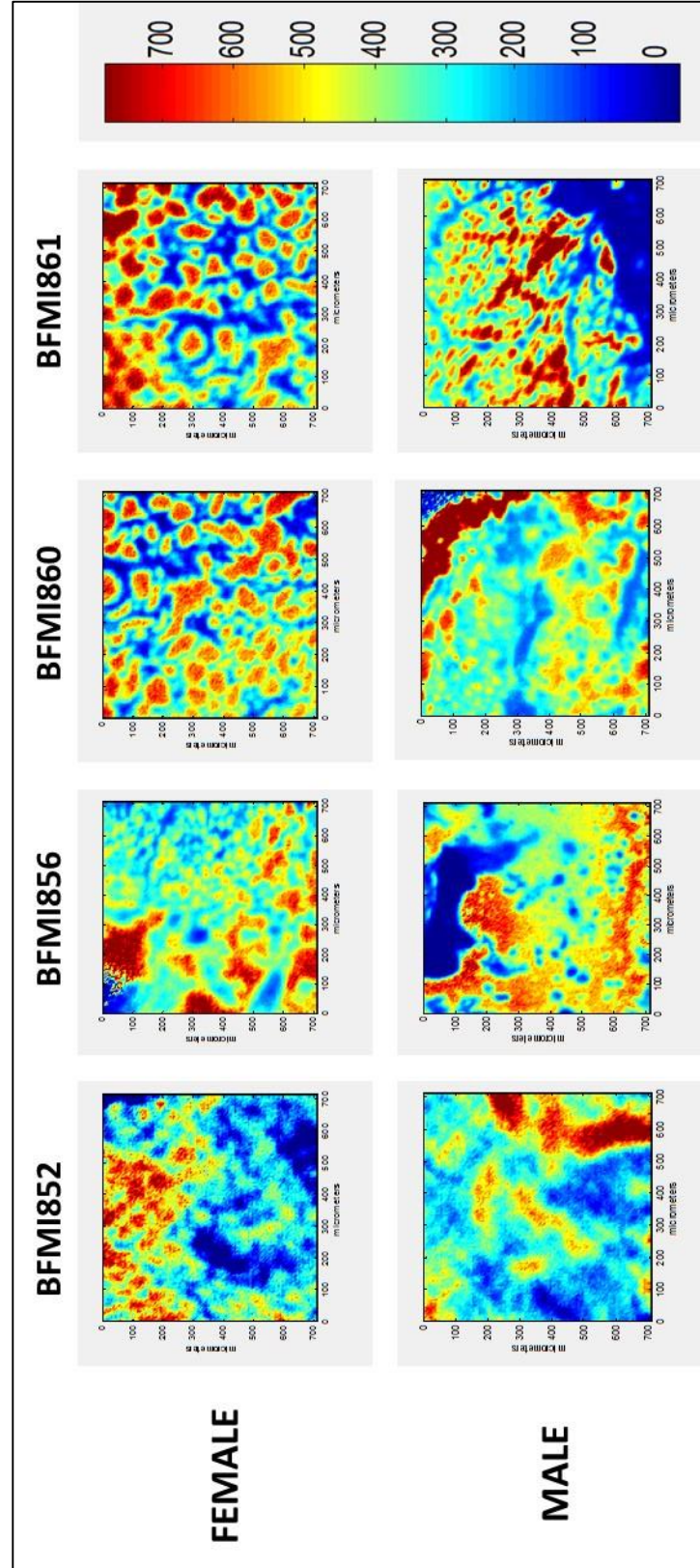


**Figure 46.** Representative images of the lipid/protein ratio in SCAT of male and female groups



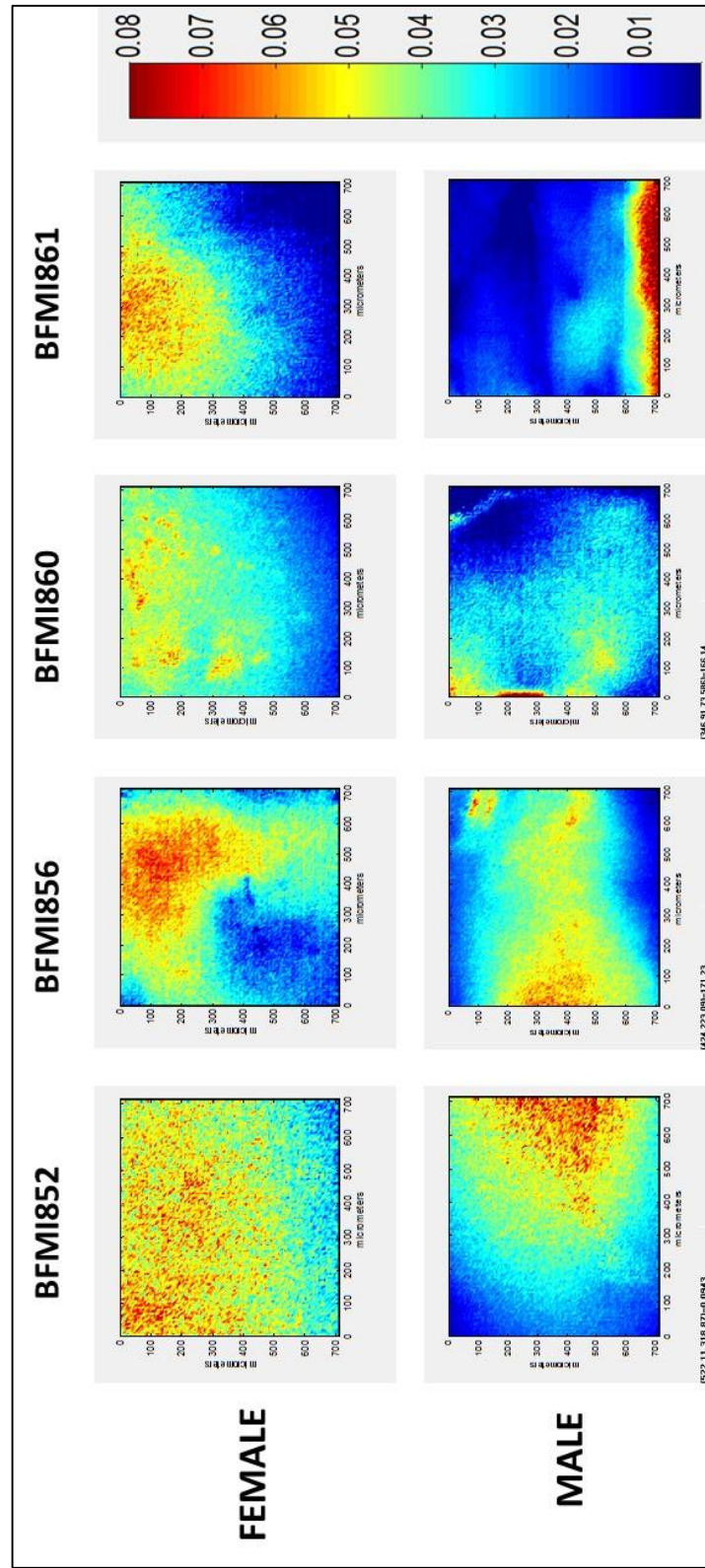


**Figure 47.** Representative images of the olefinic/lipid ratio in VAT of male and female groups.



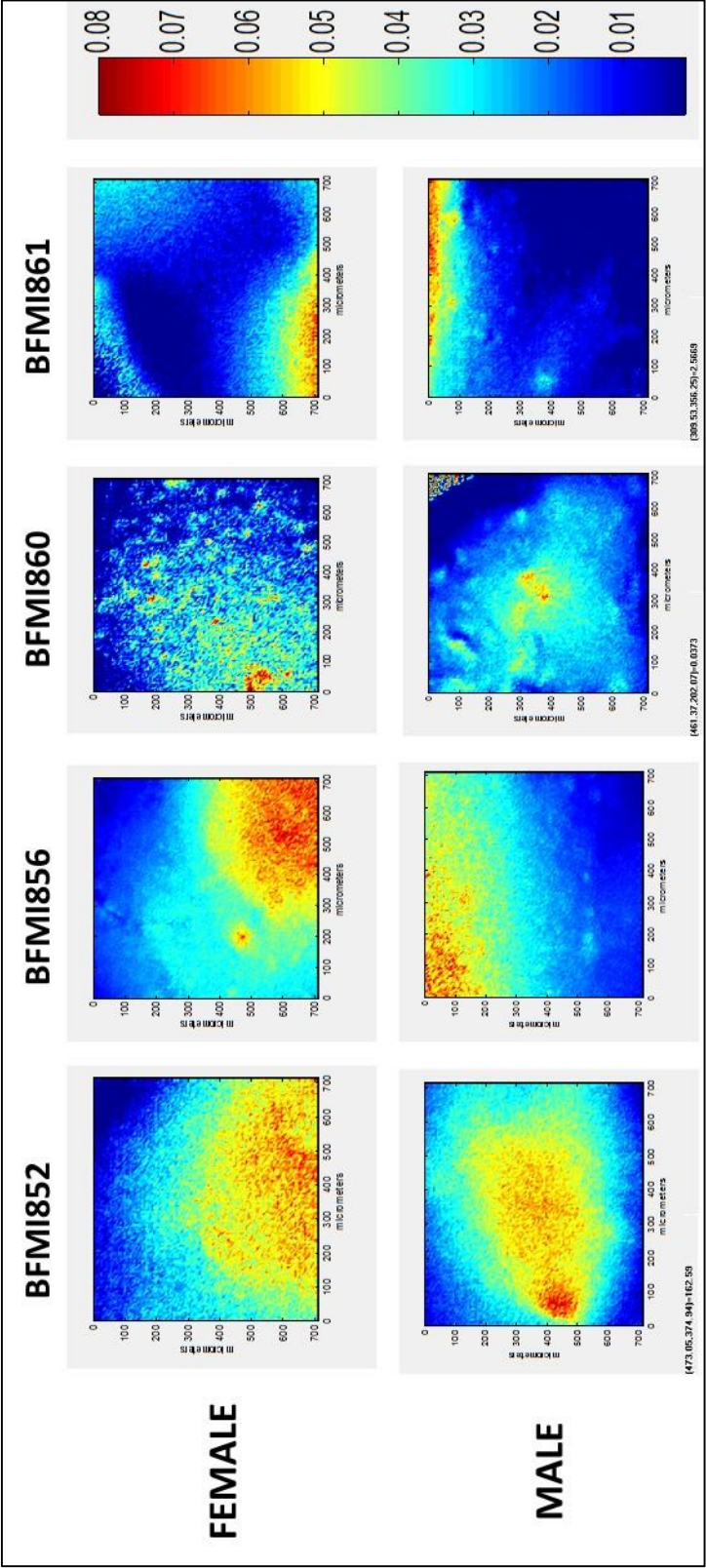
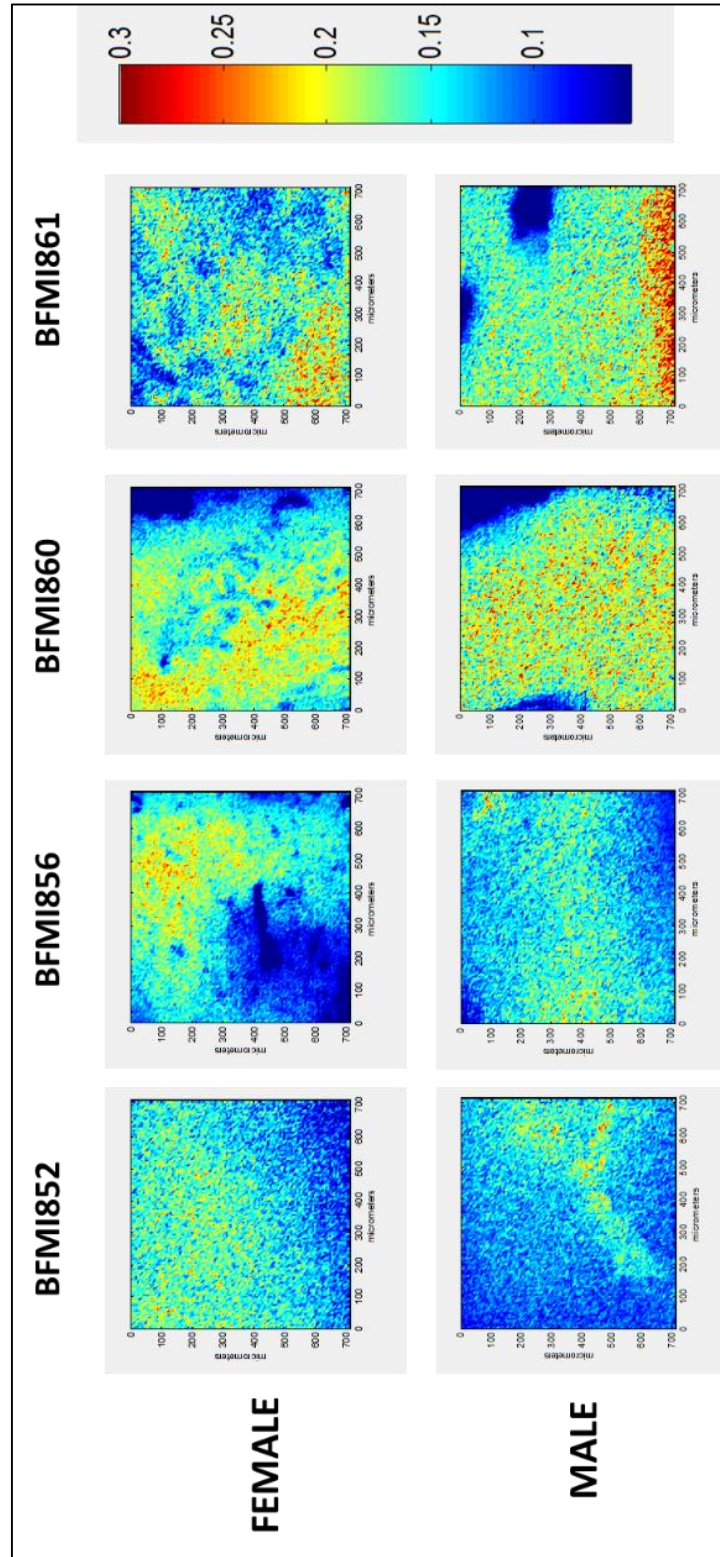
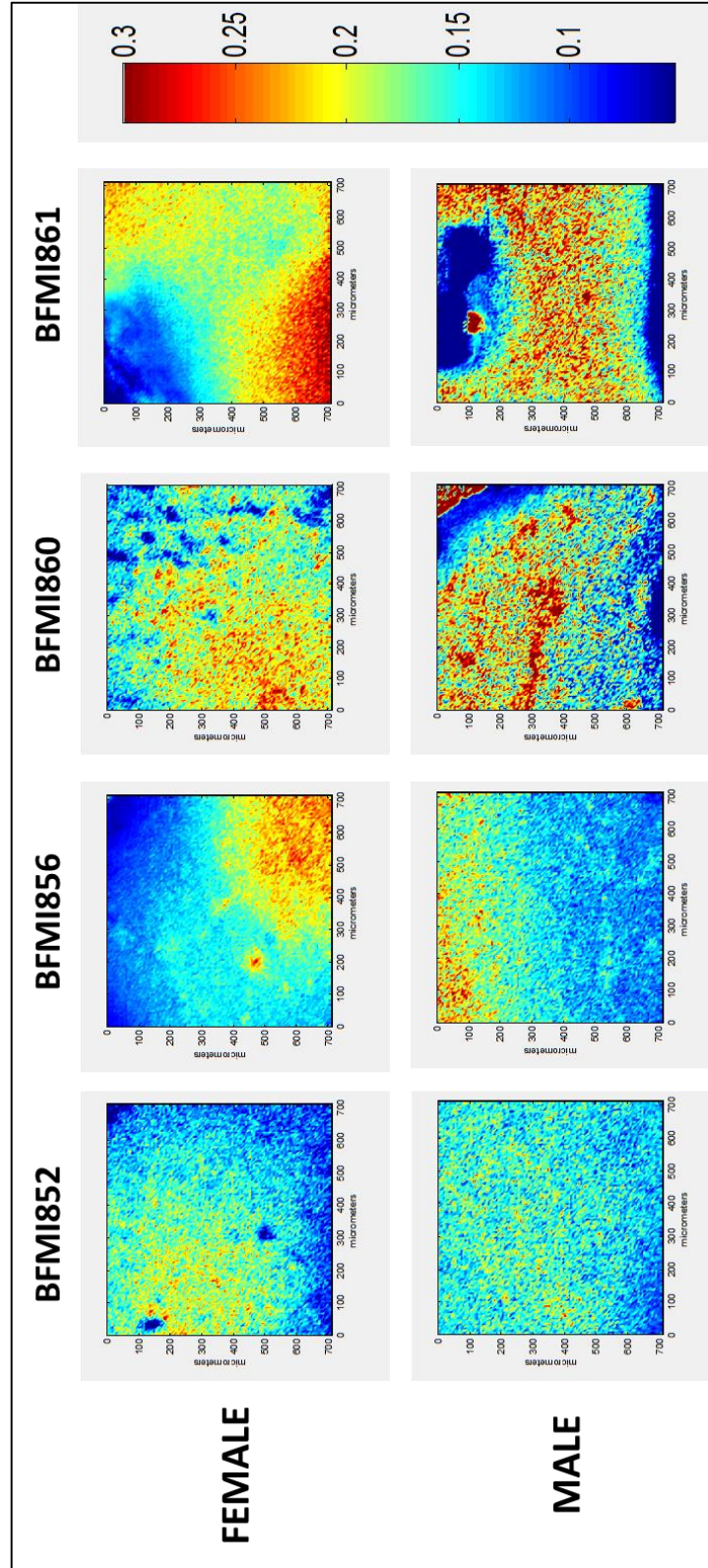


Figure 48. Representative images of the olefinic/lipid ratio in SCAT of male and female groups.



**Figure 49.** Representative images of the carbonyl/lipid ratio in VAT of male and female groups.



**Figure 50.** Representative images of the carbonyl/lipid ratio in SCAT of male and female groups.



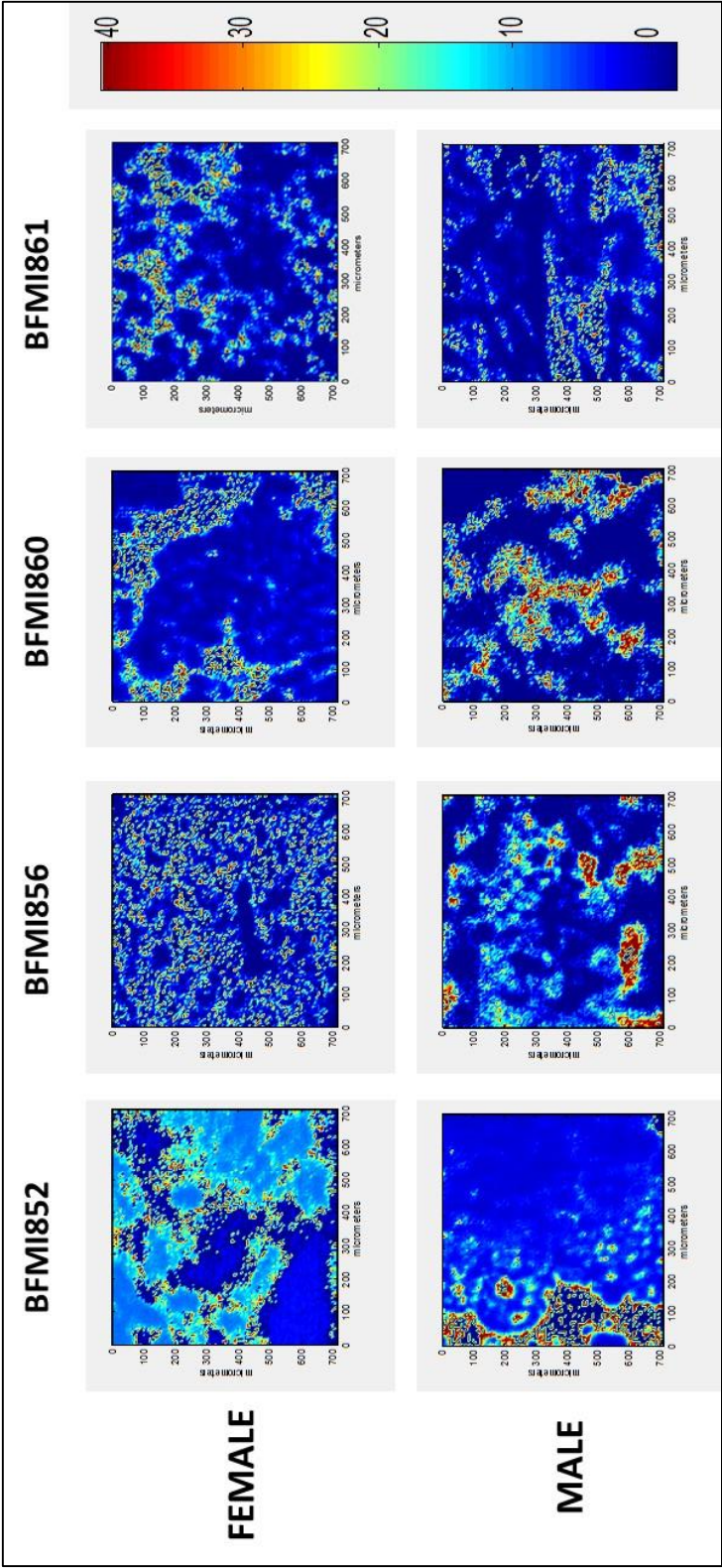


**Figure 51.** Representative images of the amide II/amide I ratio in VAT of male and female groups.

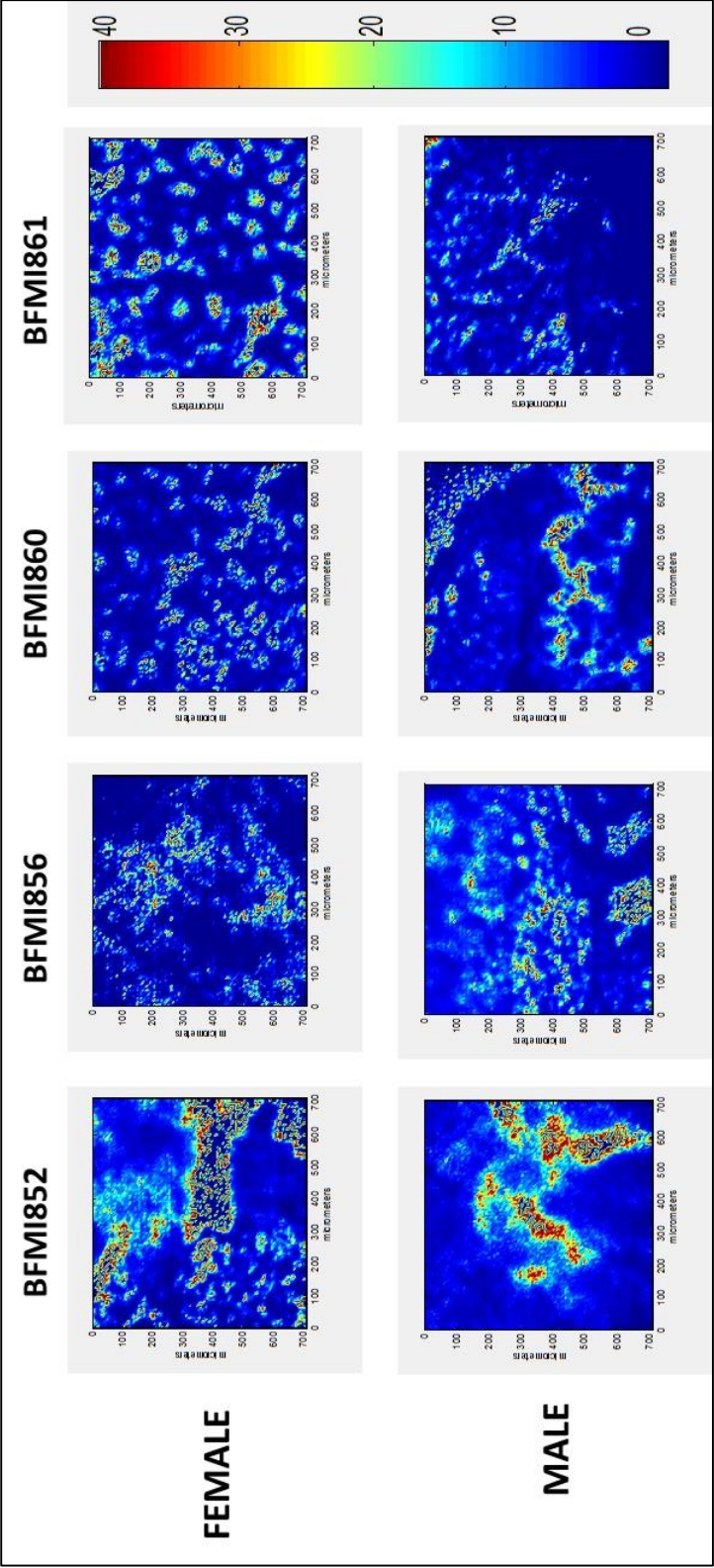


**Figure 52.** Representative images of the amide II/amide I ratio in SCAT of male and female groups.

The C-H region is a critical marker for the lipid context because it includes significant vibrations of the fatty acyl chains of membrane lipids (Bozkurt et al., 2010; Kneipp et al., 2000; Wang et al., 2005). According to the results, the C-H region has some special spectral alterations in differentiation of male and female groups. On the other hand, the amide I band which is located at fingerprint region provides information about concentration and conformation of total protein (Cakmak et al., 2012; Ishida & Griffiths, 1993). Consistently, the lipid/protein ratio can be achieved by proportioning of the certain area of the C-H region to the area of the amide I band. The Olefinic/lipid and carbonyl/lipid ratio were also calculated to get qualitative data about lipid structure of SCAT and VAT in different gender groups. Olefinic band which is located at C-H region indicates the unsaturation level in lipids of the system and olefinic/lipid ratio was calculated by proportioning of the area of the olefinic band as an unsaturated lipid to the area of the C-H region. Similarly, the carbonyl/lipid ratio was calculated by proportioning of the certain area of carbonyl band to that of C-H region. The carbonyl (C=O) ester stretching band originates from triglycerides and cholesterol esters, and carbonyl/lipid ratio gives information about carbonyl ester concentration in lipids of the system. On the other hand, the amide I/amide II ratio was calculated to investigate the alterations in protein content and structure in VAT and SCAT (Cakmak et al., 2011; Ishida & Griffiths, 1993). Figure 53 and 54 represented the comparison of all these ratios above in terms of bar graphs for the male and female obese lines for VAT and SCAT. Obviously as seen from the figure, the higher lipid/protein and carbonyl/lipid ratios and lower olefinic/lipid and amide I/ amide II ratios could be indicators of obesity, which were more significant in VAT samples of male groups and in SCAT samples of female groups.

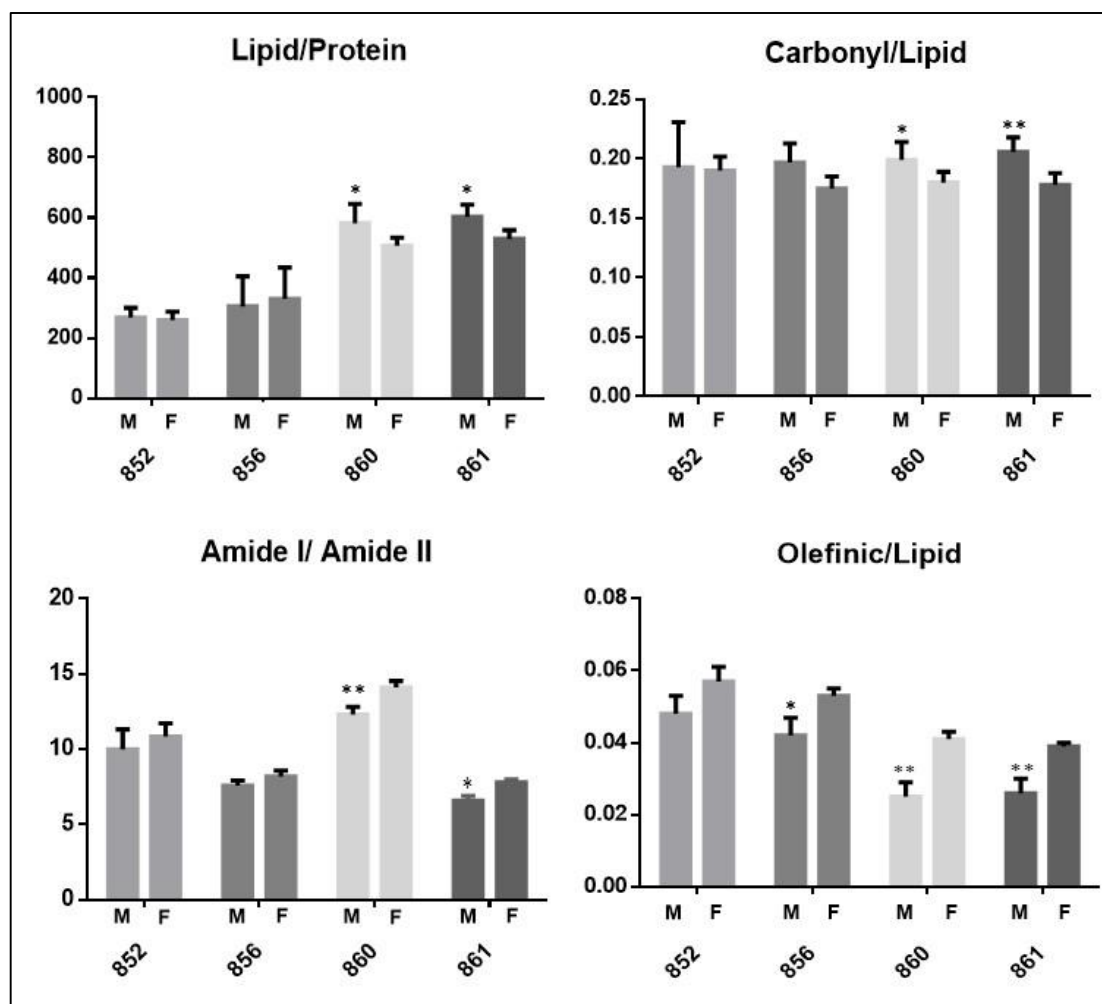


**Figure 53.** The bar graphs of the lipid/protein, olefinic/lipid, carbonyl/lipid, amide I/amide II ratios of male and female groups in VAT.

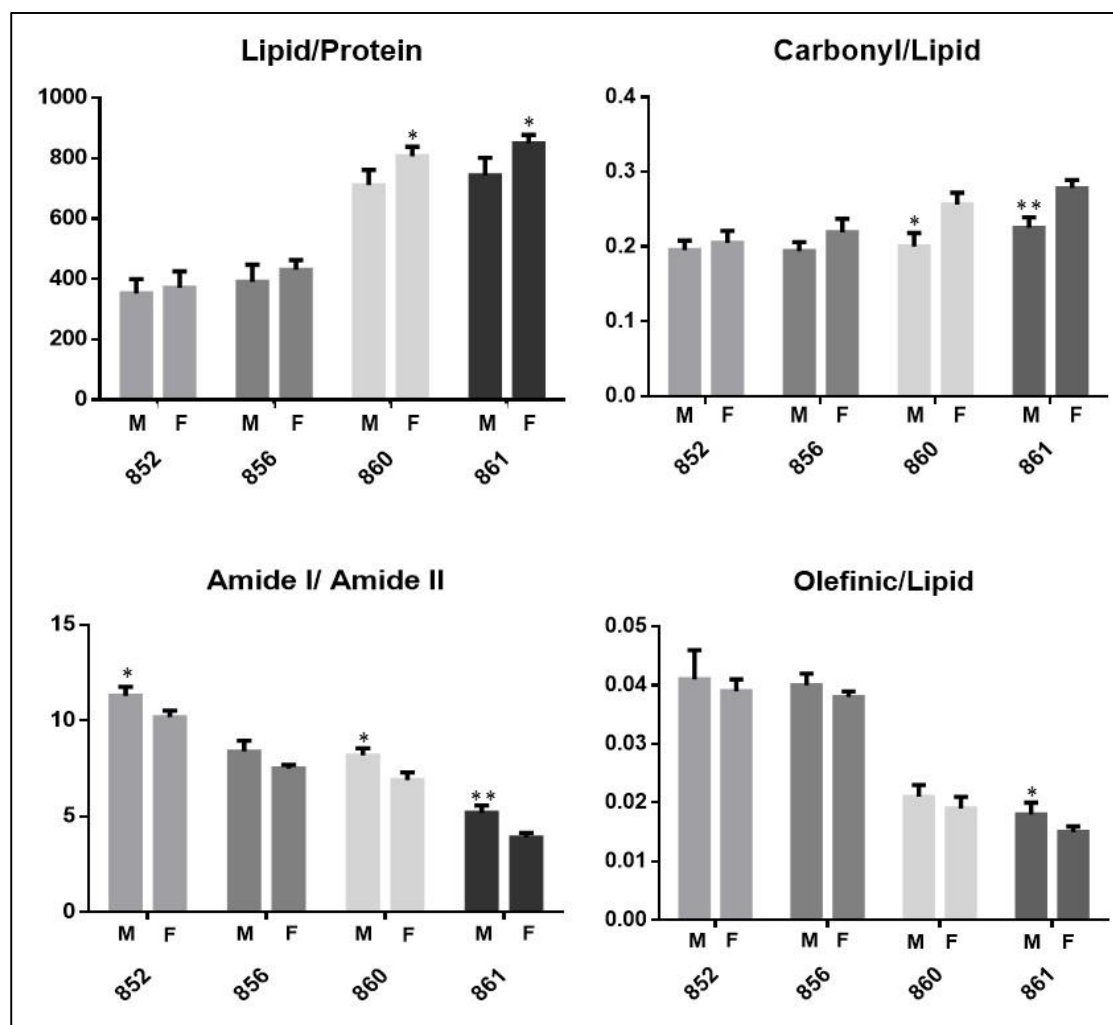


**Figure 54.** The bar graphs of the lipid/protein, olefinic/lipid, carbonyl/lipid, amide I/amide II ratios of male and female groups in SCAT.



The lipid/protein ratio provides information about alterations in lipid context compared to protein context (Bozkurt et al., 2010). Considering only VAT samples, an enhanced lipid/protein ratio was achieved in male groups compared to the female group. Especially, the male groups of BFMI860 and 861 lines showed a significant increase in this ratio in comparison to females. On the other hand, SCAT samples had a reverse situation; the female groups had a higher lipid/protein ratio compared to the male group especially for the BFMI860 and 861 lines. As stated in the literature, gender disparities can cause the alterations in the distribution and composition of lipid depots in the body. While females predominantly accumulate subcutaneous fat, males store considerably more visceral fat (Kotani et al., 1994; Macotela et al., 2009). Females have a higher amount of body fat in the gluteal-femoral region, whereas males store body fat in the visceral region. Therefore, upper body obesity and lower body obesity are referred to as android and gynoid obesity (Blaak, 2001). It has been reported that estrogen promotes the accumulation of SCAT in females (Ibrahim, 2010), which is in accordance with our results which revealed an increased amount of lipids in female SCAT tissues in comparison to male group. After menopause, the increment of body VAT in women is related to the deficiency of estrogen (Björntorp, 1995; Freedland, 2004). This reduction of estrogen after menopause is often followed by an increase in VAT, hyperinsulinemia and increase in IL-6 production (Freedland, 2004). Postmenopausal women at older ages have increased amount of VAT emphasizing the role of gonadal steroids in this phenomenon (Camhi et al., 2011; Goodman-Gruen & Barrett-Connor, 1996). When it comes to the results of males, VAT samples had higher lipid/ protein ratio in all lines. Androgens also have gender specific effects on adipose tissue distribution. Obese men are characterized by a progressive decrease of testosterone levels with increasing body weight (Pasquali, 2006). In males, this testosterone deficiency can stimulate the VAT mass and it may be associated with insulin resistance (White & Tchoukalova, 2014). It has been reported that the testosterone therapy in aging men can diminish VAT and increases lean muscle mass (Allan et al., 2008). Additionally, obese postmenopausal women treated with testosterone developed significantly increased VAT (Lovejoy et al., 1996).

The Carbonyl/lipid ratio is an indicator of the triglycerides and cholesterol ester levels in the system. (Nara et al., 2002; Ozek et al., 2009; Voortman et al., 2002). If we take into consideration only VAT samples, male groups indicated a higher carbonyl/lipid ratio in comparison to the female groups, especially in BFMI860 and 861. On the contrary, female groups showed a higher carbonyl/lipid ratio compared to male groups in SCAT results. In harmony with our results, it was stated that more FFAs may be taken up by the VAT depots in males. Moreover, visceral uptake of triglyceride and FFAs was found to be more intensive in males compared to in females (Nguyen et al., 1996). The accumulation of triglycerides and FFAs in adipose tissue is positively correlated with insulin resistance. The excess lipolysis of triglycerides leads to the release of FFAs, and then these FFAs especially from VAT release into liver through portal vein. VAT is considered as a major source of FFAs in the portal vein and this process has a critical role in the development of insulin resistance. (Hotamisligil et al., 1995; Paschos & Paletas, 2009). Since this FFA streaming rates can be seen as higher in upper-body obesity than in lower-body obesity, android obesity in males can be more harmful than gynoid obesity in females because of excess release of FFAs into circulatory system (Horowitz et al., 1999; Jensen et al., 1989). Regarding the size of adipocytes, SCAT is reported to have larger adipocytes in females than males (Fried & Kral, 1987). Consistently, female groups showed a higher carbonyl/lipid ratio compared to male groups indicating a higher triglyceride level in SCAT results. It has been reported that larger adipocytes belonging to SCAT cause an increased synthesis of triglycerides than smaller adipocytes belonging to VAT (Edens et al., 1993; Farnier et al., 2003).

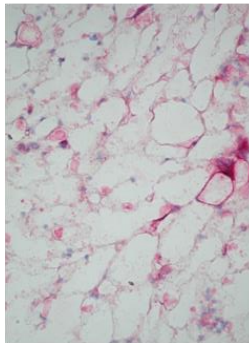
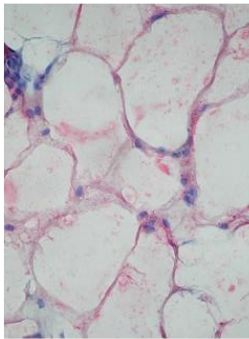
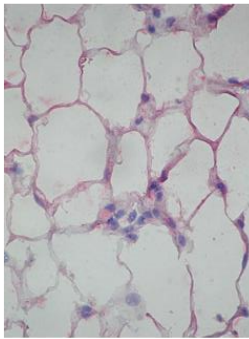
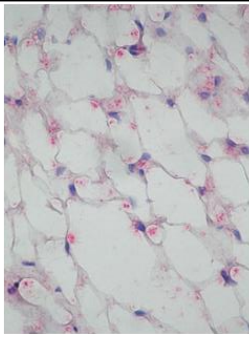
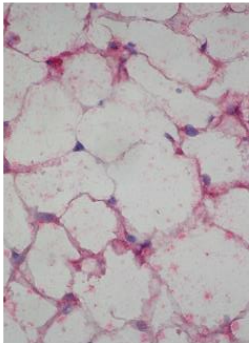
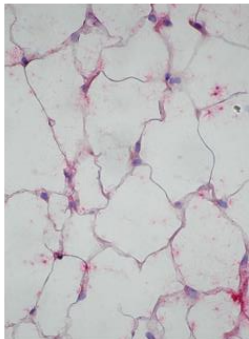
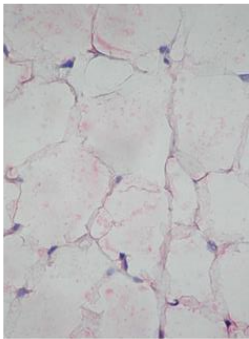
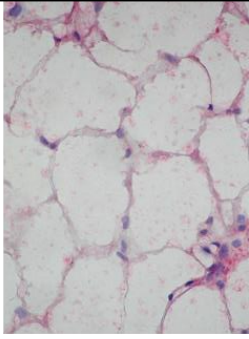
The olefinic/lipid ratio, as an index of double bonds, gives information about the relative amount of unsaturated lipids in the total lipid composition. (Cakmak et al., 2012; Kneipp et al., 2000). When we compared to male and female groups according to VAT results, the significant decrease in olefinic/lipid ratio indicates a lower content of unsaturated lipids in males in comparison to that of females, more profoundly in BFMI856 860 and 861 lines. However, in SCAT results, female groups indicated a lower olefinic/lipid ratio in comparison to male groups particularly for BFMI861 line. The fatty acid content of VAT

has lower amount of unsaturated fatty acids compared to SCAT (Garaulet et al., 2001; Machann et al., 2012). Since male groups have the higher level of VAT compared to the female groups, it can be concluded that the lower olefinic/lipid ratio in male groups indicates a lower amount of unsaturated fatty acids in accordance with the literature (Cheung & Cheng, 2016). Since females have larger amount of adipocytes of SCAT than VAT indicating a lower storage capacity in visceral depots for triglycerides and creating higher lipid saturation (Tchoukalova et al., 2008)., the female groups indicated a lower amount of unsaturated lipids in comparison to the male groups in SCAT.

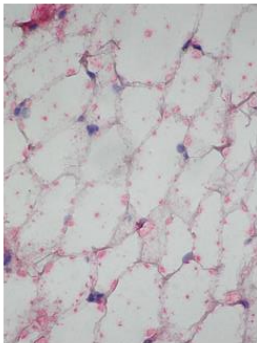
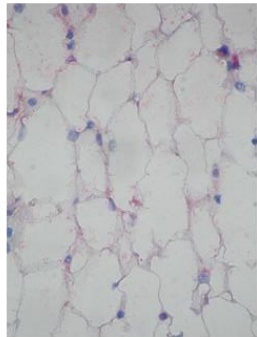
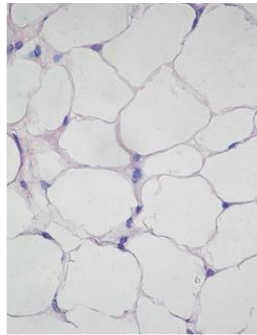
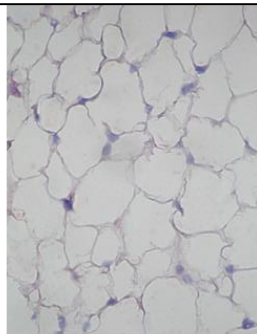
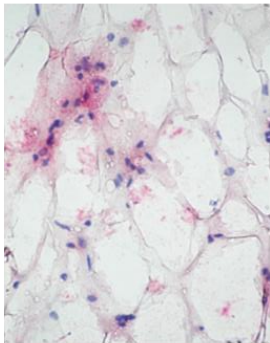
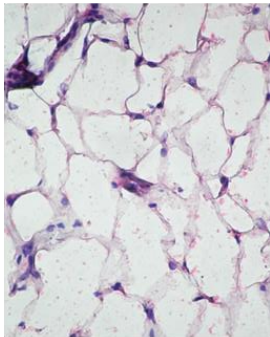
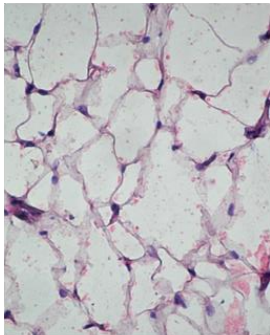
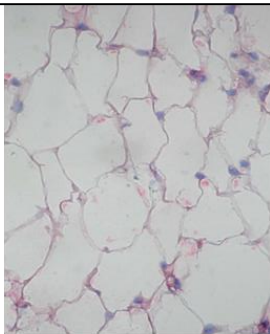
The band area ratio of amide I/ amide II was also calculated to get more information about protein structural and compositional alterations. This ratio was obtained as lower in VAT samples belonging to male groups and in SCAT samples belonging to female groups when compared to the other group. Since amide I and II bands are based on the protein structure, these decreases indicate some global changes in protein conformation. (Cakmak et al., 2011; Schmidt et al., 2007; Yu et al., 2008). Previous studies have shown that increased mass of adipose tissue was found to be correlated with the decreased relative total protein content (Seraphim et al., 2001). Adiponectin, an insulin-sensitizing hormone, is only expressed from white adipocytes (Makki et al., 2013; Piya et al., 2013). Adiponectin is significantly higher in women compared with men due to differences in sex hormones or adipose tissue distribution (Geer & Shen, 2009). WAT and BAT amounts of different gender groups also alter the protein composition due to UCP1 protein. These differences between males and females can clarify the changes in the protein conformation.

To investigate of gender-based differences in the effect of obesity on BAT and WAT, the immunohistological staining was performed to VAT and SCAT samples of male and female groups. Figure 55 and 56 represents the general microscope images of UCP1 stained VAT and SCAT sections of the male and female groups under 40X magnification respectively. The lower ratio of amide I/ amide II bands indicates possible alterations in protein structure and composition. The immunohistological staining results supported

these FTIRM results with a decreased amount of UCP1 proteins in VAT samples of male groups and SCAT samples of female groups.

|      |         |   |  |         |  |   |         |   |  |         |   |  |       |
|------|---------|---|--|---------|--|---|---------|---|--|---------|---|--|-------|
| MALE | BFMI852 |  | 9.6 %  | BFMI856 |  | 6.2 %   | BFMI860 |  | 3.5 %  | BFMI861 |  | 3.1 %  |       |
|      | FEMALE  |   |  |         |  |   |         |   |  |         |   |  |       |
|      |         |   |  | 10.6 %  |  |  | 7.1 %   |   |  | 6.9 %   |   |  | 6.6 % |
|      |         |   |  |         |  |   |         |   |  |         |   |  |       |
|      |         |   |  |         |  |   |         |   |  |         |   |  |       |

**Figure 55. .** Microscopic images of immunohistological UCP1 staining results of male and female groups belong to the VAT under 40X magnification. The percentage values of UCP1 protein were calculated by ImageJ 1.50e.

|        |         |   |  |         |  |   |         |   |  |         |   |  |       |
|--------|---------|---|--|---------|--|---|---------|---|--|---------|---|--|-------|
| FEMALE | BFMI852 |  | 5.6 %  | BFMI856 |  | 5.1 %   | BFMI860 |  | 0.3 %  | BFMI861 |  | 0.5 %  |       |
|        | MALE    |   |  |         |  |   |         |   |  |         |   |  |       |
|        |         |   |  | 6.3 %   |  |  | 5.6 %   |   |  | 2.9 %   |   |  | 2.1 % |
|        |         |   |  |         |  |   |         |   |  |         |   |  |       |
|        |         |   |  |         |  |   |         |   |  |         |   |  |       |

**Figure 56.** Microscopic images of immunohistological UCP1 staining results of male and female groups belong to the SCAT under 40X magnification. The percentage values of UCP1 protein were calculated by ImageJ 1.50e.

The importance of sex dimorphism in control of energy metabolism under physiological and pathological conditions is implying that sex hormones may play a relevant role in the regulation of BAT activity in both males and females. The gender-based difference in adipose storage is not only in WAT depots, females also have more active BAT than males in animal models (Rodriguez-Cuenca et al., 2002). On the other hand, female BAT shows larger mitochondria and higher cristae density leading to an enhanced thermogenic activity compared with the BAT present in males (Rodriguez-Cuenca et al., 2002). In harmony with literature, UCP1 immunohistological staining results indicated that VAT samples have more UCP1 protein in females in comparison to males. On the other hand, in SCAT samples, female groups showed a significant decrease in UCP1 protein amount compared to males and a brown to white adipocyte transdifferentiation can be occurred in BFMI860 and 861 because of having more WAT. In females, deposition of accumulated WAT in lower and upper body SCAT depots prevents VAT depots to prohibit the increasing central fat expansion, insulin resistance and systemic inflammation (Bloor & Symonds, 2014).

A higher lipid/protein and carbonyl/lipid ratios accompanied with a lower olefinic/lipid and amide I/ amide II ratios can be considered as obesity-induced effects on compositional structure of adipose tissues (Kucuk Baloglu et al., 2015). If all the results given above are evaluated together, it can be concluded that these obesity-induced effects were more dramatic for male groups in VAT and for female groups in SCAT. As stated in literature, VAT accumulation is significantly higher in males in comparison to females whereas SCAT had more accumulation in females (Ibrahim, 2010; Kotani et al., 1994). It has been known that VAT accumulation in obesity cause insulin resistance and lipid accumulation in liver (Hardy et al., 2012b). Therefore, males are more prone to generation of insulin resistance. Especially BFMI 860 and 861 lines were more affected from these obesity effects in both gender groups. Consistently, it was reported that these lines showed obesity symptoms more intensely and they have obesity induced insulin resistance (Kucuk Baloglu et al., 2015). These alterations in SCAT and VAT distribution make females more insulin-sensitive because of having lower visceral and hepatic adiposity linked to insulin

resistance. Since estrogen has a positive effect on insulin and glucose homeostasis, it has a crucial role in these gender-based differences. The elevated amount of VAT and lack of the protective effect of estrogen in males can be responsible of their vulnerability to insulin resistance in comparison to females (Geer & Shen, 2009). On the other hand, in obesity, the expansion of adipose tissues is associated with an increase in adipocyte number in females and an enlargement in adipocyte size in males, this gender-based difference is most obvious in SCAT and least obvious in VAT (Cinti, 2005; Giese & French, 1955). Overall, these regional gender-based differences in the number and size of adipocytes may determine gender-based differences in the risk of obesity-induced diseases because the SCAT in females may provide a safe lipid reservoir for excess energy (Whitbeck, 1981).



## CHAPTER IV

### 4. CONCLUSION

This thesis study includes three parts investigating obesity with different approaches. The first part is aimed to characterize and compare VAT and SCAT of SBD fed BFMI mice with regard to molecular content and investigate transdifferentiation between white and brown adipocytes. In addition, the second part of this study is addressed to propose triglyceride bands located at  $1770\text{-}1720\text{ cm}^{-1}$  spectral region as a more sensitive obesity related biomarker using the diagnostic potential of FTIR spectroscopy in SCAT and VAT. The purpose of third part of the study is to determine gender dependent differences in the effect of obesity on VAT and SCAT in obese mice lines.

The results of the first part indicated an enhanced lipid concentration and considerably decreased UCP1 protein content, implying a transdifferentiation of brown to white adipocytes in both adipose tissues of obese groups. These results revealed that BFMI mice lines had a lower amount of brown adipocytes in VAT and SCAT referring a tendency for obesity. Furthermore, the increased amount of triglycerides, the decreased unsaturation ratio, the qualitatively longer hydrocarbon acyl chain length of lipids obtained by FTIR microspectroscopy showed that both types of adipose tissues, especially SCAT, were prone to lipid peroxidation. It has been reported that these kind of structural and compositional alterations in cells are closely correlated with ion channel kinetics and membrane functioning (Awayda et al., 1985). Besides obesity, these obesity-induced

alterations of lipids and proteins in adipose tissues can be symptoms of insulin resistance in BFMI lines, especially for BFMI861. Another important result of the study is that both VAT and predominately SCAT indicated remarkable obesity-induced alterations, for this reason both tissues have crucial roles in the progression of obesity. As a result, the power of FTIR microspectroscopy was directly revealed in the detection of spectral variations in adipose tissue components of obese mice lines.

The second part of the study focused on spectral differences in the triglyceride region of SCAT and VAT belonging to male obese mice. By using triglyceride band as base, a successful differentiation between control, obesity related insulin resistant and obese groups was achieved with high sensitivity and specificity in the adipose tissue samples. The discriminatory power of FTIR spectroscopy coupled with multivariate analysis was revealed in diagnosis of obesity in SCAT and VAT samples and so it was revealed that the triglyceride band can be used as a biomarker in diagnosis of obesity. Another finding also indicated that obesity effects on SCAT and VAT at different rates and FTIR spectroscopy coupled with chemometrics can distinguish these effects in adipose tissues of different BFMI mice lines. Since these special mice lines develops spontaneous obesity, pure and reliable data can be achieved about related diseases. For this reason, the findings of this animal study can be transferred to medicinal investigations in the field of differential diagnosis of obesity. Since the SCAT is more accessible than the VAT for medical operations, it can be preferred in biopsies and bariatric interventions. Consistently, the SCAT is closely correlated with the VAT in regard to metabolic effects of obesity such as insulin resistance. Moreover, the results have revealed that ATR-FTIR spectroscopy coupled with chemometrics can be used to sensitively examine SCAT and VAT in obesity and this technique will shed light on the internal diagnosis of obesity in medicine.

The third part of the study aimed to detect gender-based differences in obesity by comparing molecular content of SCAT and VAT in male and female mice lines. The obesity effects on compositional structure of adipose tissues such as higher of lipid/protein

ratio, lower unsaturation/saturation ratio, higher amount of triglycerides, were more significant for male groups in VAT and for female groups in SCAT. Consistently, it is known that the VAT accumulation is higher in males than in females whereas SCAT is more accumulated in females than males. Since sex hormones naturally affect adipose tissue function and distribution, males tend to have a classic android body shape which has been closely correlated to insulin resistance. On the other hand, females develop a gynoid body shape providing a protection from the negative consequences associated with obesity and the metabolic syndrome. As a result, the samples of male and female can be distinguished by ATR-FTIR spectroscopy coupled with chemometrics and the gender-based differences in composition of SCAT and VAT were revealed by FTIR microspectroscopy and UCP1 immunohistological staining. Understanding how structure and composition of adipose tissue differ by gender can enable personalized and gender-based treatments.



## REFERENCES

- Abate, N., Garg, A., Peshock, R. M., Stray-Gundersen, J., & Grundy, S. M. (1995). Relationships of generalized and regional adiposity to insulin sensitivity in men. *The Journal of Clinical Investigation*, 96, 88–98.
- Ahima, R. S. (2006). Adipose Tissue as an Endocrine Organ. *Obesity*, 14, 242S–249S.
- Aksoy, C., Guliyev, a, Kilic, E., Uckan, D., & Severcan, F. (2012). Bone marrow mesenchymal stem cells in patients with beta thalassemia major: Molecular analyses with attenuated total reflection-fourier transform infrared (ATR-FTIR) spectroscopy study as a novel method. *Stem Cells Dev*, 21, 2000–11.
- Aksu, S., Koczan, D., Renne, U., Thiesen, H.-J., & Brockmann, G. A. (2007). Differentially expressed genes in adipose tissues of high body weight-selected (obese) and unselected (lean) mouse lines. *Journal of Applied Genetics*, 48, 133–143.
- Albu, J. B., Curi, M., Shur, M., Murphy, L., Matthews, D. E., & Pi-Sunyer, F. X. (1999). Systemic resistance to the antilipolytic effect of insulin in black and white women with visceral obesity. *The American Journal of Physiology*, 277, E551-60.
- Alderete, T. L., Sattler, F. R., Sheng, X., Tucci, J., Mittelman, S. D., Grant, E. G., & Goran, M. I. (2014). A novel biopsy method to increase yield of subcutaneous abdominal adipose tissue. *International Journal of Obesity (2005)*, 39, 1–4.
- Allan, C. A., Strauss, B. J. G., Burger, H. G., Forbes, E. A., & McLachlan, R. I. (2008). Testosterone Therapy Prevents Gain in Visceral Adipose Tissue and Loss of Skeletal Muscle in Nonobese Aging Men. *The Journal of Clinical Endocrinology & Metabolism*, 93, 139–146.
- Almind, K., Manieri, M., Sivitz, W. I., Cinti, S., & Kahn, C. R. (2007). Ectopic brown

- adipose tissue in muscle provides a mechanism for differences in risk of metabolic syndrome in mice. *Proceedings of the National Academy of Sciences*, 104, 2366–2371.
- Amhmed A. Bhiih, Princy Johnson, M. R. (2015). EM Clustering Approach for Multi-Dimensional Analysis of Big Data Set. *International Journal of Engineering Research & Technology (IJERT)*, Vol. 4-I. Retrieved from <http://www.ijert.org/view-pdf/12255/em-clustering-approach-for-multi-dimensional-analysis-of-big-data-set>
- Antoine, K. M., Mortazavi, S., Miller, A. D., & Miller, L. M. (2010). Chemical Differences Are Observed in Children's Versus Adults' Latent Fingerprints as a Function of Time. *Journal of Forensic Sciences*, 55, 513–8.
- Arita, Y., Kihara, S., Ouchi, N., Takahashi, M., Maeda, K., Miyagawa, J., ... Matsuzawa, Y. (2012). Paradoxical decrease of an adipose-specific protein, adiponectin, in obesity. 1999. *Biochemical and Biophysical Research Communications*, 425, 560–4.
- Arner, P. (1995). Differences in lipolysis between human subcutaneous and omental adipose tissues. *Annals of Medicine*, 27, 435–8.
- Arner, P. (1999). Catecholamine-induced lipolysis in obesity. *International Journal of Obesity and Related Metabolic Disorders : Journal of the International Association for the Study of Obesity*, 23 Suppl 1, 10–3.
- Awayda, M. S., Shao, W., Guo, F., Zeidel, M., & Hill, W. G. (2004). ENaC-membrane interactions: regulation of channel activity by membrane order. *The Journal of General Physiology*, 123, 709–27.
- Azizian, H., Kramer, J. K. G., Heymsfield, S. B., & Winsborough, S. (2008). Fourier transform near infrared spectroscopy: A newly developed, non-invasive method to measure body fat - Non-invasive body fat content measurement using FT-NIR. *Lipids*, 43, 97–103.
- Baser, T. (2013). *Determination of inbred obese mouse adipose tissue lipid profiles by high performance liquid chromatography*. METU, Ankara, TURKEY.

- Bashkatov, A. N., Genina, E. A., Kochubey, V. I., & Tuchin, V. V. (2005). Optical properties of human skin, subcutaneous and mucous tissues in the wavelength range from 400 to 2000 nm. *J. Phys. D: Appl. Phys.* *38*, 2543–2555.
- Batsis, J. A., Mackenzie, T. A., Bartels, S. J., Sahakyan, K. R., Somers, V. K., & Lopez-Jimenez, F. (2015). Diagnostic accuracy of body mass index to identify obesity in older adults: NHANES 1999-2004. *International Journal of Obesity (2005)*, *40*, 761–7.
- Bays, H. E., González-Campoy, J. M., Bray, G. a, Kitabchi, A. E., Bergman, D. a, Schorr, A. B., ... Henry, R. R. (2008). Pathogenic potential of adipose tissue and metabolic consequences of adipocyte hypertrophy and increased visceral adiposity. *Expert Review of Cardiovascular Therapy*, *6*, 343–368.
- Bechtel, H. A., Martin, M. C., May, T. E., & Lerch, P. (2009). Improved spatial resolution for reflection mode infrared microscopy. *Review of Scientific Instruments*, *80*, 126106.
- Bellisola, G., & Sorio, C. (2012). Infrared spectroscopy and microscopy in cancer research and diagnosis. *American Journal of Cancer Research*, *2*, 1–21.
- Berg, A. H., Combs, T. P., Du, X., Brownlee, M., & Scherer, P. E. (2001). The adipocyte-secreted protein Acrp30 enhances hepatic insulin action. *Nature Medicine*, *7*, 947–53.
- Bi, X., Li, G., Doty, S. B., & Camacho, N. P. (2005). A novel method for determination of collagen orientation in cartilage by Fourier transform infrared imaging spectroscopy (FT-IRIS). *Osteoarthritis and Cartilage*, *13*, 1050–8.
- Bigornia, S. J., Farb, M. G., Mott, M. M., Hess, D. T., Carmine, B., Fiscale, A., ... Gokce, N. (2012). Relation of depot-specific adipose inflammation to insulin resistance in human obesity. *Nutrition & Diabetes*, *2*, e30.
- Björntorp, P. (1990). “Portal” adipose tissue as a generator of risk factors for cardiovascular disease and diabetes. *Arteriosclerosis, Thrombosis, and Vascular*

*Biology*, 10, 493–497.

- Björntorp, P. (1995). Endocrine abnormalities of obesity. *Metabolism*, 44, 21–23.
- Blaak, E. (2001). Gender differences in fat metabolism. *Current Opinion in Clinical Nutrition and Metabolic Care*, 4, 499–502.
- Bloor, I. D., & Symonds, M. E. (2014). Sexual dimorphism in white and brown adipose tissue with obesity and inflammation. *Hormones and Behavior*, 66, 95–103.
- Boden, G., & Shulman, G. I. (2002). Free fatty acids in obesity and type 2 diabetes: defining their role in the development of insulin resistance and beta-cell dysfunction. *European Journal of Clinical Investigation*, 32 Suppl 3, 14–23.
- Bonora, E., Del Prato, S., Bonadonna, R. C., Gulli, G., Solini, A., Shank, M. L., ... DeFronzo, R. a. (1992). Total body fat content and fat topography are associated differently with in vivo glucose metabolism in nonobese and obese nondiabetic women. *Diabetes*, 41, 1151–1159.
- Bortolotto, J. W., Reis, C., Ferreira, A., Costa, S., Mottin, C. C., Souto, A. A., & Guaragna, R. M. (2005). Higher content of trans fatty acids in abdominal visceral fat of morbidly obese individuals undergoing bariatric surgery compared to non-obese subjects. *Obesity Surgery*, 15, 1265–70.
- Boskey, A. L., Goldberg, M., Kulkarni, A., & Gomez, S. (2006). Infrared imaging microscopy of bone: illustrations from a mouse model of Fabry disease. *Biochimica et Biophysica Acta*, 1758, 942–7.
- Bourlier, V., Zakaroff-Girard, A., Miranville, A., De Barros, S., Maumus, M., Sengenès, C., ... Bouloumie, A. (2008). Remodeling phenotype of human subcutaneous adipose tissue macrophages. *Circulation*, 117, 806–15.
- Bozkurt, O., Haman Bayari, S., Severcan, M., Krafft, C., Popp, J., & Severcan, F. (2012). Structural alterations in rat liver proteins due to streptozotocin-induced diabetes and the recovery effect of selenium: fourier transform infrared microspectroscopy and



- neural network study. *Journal of Biomedical Optics*, 17, 76023.
- Bozkurt, O., Severcan, M., & Severcan, F. (2010). Diabetes induces compositional, structural and functional alterations on rat skeletal soleus muscle revealed by FTIR spectroscopy: a comparative study with EDL muscle. *The Analyst*, 135, 3110–3119.
- Brereton, R. G. (2003). *Chemometrics : data analysis for the laboratory and chemical plant*. Wiley.
- Brochu, M., Starling, R. D., Tchernof, A., Matthews, D. E., Garcia-Rubi, E., & Poehlman, E. T. (2000). Visceral adipose tissue is an independent correlate of glucose disposal in older obese postmenopausal women. *The Journal of Clinical Endocrinology and Metabolism*, 85, 2378–84.
- Brown, C. D., Vega-Montoto, L., & Wentzell, P. D. (2000). Derivative preprocessing and optimal corrections for baseline drift in multivariate calibration. *Applied Spectroscopy*, 54, 1055–1068.
- Cakmak, G., Miller, L. M., Zorlu, F., & Severcan, F. (2012). Amifostine, a radioprotectant agent, protects rat brain tissue lipids against ionizing radiation induced damage: an FTIR microspectroscopic imaging study. *Archives of Biochemistry and Biophysics*, 520, 67–73.
- Cakmak, G., Togan, I., & Severcan, F. (2006). 17Beta-estradiol induced compositional, structural and functional changes in rainbow trout liver, revealed by FT-IR spectroscopy: a comparative study with nonylphenol. *Aquatic Toxicology (Amsterdam, Netherlands)*, 77, 53–63.
- Cakmak, G., Zorlu, F., Severcan, M., & Severcan, F. (2011). Screening of protective effect of amifostine on radiation-induced structural and functional variations in rat liver microsomal membranes by FT-IR spectroscopy. *Analytical Chemistry*, 83, 2438–44.
- Camhi, S. M., Bray, G. A., Bouchard, C., Greenway, F. L., Johnson, W. D., Newton, R. L., ... Katzmarzyk, P. T. (2011). The Relationship of Waist Circumference and BMI to Visceral, Subcutaneous, and Total Body Fat: Sex and Race Differences. *Obesity*,

19, 402–408.

Campbell, I. D., & Dwek, R. A. (1984). *Biological spectroscopy*. Benjamin/Cummings Pub. Co.

Campbell, P. J., Carlson, M. G., & Nurjhan, N. (1994). Fat metabolism in human obesity. *The American Journal of Physiology*, 266, E600-5.

Cancello, R., Zingaretti, M. C., Sarzani, R., Ricquier, D., & Cinti, S. (1998). Leptin and UCP1 genes are reciprocally regulated in brown adipose tissue. *Endocrinology*, 139, 4747–50.

Cannon, B., Hedin, A., & Nedergaard, J. (1982). Exclusive occurrence of thermogenin antigen in brown adipose tissue. *FEBS Letters*, 150, 129–32.

Cannon, B., & Nedergaard, J. (2004). Brown adipose tissue: function and physiological significance. *Physiological Reviews*, 84, 277–359.

Chen, H., Lin, Z., Wu, H., Wang, L., Wu, T., & Tan, C. (2015). Diagnosis of colorectal cancer by near-infrared optical fiber spectroscopy and random forest. *Spectrochimica Acta - Part A: Molecular and Biomolecular Spectroscopy*, 135, 185–191.

Cheung, O. K.-W., & Cheng, A. S.-L. (2016). Gender Differences in Adipocyte Metabolism and Liver Cancer Progression. *Frontiers in Genetics*, 7, 168.

Ci, Y. X., Gao, T. Y., Feng, J., & Guo, Z. Q. (1999). Fourier Transform Infrared Spectroscopic Characterization of Human Breast Tissue: Implications for Breast Cancer Diagnosis. *Applied Spectroscopy*, Vol. 53, Issue 3, Pp. 312-315, 53, 312–315.

Cinti, S. (2005). The adipose organ. *Prostaglandins Leukotrienes and Essential Fatty Acids*, 73, 9–15.

Cinti, S. (2006). The role of brown adipose tissue in human obesity. *Nutrition, Metabolism and Cardiovascular Diseases*, 16, 569–574.

Cinti, S. (2008). Reversible transdifferentiation in the adipose organ. *International Journal of Pediatric Obesity: IJPO: An Official Journal of the International*

*Association for the Study of Obesity*, 3 Suppl 2, 21–6.

- Cinti, S. (2009). Transdifferentiation properties of adipocytes in the adipose organ. *AJP: Endocrinology and Metabolism*, 297, E977–E986.
- Cnop, M., Havel, P. J., Utzschneider, K. M., Carr, D. B., Sinha, M. K., Boyko, E. J., ... Kahn, S. E. (2003). Relationship of adiponectin to body fat distribution, insulin sensitivity and plasma lipoproteins: evidence for independent roles of age and sex. *Diabetologia*, 46, 459–469.
- Coelho, M., Oliveira, T., & Fernandes, R. (2013). Biochemistry of adipose tissue: an endocrine organ. *Archives of Medical Science : AMS*, 9, 191–200.
- Cohen, D. H., & LeRoith, D. (2012). Obesity, type 2 diabetes, and cancer: the insulin and IGF connection. *Endocrine Related Cancer*, 19, F27–F45.
- Conway, J. M., Norris, K. H., & Bodwell, C. E. (1984). A new approach for the estimation of body composition: infrared interactance. *The American Journal of Clinical Nutrition*, 40, 1123–30.
- Cox, T. F. (2005). *An introduction to multivariate data analysis*. Hodder Education.
- Çakmak, G., Togan, I., Uğuz, C., & Severcan, F. (2003). FT-IR spectroscopic analysis of rainbow trout liver exposed to nonylphenol. *Applied Spectroscopy*, 57, 835–841.
- de Ferranti, S., & Mozaffarian, D. (2008). The Perfect Storm: Obesity, Adipocyte Dysfunction, and Metabolic Consequences. *Clinical Chemistry*, 54.
- Derenne, A., Vandersleyen, O., & Goormaghtigh, E. (2014). Lipid quantification method using FTIR spectroscopy applied on cancer cell extracts. *Biochimica et Biophysica Acta*, 1841, 1200–9.
- Diem, M. (1993). *Introduction to modern vibrational spectroscopy*. Wiley.
- Díez, J. J., & Iglesias, P. (2003). The role of the novel adipocyte-derived hormone adiponectin in human disease. *European Journal of Endocrinology*, 148, 293–300.

- Dogan, A., Ergen, K., Budak, F., & Severcan, F. (2007). Evaluation of disseminated candidiasis on an experimental animal model: a fourier transform infrared study. *Applied Spectroscopy*, *61*, 199–203.
- Dogan, A., Lasch, P., Neuschl, C., Millrose, M. K., Alberts, R., Schughart, K., ... Brockmann, G. A. (2013). ATR-FTIR spectroscopy reveals genomic loci regulating the tissue response in high fat diet fed BXD recombinant inbred mouse strains. *BMC Genomics*, *14*, 386.
- Drolet, R., Richard, C., Sniderman, A. D., Mailloux, J., Fortier, M., Huot, C., ... Tchernof, A. (2008). Hypertrophy and hyperplasia of abdominal adipose tissues in women. *International Journal of Obesity*, *32*, 283–291.
- Duplus, E., Glorian, M., & Forest, C. (2000). Fatty acid regulation of gene transcription. *The Journal of Biological Chemistry*, *275*, 30749–52.
- Edens, N. K., Fried, S. K., Kral, J. G., Hirsch, J., & Leibel, R. L. (1993). In vitro lipid synthesis in human adipose tissue from three abdominal sites. *The American Journal of Physiology*, *265*, E374-9.
- Fabian, H., Jackson, M., Murphy, L., Watson, P. H., Fichtner, I., & Mantsch, H. H. (1995). A comparative infrared spectroscopic study of human breast tumors and breast tumor cell xenografts. *Biospectroscopy*, *1*, 37–45.
- Farhan, K. M., Sastry, T. P., & Mandal, A. B. (2011). *Comparative study on secondary structural changes in diabetic and non-diabetic human finger nail specimen by using FTIR spectra. Clinica Chimica Acta* (Vol. 412).
- Farnier, C., Krief, S., Blache, M., Diot-Dupuy, F., Mory, G., Ferre, P., & Bazin, R. (2003). Adipocyte functions are modulated by cell size change: potential involvement of an integrin/ERK signalling pathway. *International Journal of Obesity and Related Metabolic Disorders: Journal of the International Association for the Study of Obesity*, *27*, 1178–86.
- Fernández-Real, J. M., & Ricart, W. (2003). Insulin Resistance and Chronic

- Cardiovascular Inflammatory Syndrome. *Endocrine Reviews*, 24, 278–301.
- Fox, C. S., Massaro, J. M., Hoffmann, U., Pou, K. M., Maurovich-Horvat, P., Liu, C.-Y., ... O'Donnell, C. J. (2007). Abdominal Visceral and Subcutaneous Adipose Tissue Compartments: Association With Metabolic Risk Factors in the Framingham Heart Study. *Circulation*, 116, 39–48.
- Frayn, K. N. (2000). Visceral fat and insulin resistance--causative or correlative? *The British Journal of Nutrition*, 83 Suppl 1, S71-7.
- Freedland, E. S. (2004). Role of a critical visceral adipose tissue threshold (CVATT) in metabolic syndrome: implications for controlling dietary carbohydrates: a review. *Nutrition & Metabolism*, 1, 12.
- Freifelder, D. (1982). *Physical Biochemistry, Application to Biochemistry and Molecular Biology*. Physical Biochemistry, Application to Biochemistry and Molecular Biology. W.H. Freeman.
- Fried, S. K., Bunkin, D. A., & Greenberg, A. S. (1998). Omental and Subcutaneous Adipose Tissues of Obese Subjects Release Interleukin-6: Depot Difference and Regulation by Glucocorticoid <sup>1</sup>. *The Journal of Clinical Endocrinology & Metabolism*, 83, 847–850.
- Fried, S. K., & Kral, J. G. (1987). Sex differences in regional distribution of fat cell size and lipoprotein lipase activity in morbidly obese patients. *International Journal of Obesity*, 11, 129–40.
- Friedman, J. M., & Halaas, J. L. (1998). Leptin and the regulation of body weight in mammals. *Nature*, 395, 763–770.
- Fung Kee Fung, M., Senterman, M., Eid, P., Faught, W., Mikhael, N. Z., & Wong, P. T. (1997). Comparison of Fourier-transform infrared spectroscopic screening of exfoliated cervical cells with standard Papanicolaou screening. *Gynecologic Oncology*, 66, 10–15.

- Gaigneaux, A., Ruysschaert, J. M., & Goormaghtigh, E. (2006). Cell Discrimination by Attenuated Total Reflection–Fourier Transform Infrared Spectroscopy: The Impact of Preprocessing of Spectra. *Applied Spectroscopy*, *60*, 1022–1028.
- Garaulet, M., Hernandez-Morante, J. J., Lujan, J., Tebar, F. J., & Zamora, S. (2006). Relationship between fat cell size and number and fatty acid composition in adipose tissue from different fat depots in overweight/obese humans. *International Journal of Obesity*, *30*, 899–905.
- Garaulet, M., Pérez-Llamas, F., Pérez-Ayala, M., Martínez, P., de Medina, F. S., Tebar, F. J., & Zamora, S. (2001). Site-specific differences in the fatty acid composition of abdominal adipose tissue in an obese population from a Mediterranean area: relation with dietary fatty acids, plasma lipid profile, serum insulin, and central obesity. *The American Journal of Clinical Nutrition*, *74*, 585–91.
- Garip, S., Bayari, S. H., Severcan, M., Abbas, S., Lednev, I. K., & Severcan, F. (2016). Structural effects of simvastatin on liver rat [corrected] tissue: Fourier transform infrared and Raman microspectroscopic studies. *Journal of Biomedical Optics*, *21*, 25008.
- Garip, S., Bozoglu, F., & Severcan, F. (2007). Differentiation of Mesophilic and Thermophilic Bacteria with Fourier Transform Infrared Spectroscopy. *Applied Spectroscopy*, *61*, 186–192.
- Garip, S., Gozen, A. C., & Severcan, F. (2009). Use of Fourier transform infrared spectroscopy for rapid comparative analysis of *Bacillus* and *Micrococcus* isolates. *Food Chemistry*, *113*, 1301–1307.
- Garip, S., Yapici, E., Ozek, N. S., Severcan, M., & Severcan, F. (2010). Evaluation and discrimination of simvastatin-induced structural alterations in proteins of different rat tissues by FTIR spectroscopy and neural network analysis. *The Analyst*, *135*, 3233–41.
- Gaspar, R., Dewelle, J., Kiss, R., Mijatovic, T., & Goormaghtigh, E. (2009). IR

- spectroscopy as a new tool for evidencing antitumor drug signatures. *Biochimica et Biophysica Acta*, 1788, 1263–70.
- Gasper, R., Mijatovic, T., Bénard, A., Derenne, A., Kiss, R., & Goormaghtigh, E. (2010). FTIR spectral signature of the effect of cardiogenic steroids with antitumoral properties on a prostate cancer cell line. *Biochimica et Biophysica Acta*, 1802, 1087–94.
- Gastaldelli, A., Miyazaki, Y., Pettiti, M., Matsuda, M., Mahankali, S., Santini, E., ... Ferrannini, E. (2002). Metabolic effects of visceral fat accumulation in type 2 diabetes. *The Journal of Clinical Endocrinology and Metabolism*, 87, 5098–103.
- Gazi, E., Baker, M., Dwyer, J., Lockyer, N. P., Gardner, P., Shanks, J. H., ... Brown, M. D. (2006). A Correlation of FTIR Spectra Derived from Prostate Cancer Biopsies with Gleason Grade and Tumour Stage. *European Urology*, 50, 750–761.
- Geer, E. B., & Shen, W. (2009). Gender differences in insulin resistance, body composition, and energy balance. *Gender Medicine*, 6 Suppl 1, 60–75.
- Giese, A. T., & French, C. S. (1955). The Analysis of Overlapping Spectral Absorption Bands by Derivative Spectrophotometry. *Applied Spectroscopy*, 9, 78–96.
- Gok, S., Aydin, O. Z., Sural, Y. S., Zorlu, F., Bayol, U., & Severcan, F. (2016). Bladder cancer diagnosis from bladder wash by Fourier transform infrared spectroscopy as a novel test for tumor recurrence. *Journal of Biophotonics*, 9, 967–75.
- Goodman-Gruen, D., & Barrett-Connor, E. (1996). Sex differences in measures of body fat and body fat distribution in the elderly. *American Journal of Epidemiology*, 143, 898–906.
- Goormaghtigh, E., Raussens, V., & Ruyschaert, J. M. (1999). Attenuated total reflection infrared spectroscopy of proteins and lipids in biological membranes. *Biochimica et Biophysica Acta*, 1422, 105–85.
- Gray, D. S., & Fujioka, K. (1991). Use of relative weight and Body Mass Index for the

- determination of adiposity. *Journal of Clinical Epidemiology*, 44, 545–50.
- Gregor, M. F., & Hotamisligil, G. S. (2007). Thematic review series: Adipocyte Biology. Adipocyte stress: the endoplasmic reticulum and metabolic disease. *The Journal of Lipid Research*, 48, 1905–1914.
- Guilherme, A., Virbasius, J. V, Puri, V., & Czech, M. P. (2008). Adipocyte dysfunctions linking obesity to insulin resistance and type 2 diabetes. *Nature Reviews. Molecular Cell Biology*, 9, 367–77.
- Gunawardana, S. C., & Piston, D. W. (2012). Reversal of type 1 diabetes in mice by brown adipose tissue transplant. *Diabetes*, 61, 674–82.
- Hageman, R. S., Wagener, A., Hantschel, C., Svenson, K. L., Churchill, G. A., & Brockmann, G. A. (2010). High-fat diet leads to tissue-specific changes reflecting risk factors for diseases in DBA/2J mice. *Physiological Genomics*, 42, 55–66.
- Hagman, D. K., Kuzma, J. N., Larson, I., Foster-Schubert, K. E., Kuan, L.-Y., Cignarella, A., ... Kratz, M. (2012). Characterizing and quantifying leukocyte populations in human adipose tissue: impact of enzymatic tissue processing. *Journal of Immunological Methods*, 386, 50–9.
- Hajer, G. R., van Haeften, T. W., & Visseren, F. L. J. (2008). Adipose tissue dysfunction in obesity, diabetes, and vascular diseases. *European Heart Journal*, 29, 2959–2971.
- Hantschel, C., Wagener, A., Neuschl, C., Teupser, D., & Brockmann, G. A. (2011). Features of the metabolic syndrome in the Berlin fat mouse as a model for human obesity. *Obesity Facts*, 4, 270–277.
- Hardy, O. T., Czech, M. P., & Corvera, S. (2012a). What causes the insulin resistance underlying obesity? *Current Opinion in Endocrinology, Diabetes, and Obesity*, 19, 81–7.
- Hardy, O. T., Czech, M. P., & Corvera, S. (2012b). What causes the insulin resistance underlying obesity? *Current Opinion in Endocrinology, Diabetes, and Obesity*, 19,



- Haris, P. I., & Severcan, F. (1999). FTIR spectroscopic characterization of protein structure in aqueous and non-aqueous media. *Journal of Molecular Catalysis B: Enzymatic*, 7, 207–221.
- Heilbronn, L. K., & Campbell, L. V. (2008). Adipose tissue macrophages, low grade inflammation and insulin resistance in human obesity. *Current Pharmaceutical Design*, 14, 1225–30.
- Hof, M., Hutterer, R., & Fidler, V. (Eds.). (2005). *Fluorescence Spectroscopy in Biology* (Vol. 3). Berlin/Heidelberg: Springer-Verlag. doi:10.1007/b138383
- Hoi-Ying N Holman. (2013). Catheter based mid-infrared reflectance and reflectance generated absorption spectroscopy. Retrieved from <https://www.google.com/patents/US8571640>
- Hormoz Azizian, Suzanna Winsborough, Michael Younikian, C. W. (2003). Method of in-vivo measurement of fat content of a body and apparatus therefor. Retrieved from <https://www.google.com/patents/CA2404891C?cl=en>
- Horowitz, J. F., Coppack, S. W., Paramore, D., Cryer, P. E., Zhao, G., & Klein, S. (1999). Effect of short-term fasting on lipid kinetics in lean and obese women. *The American Journal of Physiology*, 276, E278-84.
- Hosogai, N., Fukuhara, A., Oshima, K., Miyata, Y., Tanaka, S., Segawa, K., ... Shimomura, I. (2007). Adipose Tissue Hypoxia in Obesity and Its Impact on Adipocytokine Dysregulation. *Diabetes*, 56, 901–911.
- Hossain, P., Kavar, B., & El Nahas, M. (2007). Obesity and diabetes in the developing world--a growing challenge. *The New England Journal of Medicine*, 356, 213–5.
- Hotamisligil, G. S., Arner, P., Caro, J. F., Atkinson, R. L., & Spiegelman, B. M. (1995). Increased adipose tissue expression of tumor necrosis factor-alpha in human obesity and insulin resistance. *The Journal of Clinical Investigation*, 95, 2409–15.

- Hotamisligil, G. S., Shargill, N. S., & Spiegelman, B. M. (1993). Adipose expression of tumor necrosis factor- $\alpha$ : direct role in obesity-linked insulin resistance. *Science (New York, N.Y.)*, 259, 87–91.
- Howard, J. K., & Flier, J. S. (2006). Attenuation of leptin and insulin signaling by SOCS proteins. *Trends in Endocrinology & Metabolism*, 17, 365–371.
- Hsieh, P.-S. (2011). Obesity-Induced Adipose Tissue Inflammation and Insulin Resistance. In *Role of the Adipocyte in Development of Type 2 Diabetes*. InTech. doi:10.5772/20561
- Huang, C.-Y., Huang, H.-L., Yang, K.-C., Lee, L.-T., Yang, W.-S., Huang, K.-C., & Tseng, F.-Y. (2015). Serum Triglyceride Levels Independently Contribute to the Estimation of Visceral Fat Amount Among Nondiabetic Obese Adults. *Medicine*, 94, e965.
- Ibrahim, M. M. (2010). Subcutaneous and visceral adipose tissue: Structural and functional differences. *Obesity Reviews*, 11, 11–18.
- Ishida, K. P., & Griffiths, P. R. (1993). Comparison of the Amide I/II Intensity Ratio of Solution and Solid-State Proteins Sampled by Transmission, Attenuated Total Reflectance, and Diffuse Reflectance Spectrometry. *Applied Spectroscopy*, Vol. 47, Issue 5, Pp. 584-589, 47, 584–589.
- Jackson, M., Ramjiawan, B., Hewko, M., & Mantsch, H. H. (1998). Infrared microscopic functional group mapping and spectral clustering analysis of hypercholesterolemic rabbit liver. *Cellular and Molecular Biology (Noisy-Le-Grand, France)*, 44, 89–98.
- Jensen, M. D., Haymond, M. W., Rizza, R. A., Cryer, P. E., & Miles, J. M. (1989). Influence of body fat distribution on free fatty acid metabolism in obesity. *The Journal of Clinical Investigation*, 83, 1168–73.
- Josse, A. R., Azizian, H., French, S. B., Kramer, J. K. G., & Phillips, S. M. (2011). Body Fat Content Determination in Premenopausal, Overweight, and Obese Young Women Using DXA and FT-NIR. *Obesity*, 19, 1497–1502.

- Jung, U., & Choi, M.-S. (2014). Obesity and Its Metabolic Complications: The Role of Adipokines and the Relationship between Obesity, Inflammation, Insulin Resistance, Dyslipidemia and Nonalcoholic Fatty Liver Disease. *International Journal of Molecular Sciences*, *15*, 6184–6223.
- Kahn, B. B., & Flier, J. S. (2000). Obesity and insulin resistance. *The Journal of Clinical Investigation*, *106*, 473–81.
- Kastorini, C.-M., Milionis, H. J., Esposito, K., Giugliano, D., Goudevenos, J. A., & Panagiotakos, D. B. (2011). The Effect of Mediterranean Diet on Metabolic Syndrome and its Components. *Journal of the American College of Cardiology*, *57*, 1299–1313.
- Katiyar, D., Singh, B., Lall, A. M., & Haldar, C. (2011). Efficacy of chitooligosaccharides for the management of diabetes in alloxan induced mice: A correlative study with antihyperlipidemic and antioxidative activity. *European Journal of Pharmaceutical Sciences*, *44*, 534–543.
- Kazarian, S. G., & Chan, K. L. A. (2006). Applications of ATR-FTIR spectroscopic imaging to biomedical samples. *Biochimica et Biophysica Acta (BBA) - Biomembranes*, *1758*, 858–867.
- Kern, P. A., Saghizadeh, M., Ong, J. M., Bosch, R. J., Deem, R., & Simsolo, R. B. (1995). The expression of tumor necrosis factor in human adipose tissue. Regulation by obesity, weight loss, and relationship to lipoprotein lipase. *Journal of Clinical Investigation*, *95*, 2111–2119.
- Kershaw, E. E., & Flier, J. S. (2004). Adipose Tissue as an Endocrine Organ. *The Journal of Clinical Endocrinology & Metabolism*, *89*, 2548–2556.
- Klaus, S., Casteilla, L., Bouillaud, F., & Ricquier, D. (1991). The uncoupling protein UCP: a membraneous mitochondrial ion carrier exclusively expressed in brown adipose tissue. *The International Journal of Biochemistry*, *23*, 791–801.
- Kneipp, J., Beekes, M., Lasch, P., & Naumann, D. (2002). Molecular changes of

- preclinical scrapie can be detected by infrared spectroscopy. *The Journal of Neuroscience : The Official Journal of the Society for Neuroscience*, 22, 2989–2997.
- Kneipp, J., Lasch, P., Baldauf, E., Beekes, M., & Naumann, D. (2000). Detection of pathological molecular alterations in scrapie-infected hamster brain by Fourier transform infrared (FT-IR) spectroscopy. *Biochimica et Biophysica Acta - Molecular Basis of Disease*, 1501, 189–199.
- Kotani, K., Tokunaga, K., Fujioka, S., Kobatake, T., Keno, Y., Yoshida, S., ... Matsuzawa, Y. (1994). Sexual dimorphism of age-related changes in whole-body fat distribution in the obese. *International Journal of Obesity and Related Metabolic Disorders : Journal of the International Association for the Study of Obesity*, 18, 207–2.
- Koyama, K., Chen, G., Lee, Y., & Unger, R. H. (1997). Tissue triglycerides, insulin resistance, and insulin production: implications for hyperinsulinemia of obesity. *The American Journal of Physiology*, 273, E708-13.
- Kretlow, A., Wang, Q., Beekes, M., Naumann, D., & Miller, L. M. (2008). Changes in protein structure and distribution observed at pre-clinical stages of scrapie pathogenesis. *Biochimica et Biophysica Acta (BBA) - Molecular Basis of Disease*, 1782, 559–565.
- Kucuk Baloglu, F., Garip, S., Heise, S., Brockmann, G., & Severcan, F. (2015). FTIR imaging of structural changes in visceral and subcutaneous adiposity and brown to white adipocyte transdifferentiation. *The Analyst*, 140, 2205–14.
- Kumar, S., Shabi, T. S., Goormaghtigh, E., Khamis, Z., Sahab, Z., Sang, Q.-X., ... Baehner, F. (2014). A FTIR Imaging Characterization of Fibroblasts Stimulated by Various Breast Cancer Cell Lines. *PLoS ONE*, 9, e111137.
- Lafontan, M., & Berlan, M. (2003). Do regional differences in adipocyte biology provide new pathophysiological insights? *Trends in Pharmacological Sciences*, 24, 276–283.
- Lago, F., Dieguez, C., Gómez-Reino, J., & Gualillo, O. (2007). Adipokines as emerging

- mediators of immune response and inflammation. *Nature Clinical Practice. Rheumatology*, 3, 716–24.
- Lasch, P., Haensch, W., Naumann, D., & Diem, M. (2004). Imaging of colorectal adenocarcinoma using FT-IR microspectroscopy and cluster analysis. *Biochimica et Biophysica Acta - Molecular Basis of Disease*, 1688, 176–186.
- Lavine, B. K. (2000). Chemometrics. *Anal. Chem.*, 72 (12), pp 91–98.
- Lemieux, I., Pascot, A., Prud'homme, D., Alméras, N., Bogaty, P., Nadeau, A., ... Després, J. P. (2001). Elevated C-reactive protein: another component of the atherothrombotic profile of abdominal obesity. *Arteriosclerosis, Thrombosis, and Vascular Biology*, 21, 961–7.
- Lemieux, S., & Després, J. P. (1994). Metabolic complications of visceral obesity: contribution to the aetiology of type 2 diabetes and implications for prevention and treatment. *Diabete & Metabolisme*, 20, 375–93.
- Levin, I. W., & Bhargava, R. (2005). Fourier transform infrared vibrational spectroscopic imaging: integrating microscopy and molecular recognition. *Annual Review of Physical Chemistry*, 56, 429–474.
- LeVine, S. M., & Wetzel, D. L. (1998). Chemical analysis of multiple sclerosis lesions by FT-IR microspectroscopy. *Free Radical Biology & Medicine*, 25, 33–41.
- Li, G.-Z., Bu, H.-L., Yang, M. Q., Zeng, X.-Q., & Yang, J. Y. (2008). Selecting subsets of newly extracted features from PCA and PLS in microarray data analysis. *BMC Genomics*, 9 Suppl 2, S24.
- Li, X., Li, Q.-B., Zhang, G.-J., Xu, Y.-Z., Sun, X.-J., Shi, J.-S., ... Wu, J.-G. (2012). Identification of Colitis and Cancer in Colon Biopsies by Fourier Transform Infrared Spectroscopy and Chemometrics. *The Scientific World Journal*, 2012, 1–4.
- Liu, X., Zheng, Z., Zhu, X., Meng, M., Li, L., Shen, Y., ... Jin, W. (2013). Brown adipose tissue transplantation improves whole-body energy metabolism. *Cell Research*, 23,

851–854.

- Lovejoy, J. C., Bray, G. A., Bourgeois, M. O., Macchiavelli, R., Rood, J. C., Greeson, C., & Partington, C. (1996). Exogenous androgens influence body composition and regional body fat distribution in obese postmenopausal women--a clinical research center study. *The Journal of Clinical Endocrinology & Metabolism*, 81, 2198–2203.
- Machann, J., Stefan, N., Schabel, C., Schleicher, E., Fritsche, A., Würslin, C., ... Schick, F. (2012). Fraction of unsaturated fatty acids in visceral adipose tissue (VAT) is lower in subjects with high total VAT volume - a combined <sup>1</sup>H MRS and volumetric MRI study in male subjects. *NMR in Biomedicine*, 26, 232–236.
- Macotela, Y., Boucher, J., Tran, T. T., & Kahn, C. R. (2009). Sex and Depot Differences in Adipocyte Insulin Sensitivity and Glucose Metabolism. *Diabetes*, 58, 803–812.
- Maeda, N., Shimomura, I., Kishida, K., Nishizawa, H., Matsuda, M., Nagaretani, H., ... Matsuzawa, Y. (2002). Diet-induced insulin resistance in mice lacking adiponectin/ACRP30. *Nature Medicine*, 8, 731–737.
- Makki, K., Froguel, P., & Wolowczuk, I. (2013). Adipose tissue in obesity-related inflammation and insulin resistance: cells, cytokines, and chemokines. *ISRN Inflammation*, 2013, 139239.
- Manoharan, R., Baraga, J. J., Rava, R. P., Dasari, R. R., Fitzmaurice, M., & Feld, M. S. (1993). Biochemical analysis and mapping of atherosclerotic human artery using FT-IR microspectroscopy. *Atherosclerosis*, 103, 181–93.
- Manoharan, R., Wang, Y., & Feld, M. S. (1996). Histochemical analysis of biological tissues using Raman spectroscopy. *Spectrochimica Acta Part A: Molecular and Biomolecular Spectroscopy*, 52, 215–249.
- Mantsch, H. H. (1984). Biological applications of fourier transform infrared spectroscopy: a study of phase transitions in biomembranes. *Journal of Molecular Structure*, 113, 201–212.

- Marcelli, A., Cricenti, A., Kwiatek, W. M., & Petibois, C. (2012). Biological applications of synchrotron radiation infrared spectromicroscopy. *Biotechnology Advances*, 30, 1390–404.
- Mariey, L., Signolle, J. P., Amiel, C., & Traver, J. (2001). Discrimination, classification, identification of microorganisms using FTIR spectroscopy and chemometrics. *Vibrational Spectroscopy*, 26, 151–159.
- Mårin, P., Andersson, B., Ottosson, M., Olbe, L., Chowdhury, B., Kvist, H., ... Björntorp, P. (1992). The morphology and metabolism of intraabdominal adipose tissue in men. *Metabolism: Clinical and Experimental*, 41, 1242–8.
- Mark, H., Workman, J., Mark, H., & Workman, J. (2007). 55 – Derivatives in Spectroscopy: Part 2 – The “True” Derivative. In *Chemometrics in Spectroscopy* (p. 351–XIX).
- Massart D, Vandeginste B, Deming S, Michotte Y, K. L. (2003). *Evaluation of precision and accuracy. Comparison of two procedures. Chemometrics: a textbook*. Elsevier Science, BV, Amsterdam, The Netherlands.
- McArdle, M. A., Finucane, O. M., Connaughton, R. M., McMorrow, A. M., & Roche, H. M. (2013). Mechanisms of Obesity-Induced Inflammation and Insulin Resistance: Insights into the Emerging Role of Nutritional Strategies. *Frontiers in Endocrinology*, 4. doi:10.3389/fendo.2013.00052
- Meek, S. E., Nair, K. S., & Jensen, M. D. (1999). Insulin regulation of regional free fatty acid metabolism. *Diabetes*, 48, 10–4.
- Melin, A.-M., Perromat, A., & Déléris, G. (2000). Pharmacologic application of Fourier transform IR spectroscopy: In vivo toxicity of carbon tetrachloride on rat liver. *Biopolymers*, 57, 160–168.
- Mendelsohn R, M. H. (1986). *Fourier transform infrared studies of lipidprotein interaction, Progress in Protein-Lipid Interactions* (vol 2). Netherlands: Elsevier Science Publishers.

- Meyer, C. W., Wagener, A., Rink, N., Hantschel, C., Heldmaier, G., Klingenspor, M., & Brockmann, G. A. (2009). High Energy Digestion Efficiency and Altered Lipid Metabolism Contribute to Obesity in BFM1 Mice. *Obesity*, *17*, 1988–1993.
- Misra, A., & Vikram, N. K. (2003). Clinical and Pathophysiological Consequences of Abdominal Adiposity and Abdominal Adipose Tissue Depots. *Nutrition*, *19*, 457–66.
- Misra, A., Wasir, J. S., & Vikram, N. K. (2005). Waist circumference criteria for the diagnosis of abdominal obesity are not applicable uniformly to all populations and ethnic groups. *Nutrition (Burbank, Los Angeles County, Calif.)*, *21*, 969–76.
- Mittra, S., Bansal, V. S., & Bhatnagar, P. K. (2008). From a glucocentric to a lipocentric approach towards metabolic syndrome. *Drug Discovery Today*, *13*, 211–218.
- Motoshima, H., Wu, X., Sinha, M. K., Hardy, V. E., Rosato, E. L., Barbot, D. J., ... Goldstein, B. J. (2002). Differential Regulation of Adiponectin Secretion from Cultured Human Omental and Subcutaneous Adipocytes: Effects of Insulin and Rosiglitazone. *The Journal of Clinical Endocrinology & Metabolism*, *87*, 5662–5667.
- Mourant, J. R., Yamada, Y. R., Carpenter, S., Dominique, L. R., & Freyer, J. P. (2003). FTIR Spectroscopy Demonstrates Biochemical Differences in Mammalian Cell Cultures at Different Growth Stages. *Biophysical Journal*, *85*, 1938–1947.
- Movasaghi, Z., Rehman, S., & ur Rehman, D. I. (2008). Fourier Transform Infrared (FTIR) Spectroscopy of Biological Tissues. *Applied Spectroscopy Reviews*, *43*, 134–179.
- Müller, G., Ertl, J., Gerl, M., & Preibisch, G. (1997). Leptin impairs metabolic actions of insulin in isolated rat adipocytes. *The Journal of Biological Chemistry*, *272*, 10585–93.
- Nakamura, T., Kelly, J. G., Trevisan, J., Cooper, L. J., Bentley, A. J., Carmichael, P. L., ... Martin, F. L. (2010). Microspectroscopy of spectral biomarkers associated with



- human corneal stem cells. *Molecular Vision*, *16*, 359–68.
- Nara, M., Okazaki, M., & Kagi, H. (2002). Infrared study of human serum very-low-density and low-density lipoproteins. Implication of esterified lipid C=O stretching bands for characterizing lipoproteins. *Chemistry and Physics of Lipids*, *117*, 1–6.
- Naumann Dieter, Fabian Heinz, L. P. (2009). *Biological and Biomedical Infrared Spectroscopy*. IOS Press. doi:10.3233/978-1-60750-045-2-312
- Neuschl, C., Hantschel, C., Wagener, A., Schmitt, A. O., Illig, T., & Brockmann, G. A. (2010). A unique genetic defect on chromosome 3 is responsible for juvenile obesity in the Berlin Fat Mouse. *International Journal of Obesity*, *34*, 1706–1714.
- Nguyen, T. T., Hernández Mijares, A., Johnson, C. M., & Jensen, M. D. (1996). Postprandial leg and splanchnic fatty acid metabolism in nonobese men and women. *The American Journal of Physiology*, *271*, E965-72.
- Oka, R., Miura, K., Sakurai, M., Nakamura, K., Yagi, K., Miyamoto, S., ... Yamagishi, M. (2010). Impacts of Visceral Adipose Tissue and Subcutaneous Adipose Tissue on Metabolic Risk Factors in Middle-aged Japanese. *Obesity*, *18*, 153–160.
- Ouchi, N., Kihara, S., Arita, Y., Okamoto, Y., Maeda, K., Kuriyama, H., ... Matsuzawa, Y. (2000). Adiponectin, an adipocyte-derived plasma protein, inhibits endothelial NF-kappaB signaling through a cAMP-dependent pathway. *Circulation*, *102*, 1296–301.
- Ouchi, N., Parker, J. L., Lugus, J. J., & Walsh, K. (2011). Adipokines in inflammation and metabolic disease. *Nature Reviews Immunology*, *11*, 85–97.
- Ozek Simsek, N., Sara, Y., Onur, R., & Severcan, F. (2009). Low dose simvastatin induces compositional, structural and dynamic changes in rat skeletal extensor digitorum longus muscle tissue. *Bioscience Reports*, *30*, 41–50.
- Ozek, N. S., Tuna, S., Erson-Bensan, A. E., & Severcan, F. (2010). Characterization of microRNA-125b expression in MCF7 breast cancer cells by ATR-FTIR

- spectroscopy. *The Analyst*, *135*, 3094–102.
- Pan, D. A., Lillioja, S., Kriketos, A. D., Milner, M. R., Baur, L. A., Bogardus, C., ... Storlien, L. H. (1997). Skeletal muscle triglyceride levels are inversely related to insulin action. *Diabetes*, *46*, 983–8.
- Paschos, P., & Paletas, K. (2009). Non alcoholic fatty liver disease and metabolic syndrome. *Hippokratia*, *13*, 9–19.
- Pasquali, R. (2006). Obesity and androgens: facts and perspectives. *Fertility and Sterility*, *85*, 1319–1340.
- Pepys, M. B., & Hirschfield, G. M. (2003). C-reactive protein: a critical update. *Journal of Clinical Investigation*, *111*, 1805–1812.
- Pérez, C., Fernández-Galaz, C., Fernández-Agulló, T., Arribas, C., Andrés, A., Ros, M., & Carrascosa, J. M. (2004). Leptin Impairs Insulin Signaling in Rat Adipocytes. *Diabetes*, *53*.
- Phillips, D. I., Caddy, S., Ilic, V., Fielding, B. A., Frayn, K. N., Borthwick, A. C., & Taylor, R. (1996). Intramuscular triglyceride and muscle insulin sensitivity: evidence for a relationship in nondiabetic subjects. *Metabolism: Clinical and Experimental*, *45*, 947–50.
- Piya, M. K., McTernan, P. G., & Kumar, S. (2013). Adipokine inflammation and insulin resistance: the role of glucose, lipids and endotoxin. *The Journal of Endocrinology*, *216*, T1–T15.
- Popkin, B. M., Paeratakul, S., Zhai, F., & Ge, K. (1995). A review of dietary and environmental correlates of obesity with emphasis on developing countries. *Obesity Research*, *3 Suppl 2*, 145s–153s.
- Pou, K. M., Massaro, J. M., Hoffmann, U., Vasan, R. S., Maurovich-Horvat, P., Larson, M. G., ... Fox, C. S. (2007). Visceral and subcutaneous adipose tissue volumes are cross-sectionally related to markers of inflammation and oxidative stress: The

- Framingham Heart Study. *Circulation*, 116, 1234–1241.
- Pouliot, M. C., Després, J. P., Lemieux, S., Moorjani, S., Bouchard, C., Tremblay, A., ... Lupien, P. J. (1994). Waist circumference and abdominal sagittal diameter: best simple anthropometric indexes of abdominal visceral adipose tissue accumulation and related cardiovascular risk in men and women. *The American Journal of Cardiology*, 73, 460–8.
- Prieto-Hontoria, P. L., Pérez-Matute, P., Fernández-Galilea, M., Bustos, M., Martínez, J. A., & Moreno-Aliaga, M. J. (2011). Role of obesity-associated dysfunctional adipose tissue in cancer: A molecular nutrition approach. *Biochimica et Biophysica Acta (BBA) - Bioenergetics*, 1807, 664–678.
- Purnell, J. Q., Kahn, S. E., Samuels, M. H., Brandon, D., Loriaux, D. L., & Brunzell, J. D. (2009). Enhanced cortisol production rates, free cortisol, and 11 $\beta$ -HSD-1 expression correlate with visceral fat and insulin resistance in men: effect of weight loss. *American Journal of Physiology. Endocrinology and Metabolism*, 296, E351-7.
- Qatanani, M., & Lazar, M. A. (2007). Mechanisms of obesity-associated insulin resistance: many choices on the menu. *Genes & Development*, 21, 1443–55.
- Rajala, M. W., & Scherer, P. E. (2003). Minireview: The Adipocyte—At the Crossroads of Energy Homeostasis, Inflammation, and Atherosclerosis. *Endocrinology*, 144, 3765–3773.
- Reaven, G. M. (1997). Banting Lecture 1988. Role of insulin resistance in human disease. 1988. *Nutrition (Burbank, Los Angeles County, Calif.)*, 13, 65; discussion 64, 66.
- Reichart, U., Renne, U., Aigner, B., Kratzsch, J., & Brockmann, G. A. (2003). A Novel Leptin Receptor Variant with a Conservative Amino Acid Substitution (I359 V) in Body Weight Selected and Unselected Mouse Lines. *Experimental and Clinical Endocrinology & Diabetes*, 111, 283–287.
- Rieppo, L., Saarakkala, S., Närhi, T., Helminen, H. J., Jurvelin, J. S., Rieppo, J., ... Rieppo, J. (2012). Application of second derivative spectroscopy for increasing

- molecular specificity of fourier transform infrared spectroscopic imaging of articular cartilage. *Osteoarthritis and Cartilage*, 20, 451–459.
- Rigas, B., Morgello, S., Goldman, I. S., & Wong, P. T. (1990). Human colorectal cancers display abnormal Fourier-transform infrared spectra. *Proceedings of the National Academy of Sciences of the United States of America*, 87, 8140–4.
- Rodriguez-Cuenca, S., Pujol, E., Justo, R., Frontera, M., Oliver, J., Gianotti, M., & Roca, P. (2002). Sex-dependent Thermogenesis, Differences in Mitochondrial Morphology and Function, and Adrenergic Response in Brown Adipose Tissue. *Journal of Biological Chemistry*, 277, 42958–42963.
- Ruan, H., Hacohen, N., Golub, T. R., Van Parijs, L., & Lodish, H. F. (2002). Tumor necrosis factor-alpha suppresses adipocyte-specific genes and activates expression of preadipocyte genes in 3T3-L1 adipocytes: nuclear factor-kappaB activation by TNF-alpha is obligatory. *Diabetes*, 51, 1319–36.
- Russo, G. L. (2009). Dietary n–6 and n–3 polyunsaturated fatty acids: From biochemistry to clinical implications in cardiovascular prevention. *Biochemical Pharmacology*, 77, 937–946.
- Ryo, M., Nakamura, T., Kihara, S., Kumada, M., Shibazaki, S., Takahashi, M., ... Funahashi, T. (2004). Adiponectin as a biomarker of the metabolic syndrome. *Circulation Journal : Official Journal of the Japanese Circulation Society*, 68, 975–81.
- Rytka, J. M., Wueest, S., Schoenle, E. J., & Konrad, D. (2011). The portal theory supported by venous drainage-selective fat transplantation. *Diabetes*, 60, 56–63.
- Saely, C. H., Geiger, K., & Drexel, H. (2012). Brown versus white adipose tissue: a mini-review. *Gerontology*, 58, 15–23.
- Sallis, J. F., & Glanz, K. (2009). Physical activity and food environments: solutions to the obesity epidemic. *The Milbank Quarterly*, 87, 123–54.

- Schenk, S., Saberi, M., & Olefsky, J. M. (2008). Insulin sensitivity: modulation by nutrients and inflammation. *Journal of Clinical Investigation*, 118, 2992–3002.
- Schmidt, M., Wolfram, T., Rumpler, M., Tripp, C. P., & Grunze, M. (2007). Live cell adhesion assay with attenuated total reflection infrared spectroscopy. *Biointerphases*, 2, 1–5.
- Sen, I., Bozkurt, O., Aras, E., Heise, S., Brockmann, G. A., & Severcan, F. (2015). Lipid profiles of adipose and muscle tissues in mouse models of juvenile onset of obesity without high fat diet induction: a Fourier transform infrared (FT-IR) spectroscopic study. *Applied Spectroscopy*, 69, 679–88.
- Seni, G., & Elder, J. F. (2010). Ensemble Methods in Data Mining: Improving Accuracy Through Combining Predictions. *Synthesis Lectures on Data Mining and Knowledge Discovery*, 2, 1–126.
- Seraphim, P. M., Nunes, M. T., & Machado, U. F. (2001). GLUT4 protein expression in obese and lean 12-month-old rats: insights from different types of data analysis. *Brazilian Journal of Medical and Biological Research = Revista Brasileira de Pesquisas Medicas E Biologicas*, 34, 1353–62.
- Severcan, F., Bozkurt, O., Gurbanov, R., & Gorgulu, G. (2010). FT-IR spectroscopy in diagnosis of diabetes in rat animal model. *Journal of Biophotonics*, 3, 621–631.
- Severcan, F., & Haris, P. I. (2012). *Vibrational Spectroscopy in Diagnosis and Screening*. IOS Press. Retrieved from [https://books.google.com/books/about/Vibrational\\_Spectroscopy\\_in\\_Diagnosis\\_an.html?id=FEQVrQKJrsYC&pgis=1%5Cnhttps://books.google.com/books?id=FEQVrQKJrsYC&pgis=1](https://books.google.com/books/about/Vibrational_Spectroscopy_in_Diagnosis_an.html?id=FEQVrQKJrsYC&pgis=1%5Cnhttps://books.google.com/books?id=FEQVrQKJrsYC&pgis=1)
- Severcan, F., Okan Durmus, H., Eker, F., Akinoglu, B. G., & Haris, P. I. (2000). Vitamin D(2) modulates melittin-membrane interactions. *Talanta*, 53, 205–211.
- Shaps RH, S. J. (1980). Automated infrared spectra search and display. *European Spectroscopy News*, 32, 39–42.

- Shulman, G. I. (2000). Cellular mechanisms of insulin resistance. *The Journal of Clinical Investigation*, 106, 171–6.
- Smiley, B. L., & Richmond, G. L. (1999). Alkyl chain ordering of asymmetric phosphatidylcholines. *Journal of Physical Chemistry B*, 103, 653.
- Smith, S. R., Lovejoy, J. C., Greenway, F., Ryan, D., deJonge, L., de la Bretonne, J., ... Bray, G. A. (2001). Contributions of total body fat, abdominal subcutaneous adipose tissue compartments, and visceral adipose tissue to the metabolic complications of obesity. *Metabolism*, 50, 425–435.
- Sonmez, K., Akcakoyun, M., Akcay, A., Demir, D., Duran, N. E., Gencbay, M., ... Turan, F. (2003). Which method should be used to determine the obesity, in patients with coronary artery disease? (Body mass index, waist circumference or waist-hip ratio). *International Journal of Obesity*, 27, 341–346.
- Sopasakis, V. R., Sandqvist, M., Gustafson, B., Hammarstedt, A., Schmelz, M., Yang, X., ... Smith, U. (2004). High Local Concentrations and Effects on Differentiation Implicate Interleukin-6 as a Paracrine Regulator. *Obesity Research*, 12, 454–460.
- Spector, A. A., & Yorek, M. A. (1985). Membrane lipid composition and cellular function. *Journal of Lipid Research*, 26, 1015–35.
- Stanford, K. I., Middelbeek, R. J. W., Townsend, K. L., An, D., Nygaard, E. B., Hitchcox, K. M., ... Goodyear, L. J. (2013). Brown adipose tissue regulates glucose homeostasis and insulin sensitivity. *The Journal of Clinical Investigation*, 123, 215–23.
- Struve, W., & Mills, I. (1990). *Fundamentals of Molecular Spectroscopy. Vibrational Spectroscopy* (Vol. 1). Wiley. doi:10.1016/0924-2031(90)80014-U
- Stuart, B., & Ando, D. J. (1997). *Biological applications of infrared spectroscopy*. Published on behalf of ACOL (University of Greenwich) by John Wiley.
- Stuart, B. H. (2004). *Infrared Spectroscopy : Fundamentals and Applications*. J. Wiley.

- Sukuta, S., & Bruch, R. (1999). Factor analysis of cancer Fourier transform infrared evanescent wave fiberoptical (FTIR-FEW) spectra. *Lasers in Surgery and Medicine*, 24, 382–8.
- Susi, H., & Michael Byler, D. (1983). Protein structure by Fourier transform infrared spectroscopy: Second derivative spectra. *Biochemical and Biophysical Research Communications*, 115, 391–397.
- Svenson, K. L., Von Smith, R., Magnani, P. a, Suetin, H. R., Paigen, B., Naggert, J. K., ... Peters, L. L. (2007). Multiple trait measurements in 43 inbred mouse strains capture the phenotypic diversity characteristic of human populations. *Journal of Applied Physiology (Bethesda, Md. : 1985)*, 102, 2369–2378.
- Tchoukalova, Y. D., Koutsari, C., Karpyak, M. V, Votruba, S. B., Wendland, E., & Jensen, M. D. (2008). Subcutaneous adipocyte size and body fat distribution. *The American Journal of Clinical Nutrition*, 87, 56–63.
- Tilg, H., & Moschen, A. R. (2006). Adipocytokines: mediators linking adipose tissue, inflammation and immunity. *Nature Reviews Immunology*, 6, 772–783.
- Tordjman, J., Divoux, A., Prifti, E., Poitou, C., Pelloux, V., Hugol, D., ... Clement, K. (2012). Structural and inflammatory heterogeneity in subcutaneous adipose tissue: Relation with liver histopathology in morbid obesity. *Journal of Hepatology*, 56, 1152–1158.
- Townsend, K., & Tseng, Y.-H. (2012). Brown adipose tissue: Recent insights into development, metabolic function and therapeutic potential. *Adipocyte*, 1, 13–24.
- Toyran, N., Turan, B., & Severcan, F. (2007). Selenium alters the lipid content and protein profile of rat heart: An FTIR microspectroscopic study. *Archives of Biochemistry and Biophysics*, 458, 184–193.
- Toyran, N., Zorlu, F., Dönmez, G., Öge, K., & Severcan, F. (2004). Chronic hypoperfusion alters the content and structure of proteins and lipids of rat brain homogenates: a Fourier transform infrared spectroscopy study. *European Biophysics*

*Journal*, 33, 549–554.

- Trayhurn, P., Drevon, C. A., & Eckel, J. (2011). Secreted proteins from adipose tissue and skeletal muscle – adipokines, myokines and adipose/muscle cross-talk. *Archives of Physiology and Biochemistry*, 117, 47–56.
- Tritos, N. A., & Mantzoros, C. S. (1997). Leptin: its role in obesity and beyond. *Diabetologia*, 40, 1371–1379.
- Tulloch-Reid, M. K., Hanson, R. L., Sebring, N. G., Reynolds, J. C., Premkumar, A., Genovese, D. J., & Sumner, A. E. (2004). Both Subcutaneous and Visceral Adipose Tissue Correlate Highly with Insulin Resistance in African Americans. *Obesity Research*, 12, 1352–1359.
- Turkish Statistical Institute. (2014). Turkey health survey 2014. Retrieved February 12, 2017, from <http://www.tuik.gov.tr/PreHaberBultenleri.do?id=18854>
- van Beek, L., Lips, M. A., Visser, A., Pijl, H., Ioan-Facsinay, A., Toes, R., ... van Harmelen, V. (2014). Increased systemic and adipose tissue inflammation differentiates obese women with T2DM from obese women with normal glucose tolerance. *Metabolism*, 63, 492–501.
- van Kruijsdijk, R. C. M., van der Wall, E., & Visseren, F. L. J. (2009). Obesity and Cancer: The Role of Dysfunctional Adipose Tissue. *Cancer Epidemiology and Prevention Biomarkers*, 18.
- van Rhijn, B. W. G., van der Poel, H. G., & van der Kwast, T. H. (2009). Cytology and Urinary Markers for the Diagnosis of Bladder Cancer. *European Urology Supplements*, 8, 536–541.
- Vidal, H., Auboeuf, D., De Vos, P., Staels, B., Riou, J. P., Auwerx, J., & Laville, M. (1996). The expression of ob gene is not acutely regulated by insulin and fasting in human abdominal subcutaneous adipose tissue. *Journal of Clinical Investigation*, 98, 251–255.



- Voortman, G., Gerrits, J., Altavilla, M., Henning, M., van Bergeijk, L., & Hessels, J. (2002). Quantitative determination of faecal fatty acids and triglycerides by Fourier transform infrared analysis with a sodium chloride transmission flow cell. *Clinical Chemistry and Laboratory Medicine*, 40, 795–8.
- Wadden, T. A., & Stunkard, A. J. (n.d.). *Handbook of obesity treatment*. Guilford Press.
- Wagener, A., Goessling, H. F., Schmitt, A. O., Mauel, S., Gruber, A. D., Reinhardt, R., & Brockmann, G. A. (2010). Genetic and diet effects on Ppar- $\alpha$  and Ppar- $\gamma$  signaling pathways in the Berlin Fat Mouse Inbred line with genetic predisposition for obesity. *Lipids in Health and Disease*, 9, 99.
- Wagener, A., Schmitt, A. O., Aksu, S., Schlote, W., Neuschl, C., & Brockmann, G. A. (2006). Genetic, sex, and diet effects on body weight and obesity in the Berlin Fat Mouse Inbred lines. *Physiological Genomics*, 27, 264–270.
- Wajchenberg, B. L. (2000). Subcutaneous and Visceral Adipose Tissue: Their Relation to the Metabolic Syndrome. *Endocrine Reviews*, 21, 697–738.
- Wang, L., & Mizaikoff, B. (2008). Application of multivariate data-analysis techniques to biomedical diagnostics based on mid-infrared spectroscopy. *Analytical and Bioanalytical Chemistry*, 391, 1641–54.
- Wang, Q., Sanad, W., Miller, L. M., Voigt, A., Klingel, K., Kandolf, R., ... Baumann, G. (2005). Infrared imaging of compositional changes in inflammatory cardiomyopathy. *Vibrational Spectroscopy*, 38, 217–222.
- Wang, T. D., Triadafilopoulos, G., Crawford, J. M., Dixon, L. R., Bhandari, T., Sahbaie, P., ... Contag, C. H. (2007). Detection of endogenous biomolecules in Barrett's esophagus by Fourier transform infrared spectroscopy. *Proceedings of the National Academy of Sciences of the United States of America*, 104, 15864–9.
- Ward, J. H. (1963). Hierarchical grouping to optimize an objective function. *Journal of the American Statistical Association*.

- Weisberg, S. P., McCann, D., Desai, M., Rosenbaum, M., Leibel, R. L., & Ferrante, A. W. (2003). Obesity is associated with macrophage accumulation in adipose tissue. *Journal of Clinical Investigation*, 112, 1796–1808.
- West, P. A., Bostrom, M. P. G., Torzilli, P. A., & Camacho, N. P. (2004). Fourier transform infrared spectral analysis of degenerative cartilage: an infrared fiber optic probe and imaging study. *Applied Spectroscopy*, 58, 376–81.
- Whitbeck, M. R. (1981). Second Derivative Infrared Spectroscopy. *Applied Spectroscopy*, 35, 93–95.
- White, U. A., & Tchoukalova, Y. D. (2014). Sex dimorphism and depot differences in adipose tissue function. *Biochimica et Biophysica Acta (BBA) - Molecular Basis of Disease*, 1842, 377–392.
- WHO. (1995). Physical status: the use and interpretation of anthropometry. Report of a WHO Expert Committee. *World Health Organization Technical Report Series*.
- WHO. (2008). Waist Circumference and Waist-Hip Ratio Report of a WHO Expert Consultation. *World Health*, 8–11.
- WHO. (2014). World : Prevalence of obesity, ages 18+, age standardized: Both sexes, 2014. Retrieved from [http://gamapserver.who.int/mapLibrary/Files/Maps/Global\\_Obesity\\_2014\\_BothSexes.png](http://gamapserver.who.int/mapLibrary/Files/Maps/Global_Obesity_2014_BothSexes.png)
- WHO. (2016). BMI Classification. Retrieved from [http://apps.who.int/bmi/index.jsp?introPage=intro\\_3.html](http://apps.who.int/bmi/index.jsp?introPage=intro_3.html)
- Widiker, S., Kärst, S., Wagener, A., & Brockmann, G. A. (2010). High-fat diet leads to a decreased methylation of the Mc4r gene in the obese BFMI and the lean B6 mouse lines. *Journal of Applied Genetics*, 51, 193–197.
- World Health Organization, & Organization, W. H. (2004). Public health Appropriate body-mass index for Asian populations and its implications for policy and

- intervention strategies. *Public Health*, 363, 157–163.
- Wozniak, S. E., Gee, L. L., Wachtel, M. S., & Frezza, E. E. (2009). Adipose tissue: the new endocrine organ? A review article. *Digestive Diseases and Sciences*, 54, 1847–56.
- Xue, J., Lee, C., Wakeham, S. G., & Armstrong, R. A. (2011). Using principal components analysis (PCA) with cluster analysis to study the organic geochemistry of sinking particles in the ocean. *Organic Geochemistry*, 42, 356–367.
- Yano, K., Ohoshima, S., Shimizu, Y., Moriguchi, T., & Katayama, H. (1996). Evaluation of glycogen level in human lung carcinoma tissues by an infrared spectroscopic method. *Cancer Letters*, 110, 29–34.
- Yeagle, P. L. (2004). *The Structure of Biological Membranes*. CRC Press. Retrieved from <http://books.google.com/books?hl=en&lr=&id=Z0F0LLSJ8dIC&pgis=1>
- Yu, P., Doiron, K., & Liu, D. (2008). Shining light on the differences in molecular structural chemical makeup and the cause of distinct degradation behavior between malting- and feed-type barley using synchrotron FTIR microspectroscopy: a novel approach. *Journal of Agricultural and Food Chemistry*, 56, 3417–26.
- Zhang, Y., Proenca, R., Maffei, M., Barone, M., Leopold, L., & Friedman, J. M. (1994). Positional cloning of the mouse obese gene and its human homologue. *Nature*, 372, 425–432.
- Ziccardi, P., Nappo, F., Giugliano, G., Esposito, K., Marfella, R., Cioffi, M., ... Giugliano, D. (2002). Reduction of inflammatory cytokine concentrations and improvement of endothelial functions in obese women after weight loss over one year. *Circulation*, 105, 804–9.

Zierath, J. R., Livingston, J. N., Thörne, A., Bolinder, J., Reynisdottir, S., Lönnqvist, F., & Arner, P. (1998). Regional difference in insulin inhibition of non-esterified fatty acid release from human adipocytes: relation to insulin receptor phosphorylation and intracellular signalling through the insulin receptor substrate-1 pathway. *Diabetologia*, *41*, 1343–54.

## APPENDIX

### A. IR MAPS OBTAINED FROM FTIR MICROSCOPY

Here in this section, the IR maps of the three different randomly selected area in each adipose tissue section obtained from FTIR microscopy are presented in figure A.1.

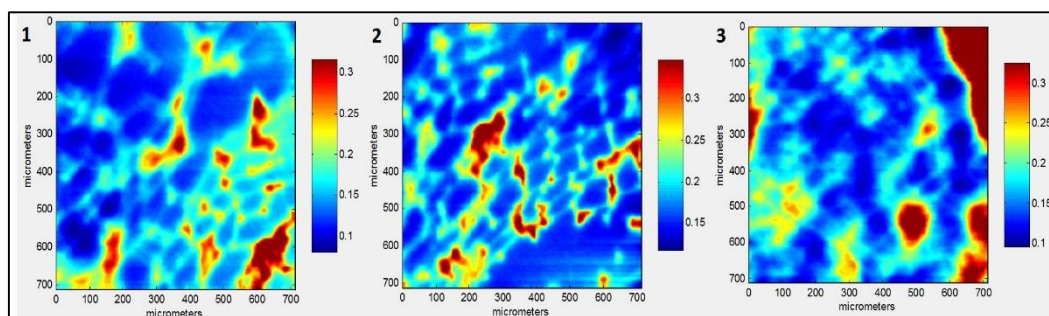


**Figure A.1.** The IR maps of the three different randomly selected area in adipose tissue section of BFMI lines obtained from FTIR microscopy.



## **CURRICULUM VITAE**

### **I. PERSONAL INFORMATION**

**Name-Surname** : Fatma KÜÇÜK BALOĞLU  
**Date of Birth/Place** : Ankara / 16.12.1984  
**Address** : Middle East Technical University  
Department of Biological Sciences  
Molecular Biophysics Laboratory  
06800, Çankaya, ANKARA  
**Phone** : +90 312 210 51 57  
**GSM** : +90 545 566 37 15  
**E-mail** : fatmakucuk1984@gmail.com  
**Marital status** : Married

### **II. EDUCATION**

#### **Ph.D. (2011 - continue)**

Middle East Technical University  
Graduate School of Applied and Natural Science  
Department of Biological Sciences, Ankara, Turkey.

PhD Qualification Major: Biophysics

PhD Qualification Minor: Physiology

Thesis: *BIOPHYSICAL CHARACTERIZATION AND DIAGNOSIS OF OBESITY FROM ADIPOSE TISSUE BY FOURIER TRANSFORM INFRARED SPECTROSCOPY AND IMAGING*

Supervisor: Prof. Dr. Feride SEVERCAN

**M.Sc. (2008 - 2010)**

Gazi University

Graduate School of Applied and Natural Science

Department of Biological Sciences, Ankara, Turkey.

Thesis: *THE EFFECT OF SYSTEMIC EGF ON LIVER TISSUE COLLAGEN AND PROTEIN LEVELS IN WOUND HEALING*

Supervisor: Assoc. Prof. Dr. Barbaros BALABANLI

**Undergraduate (2003 - 2008)**

Gazi University

Faculty of Education

Department of Biology Education, Ankara, Turkey



### **III. WORK EXPERIENCE**

#### **Research Assistant (2011 – continue)**

Middle East Technical University

Department of Biological Sciences

Ankara, Turkey

#### **Biology Teacher (2009-2010)**

The Ministry of Education ,Turkey.

### **IV. AWARDS AND SCHOLARSHIPS**

1. TUBITAK 2211-A National Scholarship Programme for PhD Students (2011-2015)
2. TUBITAK Encouragement Award for Article (2015)
3. METU Encouragement Award for Article (2015)

### **V. RESEARCH AREAS**

- Biophysical Methods
  - Fourier Transform Infrared (FTIR) Spectroscopy and Microspectroscopy
  - Differential scanning calorimetry (DSC) Technique
  - UV-Visible Spectrophotometric Method
- Laboratory Animals Using Techniques
- Histological sectioning and staining techniques
- Immunohistochemical staining methods
- Enzyme-linked immunosorbent assay
- Multivariate Data Analysis

## VI. PUBLICATIONS

### A) Articles published in SCI / SCI-Expanded indexed journals:

1. **Kucuk Baloglu F**, Garip S, Heise S, Brockmann G, Severcan F. FTIR imaging of structural changes in visceral and subcutaneous adiposity and brown to white adipocyte transdifferentiation. *Analyst* 2015; 140: 2205–14.
2. **Kucuk Baloglu F**, Baloglu O, Heise S, Brockmann G, Severcan F. Triglyceride Dependent Differentiation Of Obesity In Adipose Tissues By FTIR Spectroscopy Coupled With Chemometrics. *Journal of Biophotonics* 2017.

### B) Articles published in the other indexed journals:

1. Balabanlı B, Cevher S, **Kucuk F**. Growth Factor-Collagen Relationship in Wound Healing, *Gazi University Journal Of Science* 2015; 28 (2): 175-179.

## VII. PRESENTATIONS

### A) Abstracts published in SCI / SCI-Expanded indexed journals:

1. **Kucuk Baloglu F**, Brockmann G, Heise S, Garip S, Severcan F, Investigation of Gender Effect on Obesity using a Model of Inbred Obese Mouse Lines by Fourier Transform Infrared Imaging, **Biophysical Journal**, 108(2), Supplement 1, p626a, Biophysical Society 59th Annual Meeting, 2015, February 7-11, Baltimore, USA.

### B) Abstracts published in book of abstracts:

#### Poster Presentations

1. **Kucuk F**, Brockmann G, Heise S, Garip S, Severcan F. *Obesity-dependent structural and functional changes in different Inbred obese mouse lines of*

*gonadal and inguinal adipose tissues: a Fourier transform infrared imaging study.* FT-IR Meeting in Berlin 2013: "FT-IR Spectroscopy in Microbiological and Medical Diagnostics", Robert Koch-Institute, October 24 - 25, 2013, Berlin/ GERMANY.

2. **Kucuk F**, Brockmann G, Heise S, Garip S, Severcan F. *Obesity Dependent Structural and Functional Changes in Male And Female Inbred Obese Mouse Lines By Fourier Transform Infrared Imaging*, Abstract Book, pp:43 ITNANO 2014, 2nd International Translational Nanomedicine Conference. 25-27 July 2014, Boston, USA.
3. **Kucuk F**, Brockmann G, Heise S, Garip S, Severcan F. *Obesity-Related Structural, Functional and Ucp1 Protein Content Changes In Different Inbred Obese Male Mouse Lines Of Gonadal And Inguinal Adipose Tissues*, Abstract Book, SPEC 2014, Shedding New Light on Disease, 17-22 August 2014, Krakow, POLAND.
4. **Kucuk F**, Sen I, Baloglu O ,Severcan M, Brockmann G, Severcan M. *Differentiation Of Different Inbred Obese Mouse Lines At Adipose Tissues By ATR- FTIR Spectroscopy With Chemometric Tools*. International Turkish Congress on Molecular Spectroscopy (TURCMOS), Abstract Book, September 15-20, 2013; 187, Istanbul/TURKEY.

## VIII. NATIONAL AND INTERNATIONAL CONFERENCES

1. 24. International Biophysics Congress, Marmara University, 25-28 September 2012, İstanbul, TURKEY.
2. IV. International Congress of the Molecular Biology Association of Turkey, 27-29 November 2015, Ankara, TURKEY.

## IX. PROJECT EXPERIENCE

### International

- *Structural, Functional And Compositional Characterization Of Different Adipose Tissues In Inbred Obese Mouse Models*

The Scientific & Technological Research Council of Turkey (TUBITAK) COST project

No: SBAG- 110S235

Duration: 2010-2012

Task: Scholarship Student

Principal Investigator of Turkey side: Prof. Dr. Feride SEVERCAN

Principal Investigator of Germany side: Prof. Dr. Gudrun BROCKMANN

### National

- *Investigation of Obesity Induced Type 2 Diabetes dependent molecular alterations and therapeutic effect of Palmitoleic Acid on these alterations in adipose tissue by Fourier Transform Infrared Microspectroscopy*

The Scientific & Technological Research Council of Turkey (TUBITAK) Short Term R&D Funding Program

No: KBAG- 115Z702

Duration: 2015-2016

Task: Researcher

Principal Investigator: Prof. Dr. Feride SEVERCAN

## X. SEMINAR, SUMMER SCHOOL AND WORKSHOPS

1. 3rd International Workshop on Molecular Approaches to Obesity and Diabetes with New Implications, 15-16 March, 2012, METU, Ankara, TURKEY.

2. FT-IR Meeting in Berlin 2013: "FT-IR Spectroscopy in Microbiological and Medical Diagnostics", Robert Koch-Institute, 24 – 25 October 2013, Berlin/GERMANY.

## **XI. SEMINARS AND COURSES**

1. Light and Electron Microscope Training Course, Gazi University, December 2008, Ankara, TURKEY.
2. Applied Laboratory Animals Using Techniques Course, Bilkent University, January 2014, Ankara, TURKEY.
3. Perkin-Elmer health sciences, FT-IR Microscopy Training Course, 22 October 2015, İstanbul, TURKEY.
4. TA Instruments Roadshow, DSC Seminar, 26 April 2016, Ankara, TURKEY.

## **XII. OTHER**

### Programmes

- MS Office (Word, Excel, PowerPoint, Access, Outlook)
- OriginPro, GraphPad Prism, Perkin Elmer Spectrum, OPUS, The Unscrambler X

### English

- Foreign Language Certificate (English), METU, Ankara, TURKEY. (14.02.11-10.06.11)
- Foreign Language Certificate (English), EC Language School, MALTA. (14.06.11-02.09.11)

## **XIII. PROFESSIONAL AFFILIATIONS**

- Biophysical Society (BPS)